To the Graduate Council:

I am submitting herewith a dissertation written by Yanghui Qiu entitled "Double Ionization of Helium and H^- by High-Energy Photons". I have examined the final copy of this dissertation for form and content and recommend that it be accepted in partial fulfillment of the requirements for the degree of Doctor of Philosophy, with a major in Physics.

Joachim Burgdörfer, Major Professor

We have read this dissertation
and recommend its acceptance:

Accepted for the Council:

Associate Vice Chancellor and
Dean of the Graduate School

Double Ionization of He and H^- by High-Energy Photons

A Dissertation Presented
for the Doctor of Philosophy Degree
The University of Tennessee, Knoxville

Yanghui Qiu
December, 1997

Acknowledgments

I am highly indebted to Prof. Joachim Burgdörfer for inviting me to join his research group and introducing me to the frontier of electron correlation. As my major advisor, as a teacher and as a friend, he has provided invaluable guidance not only to the scientific projects I have been working on, but also throughout my entire graduate career.

I would also like to thank the members on my committee Prof. Charles Feigerle, Prof. David Pegg and Prof. Stuart Elston for their instruction and comments in the preparation of this thesis. I wish to thank Dr. Jianyi Wang, Dr. Jianzi Tang, Dr. Carlos Reinhold and Dr. Jörg Müller for their assistance, cooperation and discussion. I would like to thank Mr. Stefan Deutscher for his friendship and help in many computer related issues. I wish to thank Mr. Ludger Wirtz and Mr. Shuhei Yoshida for their long-term inspiration and friendship. Finally, I would like to thank my wife Qiru Xie and my son Xi (John) Qiu for their support of my study.

Abstract

We present theoretical studies on the double ionization and ionization-excitation of helium and H^- by high energy photon ($\geq$ 1 keV). With an accurate Hylleraas-type initial state wavefunction and final state wavefunctions with and without correlation we investigate the dynamic motion of the two-continuum electrons in the field of nucleus. We analyze the solution of the Schrödinger equation for the double-continuum system and demonstrate that the 3C wavefunction describes the final state to leading order in Z/k_1 in the full configuration space and satisfies the Kato cusp conditions exactly at the three two-body collision points. A new technique for the analysis of the distortion factor $D^{(-)}$ in the 3C wavefunction has been developed which can lead to an accurate evaluation of the transition probabilities. Our calculation shows that the double to single ratio and the satellite-to-1s ratio approaches the same asymptotic limit with and without final state correlation. However, at 1 keV the ratios with the 3C wavefunction are increased significantly while they are almost unchanged with the 2C solution. The double to single ratio of helium with the 3C wavefunction is 2.62 % at 1 keV and approaches an asymptotic value of $R_{ph}(\infty) = 1.65\%$, which is in excellent agreement with the measurements. For H^- we have made the first reliable calculation at the high energies. The double to single ratio is 1.87 % at 1 keV with the 3C wavefunction and approaches an asymptotic value of $R_{ph}(\infty) = 1.50\%$. We also point out that the interaction between the high energy photon and

atom is localized in a region with a distance of $\sim E^{-1/2}$ around the nucleus instead of a point at the center. We introduce a shape function into the formulas suggested by Kabir and Salpeter and by Dalgarno and Stewart which can dramatically improve the evaluation of the absolute cross sections of the double and single ionization at non-relativistic high energies. Moreover, we extend the validity of the formulas down to about 2 keV by including final-state correlation.

The thesis is based in part on the following publications:

- Y. Qiu, J. Tang, J. Burgdörfer, and J. Wang, one- and two-electron emission from H^- by high-energy photons, J. Phys. B **30**, L689 (1997).
- Y. Qiu, J. Tang, J. Burgdörfer, and J. Wang, Double photoionization of helium from threshold to high energies, to be published.
- Y. Qiu, J. Müller, and J. Burgdörfer, Periodic orbit spectra of hydrogen and helium, Phys. Rev. **54**, 1922 (1996).
- J. Burgdörfer, Y. Qiu, and J. Müller, Periodic Orbit Spectra of Simple Atoms, edited by H. Friedrich and B. Eckhardt, in Classical, semiclassical and quantum dynamics in atoms, (Springer-Verlag Berlin Heidelberg, 1997).
- J. Wang, J. H. McGuire, J. Burgdörfer, and Y. Qiu, Consistency test of double ionization of helium by photons and charged particles,, Phys. Rev. A **54**, 613 (1996).

- J. Wang, J. H. McGuire, J. Burgdörfer, and Y. Qiu, Differential double ionization of He by Compton photons and charged particles at large energy transfers, Phys. Rev. Lett. **26**, 1723 (1996).

Contents

List of Figures

List of Tables

List of frequently used abbreviations

DPI	**D**ouble **P**hotoionization
SPI	**S**ingle **P**hotoionization
2C	approximate final state wavefunction using a product of **2** Coulomb wavefunctions
3C	approximate final state wavefunction using a product of **3** Coulomb wavefunctions
WRP	**W**annier-**R**au-**P**eterkop
MBPT	**M**any-**B**ody **P**erturbation **T**heory
MCHF	**M**ulti-**C**onfiguration **H**artree-**F**ock
HSCC	**H**yperspherical **C**lose-**C**oupling

Chapter 1

Introduction

1.1 Motivation

The three-body problem is of fundamental importance in atomic and few-body physics. The understanding of correlation effects arising in the dynamics of two electrons escaping from a charged core is a tremendous challenge for atomic and molecular physicists. The double ionization of atoms and double detachment of negative ions by photoabsorption provide a sensitive test for electron-electron correlation. Double photoionization (DPI) is a process where an atom (ion) absorbs one photon γ and simultaneously ejects two electrons (Fig. 1.1).

Since the coupling between the electrons and the radiation field ($\propto \vec{p} \cdot \vec{A}$) is a single-body operator, two electron escape would be strictly prohibited without electron-electron correlation. The simultaneous ejection of two electrons is therefore mediated through the electron-electron interaction in the initial state ("ground-state correlation") and/or in the final state of two electrons in the Coulomb continuum ("final-state correlation").

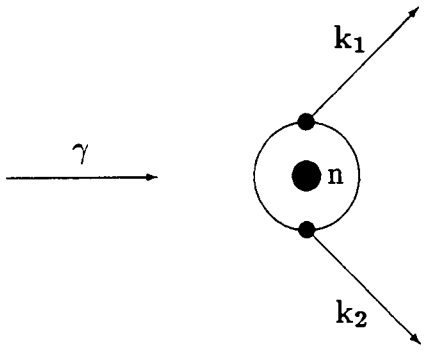

Figure 1.1: Schematic expression of the double ionization process by a single photon: the two electrons are ejected from the ground state to a double continuum state after receiving all of the photon energy.

Helium, because of its simplicity, has been the target for extensive studies from both theory and measurements in past decades. At the very low photon energies (near the DPI threshold), the studies have focused on the angular distribution of the escaping electrons and the energy dependence of the total cross section. The milestone of the studies is the Wannier-Rau-Peterkop (WRP) theory [1, 2, 3, 4] which predicted that the total DPI cross section of an atom varies above threshold as $\sigma^{++} \propto E^m$ where m is an exponent depending on the charge Z of the residual ion. The theoretical values $m = 1.127$ for $Z = 1$ and $m = 1.056$ for $Z = 2$ are consistent with recent experiments done with H^- and K^- targets [5, 6, 7, 8] and with helium target [9, 10], respectively. The WRP theory also predicted correctly the angular correlation for two-electron escape at threshold. Above but near threshold, several other independent approaches have been applied to the discussion of the angular correlation of the ejecting electrons. Rouzo and Cappello [11] calculated the

angular distribution using a highly correlated ground-state wavefunction and a double-continuum final-state wavefunction approximated by a symmetrized product of two Coulomb waves (2C) and obtained a result which disagrees with the prediction of WRP theory. Huetz, Selles, Waymel, and Mazeau [12] arrived at the angular distribution based on an approximation within the frame of WRP theory, and Maulbetsch and Briggs [13, 14] obtained the result using a correlated three-body Coulomb wavefunction (3C), which is a product of 2C wavefunction and a Coulomb distortion factor, for the final state. The result in the calculation of Maulbetsch and Briggs is in agreement with the measurement [15]. However, the 3C wavefunction is the appropriate solution of the three-body Coulomb system only in the high energy range, the agreement in the angular distribution between the theoretical prediction and measurement can not completely explain the dynamic feature of the electron-electron angular correlation.

In the higher energy range, studies have focused on the ratio of the total cross sections between double and single ionization because of the convenience for experimental set-up and for comparison between theory and measurement. At low and intermediate energies ($E \leq 1$ keV), sophisticated *ab initio* methods, such as the hyperspherical close-coupling (HSCC) [16], R-matrix [17], and complex Sturmian [18] methods have been recently developed which have led to improved agreement with most recent measurements [19, 20, 21]. At high energies ($E \geq 1$ keV), several approaches have been pursued including many body perturbation theory (MBPT) [22, 23, 27], the

use of correlated 3C wavefunction as the final state [25, 26, 27, 28] and, very recently, the application of the dipole response function [29]. In this region, discrepancies between different theoretical predictions have remained unsolved and comparison with experiments is complicated by the fact that in some experiments the separation of contributions from Compton scattering and from photoionization is not possible. In this thesis, our goal is to study the double and single photoionization and their ratio at high photon energies.

1.2 General formalism

We consider a photoionization experiment where linearly polarized photons collide with two-electron atoms in their ground states. For a photon energy greater than the double ionization threshold ($\simeq$ 79 eV for helium), the collision can result in the simultaneous ejection of two electrons having the asymptotic momenta $\mathbf{k}_1$ and $\mathbf{k}_2$ in the laboratory frame. Our main purpose is to evaluate the probability of this event under unit flux of photons, i. e.,

$$\frac{d\sigma_v^{++}}{d\rho} = \frac{2\pi \left|\langle \psi_f | H_{int} | \psi_0 \rangle\right|^2 \delta(E_0 + E - E_f)}{c/(2\pi)^3}, \tag{1.1}$$

where H_{int} is the interaction operator between the electrons and the photon, ψ_0 and ψ_f are the ground- and final-state wavefunctions, respectively, E_0 and E_f are the corresponding energies, c is the velocity of the photon, E is the incident photon energy, and $d\rho$ is the final-state volume-element of the two electrons with energies E_1 and E_2

$$d\rho = \sqrt{2E_1} dE_1 d\Omega_{\hat{\mathbf{k}}_1} \sqrt{2E_2} dE_2 d\Omega_{\hat{\mathbf{k}}_2}.$$

The interaction operator between the two electrons with momenta $\mathbf{p}_1$ and $\mathbf{p}_2$ and the photon field $\mathbf{A}_i$ ($i = 1, 2$) is a sum of single-body operators

$$H_{int} = \frac{1}{c}(\mathbf{A}_1 \cdot \mathbf{p}_1 + \mathbf{A}_2 \cdot \mathbf{p}_2).$$

The vector field $\mathbf{A}_i$ (i=1,2) are given by

$$\mathbf{A}_i = \frac{c}{2\pi\sqrt{E}}\hat{\alpha}_{\mathbf{k}} e^{i\mathbf{k}\cdot\mathbf{r}_i},$$

where $\mathbf{r}_i$ (i=1,2) are the coordinates of the two electrons in configuration space and $\mathbf{k}$ and $\hat{\alpha}_{\mathbf{k}}$ are the wavevector and the polarization direction of the photon, respectively. At small and intermediate photon energies the wavelength of the photon is larger than the size of the atom, $kr_i \lesssim 1$, so we can make a dipole approximation

$$e^{i\mathbf{k}\cdot\mathbf{r}_i} \approx 1, \quad (i = 1, 2).$$

At high photon energies ($kr_i \gtrsim 1$), the dipole approximation is not automatically justified. Also because the maximum momentum of the electrons is about $\geq 0.2c$ at the very high photon energies ($\geq$ 12.0 keV), relativistic effects should be noticeable at these energies. In this thesis we apply the non-relativistic formulation and the dipole approximation in the high energy regime. The validity of the approximation will be discussed in chapter 6. Since the incident photon is linearly polarized, we can assume, in general, that the polarization is along $\hat{z}$ direction, i. e., $\hat{\alpha}_{\mathbf{k}} = \hat{z}$. Then the interaction operator is reduced to

$$H_{int} = \frac{1}{2\pi\sqrt{E}}(p_{1z} + p_{2z}),$$

where p_{iz} (i=1,2) are the z components of the momentum operators. The sixfold differential cross section is

$$\frac{d^2\sigma_v^{++}}{dE_1 dE_2 d\Omega_{\hat{\mathbf{k}}_1} d\Omega_{\hat{\mathbf{k}}_2}} = \frac{4\pi^2}{cE} |\langle\psi_f|p_{1z} + p_{2z}|\psi_0\rangle|^2 2\sqrt{E_1 E_2}\delta(E_0 + E - E_f). \quad (1.2)$$

In Eq. (1.2) the final state ψ_f is momentum normalized. If we redefine the final state wavefunction such that it is energy normalized, the sixfold differential cross section becomes

$$\frac{d^2\sigma_v^{++}}{dE_1 dE_2 d\Omega_{\hat{\mathbf{k}}_1} d\Omega_{\hat{\mathbf{k}}_2}} = \frac{4\pi^2}{cE} |\langle\psi_f|p_{1z} + p_{2z}|\psi_0\rangle|^2 \delta(E_0 + E - E_f). \quad (1.3)$$

This formula gives the probability for double ionization where one electron is ejected with the energy E_1 , (in the element dE_1), along the direction $\hat{\mathbf{k}}_1$, (in the element of solid angle $d\Omega_{\hat{\mathbf{k}}_1}$), while the other electron is ejected with E_2 and $\hat{\mathbf{k}}_2$, in the ranges of dE_2 and $d\Omega_{\hat{\mathbf{k}}_2}$, respectively. Since the total energy is conserved during the ionization process, the electron energies are not independent, so that one of them can be eliminated by the δ function. This convention, together with the use of notations $d\Omega_{\hat{\mathbf{k}}_1}$ and $d\Omega_{\hat{\mathbf{k}}_2}$ for the two-variable solid-angle element has led one to call Eq. (1.3) the triply differential cross section. Integrating over the four angles $\hat{\mathbf{k}}_1$ and $\hat{\mathbf{k}}_2$ provides the analysis of the energy distribution of the probability,

$$\frac{d\sigma_v^{++}}{dE_2} = \int \frac{d\sigma_v^{++}}{dE_1 dE_2 d\Omega_{\hat{\mathbf{k}}_1} d\Omega_{\hat{\mathbf{k}}_2}} dE_1 d\Omega_{\hat{\mathbf{k}}_1} d\Omega_{\hat{\mathbf{k}}_2}. \quad (1.4)$$

Finally, sixfold integration leads to the total cross section of the DPI

$$\sigma_v^{++} = \int \frac{d\sigma_v^{++}}{dE_1 dE_2 d\Omega_{\hat{\mathbf{k}}_1} d\Omega_{\hat{\mathbf{k}}_2}} dE_1 dE_2 d\Omega_{\hat{\mathbf{k}}_1} d\Omega_{\hat{\mathbf{k}}_2} \quad (1.5)$$

The dipole matrix element in Eq. (1.3) with the momentum operators is the velocity form of the dipole transition operator. Since

$$\begin{aligned}\langle\psi_f|p_{1z}+p_{2z}|\psi_0\rangle &= \frac{iZ}{E}\langle\psi_f|\frac{z_1}{r_1^3}+\frac{z_2}{r_2^3}|\psi_0\rangle \\ &= iE\langle\psi_f|z_1+z_2|\psi_0\rangle, \end{aligned} \tag{1.6}$$

where z_i (i=1, 2) are the z components of the two electron coordinates, we obtain the acceleration (σ_a^{++}) and length (σ_l^{++}) forms of the transition probability:

$$\sigma_a^{++} = \frac{4\pi^2 Z^2}{cE^3}\int\left|\langle\psi_f|\frac{z_1}{r_1^3}+\frac{z_2}{r_2^3}|\psi_0\rangle\right|^2 \delta(E_0+E-E_f)dE_1dE_2d\Omega_{\hat{\mathbf{k}}_1}d\Omega_{\hat{\mathbf{k}}_2}, \tag{1.7}$$

$$\sigma_l^{++} = \frac{4\pi^2 E}{c}\int|\langle\psi_f|z_1+z_2|\psi_0\rangle|^2\,\delta(E_0+E-E_f)dE_1dE_2d\Omega_{\hat{\mathbf{k}}_1}d\Omega_{\hat{\mathbf{k}}_2}. \tag{1.8}$$

For single photoionization (SPI), one of the electrons is localized in the bound state $n_2l_2m_2$ with energy $E_2 = -Z^2/(2n_2^2)$, while the other electron is ejected with the energy $E_1 = E_0 + E - E_2$, along the direction $\hat{\mathbf{k}}_1$, (in the element of solid angle $d\Omega_{\hat{\mathbf{k}}_1}$). The total cross section of the single ionization in three gauges are

$$\sigma_a^{+} = \frac{4\pi^2 Z^2}{cE^3}\sum_{n_2l_2m_2}\int\left|\langle\psi_f|\frac{z_1}{r_1^3}+\frac{z_2}{r_2^3}|\psi_0\rangle\right|^2 d\Omega_{\hat{\mathbf{k}}_1}, \tag{1.9}$$

$$\sigma_v^{+} = \frac{4\pi^2}{cE}\sum_{n_2l_2m_2}\int|\langle\psi_f|p_{1z}+p_{2z}|\psi_0\rangle|^2\,d\Omega_{\hat{\mathbf{k}}_1}, \tag{1.10}$$

and

$$\sigma_l^{+} = \frac{4\pi^2 E}{c}\sum_{n_2l_2m_2}\int|\langle\psi_f|z_1+z_2|\psi_0\rangle|^2\,d\Omega_{\hat{\mathbf{k}}_1}. \tag{1.11}$$

The ratio between the double and single ionization is therefore obtained

$$R_{ph}(E) = \frac{\sigma_i^{++}}{\sigma_i^{+}}, \tag{1.12}$$

where i refers to the three gauge labels, i. e., a, v, and l, respectively.

By the definitions, the calculation of the double photoionization requires explicit knowledge of the ground- and final-state wavefunctions and the essential contribution to the fragmentation process comes from the ground- and final-state correlation.

1.3 Plan of the thesis

The content is arranged as follows:

- In **chapter 2** we discuss the properties of the "exact" wavefunction of the two electron system in different spatial regions and emphasize the properties of the wavefunction at small and intermediate interparticle distances. We calculate the ground-state wavefunction variationally using Sturmian polynomial and Hylleraas coordinate basis sets. These are two important approaches for single-particle and correlated basis descriptions of the ground-state correlation, respectively. We discuss the convergence of the basis sets and check the properties of the ground state wavefunction obtained.

- In **chapter 3** we investigate the dynamic motion of the two-continuum electrons in the field of a nucleus. We briefly review various approximate wavefunctions available and discuss their properties and scopes of

validity. We emphasize our study of the 2C and 3C double-continuum wavefunctions, which will be used in the calculation of double photoionization.

- In **chapter 4** we study the double and single photoionization cross sections for helium and their ratio by using the accurate ground-state wavefunction in the representation of Hylleraas coordinates and the uncorrelated 2C final-state wavefunction. Detailed calculations are performed in acceleration, velocity, and length gauges and the results are displayed and compared with the experiment data. The limitation of the present work is discussed.

- In **chapter 5** we study the double and single photoionization cross sections for helium and their ratio at high energies by using the accurate ground-state wavefunction in the representation of Hylleraas coordinates and the correlated 3C final-state wavefunction. Since the acceleration gauge is the best form to calculate the dipole transition amplitude at high energies [31] we implement the calculations in acceleration form. We have developed a new technique for the analysis of the distortion factor in the 3C wavefunction such that an accurate evaluation of the dipole matrix element is possible. The results obtained are displayed together with those of other calculations and measurements.

- In **chapter 6** we investigate the double and single photoionization cross sections for helium and their ratio at and near the non-relativistic high

energy limit. We analyze the high energy behavior of the acceleration dipole matrix element and introduce a correction to the formulas suggested by Kabir and Salpeter [84] and by Dalgarno and Stewart [85]. This correction can dramatically improve the evaluation of the absolute cross sections of the double and single ionization at the non-relativistic high energy limit. Moreover, we extend the scope of validity of the formulas by introducing final-state correlation. The improved formulas work well for finite photon energy down to about 2 keV for double photoionization. Finally, we present the justification of the dipole approximation in the high energy region.

- In **chapter 7** we study the double and single photodetachment cross sections for H^- and their ratio at high energies. Unlike helium, the electron-electron repulsion in H^- almost matches in strength the electron-nucleus attraction. Here the electron moving in the outer region of the configuration space only experiences the effect of the dipole-term potential field which is in short range. This property has significant implications for the detachment-excitation and DPI. We have made the first reliable calculations of the double and single photodetachment cross sections by using the accurate ground-state wavefunction and the correlated 3C final-state wavefunction. Detailed results of the detachment-excitation and DPI are displayed and compared with the results obtained without final state correlation. It is hoped that the present result will stimulate measurements in the near future.

Atomic units (a.u.) ($\hbar \equiv 1,\ e \equiv 1,\ m_e \equiv 1$) are used through the thesis unless otherwise noted. Other units used and related to a.u. are

$$\begin{aligned} &\text{the speed of light in vacuum c} = 137.03599 \text{ a.u.} \\ &1 \text{ eV} = 1/27.2113957 \text{ a.u.} \\ &1 \text{ cm} = 1/(5.2917726 \times 10^{-9}) \text{ a.u.} \end{aligned} \tag{1.13}$$

Chapter 2

Ground-state correlation

The electron-electron interaction in the ground state plays a very important role in the DPI [30]. At very high photon energies it dominates the asymptotic behavior of the ratio between the double and single ionization [31]. For a two electron atomic system the non-relativistic Hamiltonian, on neglecting the motion of nucleus, is

$$H = \frac{\mathbf{p}_1^2}{2} + \frac{\mathbf{p}_2^2}{2} - \frac{Z}{r_1} - \frac{Z}{r_2} + \frac{1}{r_{12}}, \tag{2.1}$$

where $\mathbf{p}_i$ and r_i $(i = 1, 2)$ are the momenta and position coordinates of the two electrons, r_{12} is the interelectron coordinate, and Z the charge of the nucleus. The ground state wavefunction ψ_0 is the solution of the Schrödinger equation

$$H\psi = E\psi \tag{2.2}$$

with the lowest eigenenergy E. Since it is the simplest case for studying many-electron atoms, the ground state of helium has been introduced in many text books of quantum mechanics [32]. Here the ground state wavefunction of the two-electron system is usually constructed as a product of

two hydrogenic ground-state wave functions

$$\psi_0(\mathbf{r}_1, \mathbf{r}_2) = \frac{Z^*}{\pi} e^{-Z^*(r_1+r_2)} \tag{2.3}$$

where Z^* is a variational parameter. Using the Ritz variational principle, the binding energy of the ground state obtained is 2.8474 and $Z^* = 1.6875$. Eq. (2.3) is the simplest variational description within the single-particle model for helium and the variational parameter Z^* serves as an effective screened charge felt by the electrons. With the availability of digital computers, different theoretical methods have been developed. The multi-configuration Hartree-Fock (MCHF) method based on single-particle orbits [33] and the various variational methods based on different basis sets [34, 35, 36, 37, 38, 39, 40, 41] are able to predict the binding energy with high accuracy. However, the accuracy of an approximate wavefunction is not entirely determined by the accuracy of the corresponding variational energy. Besides, in order to make an effective calculation of the DPI, a mathematically manageable solution of the ground state wavefunction is necessary. In section 2.1 of this chapter, we will discuss the properties of the "exact" wavefunction of the two electron system in different spatial regions and emphasize the properties of the wavefunction at small and intermediate interparticle distances. In section 2.2 and 2.3, we will calculate the ground state wavefunction variationally using Sturmian polynomial and Hylleraas coordinate basis sets. These are two important approaches for single-particle and correlated basis descriptions of the ground-state correlation, respectively. We will discuss the convergence of the basis sets and check the properties of the ground state

wavefunction obtained.

2.1 Properties of the ground state

As mentioned above, the accuracy of the binding energy is only a partial indication of the accuracy in the ground state wavefunction ψ_0, since the main contribution of the wavefunction to the binding energy comes from a spatial region whose distance from the nucleus is the order of the characteristic binding radius. Apart from the binding energy, other tests of the accuracy of ψ_0 are the virial theorem [42] for which the ratio between the potential energy and the kinetic energy equals -2 and the asymptotic behavior of ψ_0 at large distance:

$$\psi_0(\mathbf{r}_1, \mathbf{r}_2) \propto e^{-\sqrt{-E_0}(r_1+r_2)}, \tag{2.4}$$

where $-E_0$ is the binding energy.

In the small spatial region, the relevant measure of the accuracy of the solution ψ in the Schrödinger equation (Eq. (2.2)) is the Kato cusp conditions [43]:

$$\left(\frac{\partial\langle\psi(\mathbf{r}_1, \mathbf{r}_2)\rangle}{\partial r_1}\right)_{r_1=0} = -Z\psi(0, \mathbf{r}_2), \tag{2.5}$$

$$\left(\frac{\partial\langle\psi(\mathbf{r}_1, \mathbf{r}_2)\rangle}{\partial r_{12}}\right)_{r_{12}=0} = \frac{1}{2}\psi(\mathbf{r}_1 = \mathbf{r}_2, \mathbf{r}_2), \tag{2.6}$$

where the average is taken on a sphere of constant radius r_1 in Eq. (2.5) and r_2 in Eq. (2.6). The two cusp conditions give quantitative information on the singularity of the solution in the Schrödinger equation (Eq. (2.2)), and are especially important for double ionization by high-energy photons because the reaction zone of the photon-atom interaction is localized within

a distance of $\sim E^{-1/2}$ around the nucleus, where E is the photon energy (see chapter 5). These two conditions, while correct for any exact solutions of ψ in the Schrödinger equation including both bound and continuum states, are very difficult to evaluate in some coordinate systems. In the ground state, however, the two electrons are moving in a plane for which the system has only 3 degrees of freedom and the Eqs. (2.5) and (2.6) can be greatly simplified by the use of three interparticle coordinates. Following the classical method of Hylleraas [44], the ^1S state Schrödinger equation becomes

$$\frac{\partial^2\psi_0}{\partial r_1^2}+\frac{2}{r_1}\frac{\partial\psi_0}{\partial r_1}+\frac{\partial^2\psi_0}{\partial r_2^2}+\frac{2}{r_2}\frac{\partial\psi_0}{\partial r_2}+2\frac{\partial^2\psi_0}{\partial r_{12}^2}+\frac{4}{r_{12}}\frac{\partial\psi_0}{\partial r_{12}}$$
$$+\frac{(r_1^2-r_2^2+r_{12}^2)}{r_1 r_{12}}\frac{\partial^2\psi_0}{\partial r_1\partial r_{12}}+\frac{(r_2^2-r_1^2+r_{12}^2)}{r_2 r_{12}}\frac{\partial^2\psi_0}{\partial r_2\partial r_{12}}$$
$$=-2(E_0+\frac{Z}{r_1}+\frac{Z}{r_2}-\frac{1}{r_{12}})\psi_0. \qquad (2.7)$$

If we multiply each term on both sides of Eq. (2.7) by r_i and let $r_i \to 0$, we get

$$\left.\frac{\partial\psi_0(r_1,r_2,r_{12})}{\partial r_i}\right|_{r_i=0} = -Z\psi_0(r_1,r_2,r_{12})|_{r_i=0}\,,(i=1,2); \qquad (2.8)$$

If we multiply each term by r_{12} and let $r_{12} \to 0$, we have

$$\left.\frac{\partial\psi_0(r_1,r_2,r_{12})}{\partial r_{12}}\right|_{r_{12}=0} = \frac{1}{2}\psi_0(r_1,r_2,r_{12})\Big|_{r_{12}=0}. \qquad (2.9)$$

The Eqs. (2.8) and (2.9) are the cusp conditions for the ground state and are convenient to evaluate in the interparticle coordinates.

2.2 Ground state in Sturmian basis

The Sturmian polynomial basis method provides a single-particle description of the correlated wavefunction, which is useful for understanding single-

particle concepts of atoms and convenient for partial wave calculation of the dipole matrix element in DPI. The Sturmian polynomials are

$$| nlm\rangle_\sigma = \frac{1}{r}\sqrt{\frac{\sigma}{2n}\frac{(n-l-1)!}{(n+l)!}}(\sigma r)^{l+1}e^{-\sigma r/2}L_{n-l-1}^{2l+1}(\sigma r)Y_{lm}(\theta,\phi), \qquad (2.10)$$

where nlm are quantum numbers ($m = -l, -l+1, ..., l-1, l; l = 0, 1, ..., n-1$; $n = 1, 2, ...$), σ is the Sturmian variational parameter, r, θ, ϕ are the radial and angular coordinates, and

$$L_j^k(x) = \sum_{i=0}^{j}(-1)^i\frac{(j+k)!x^i}{(j-i)!(k+i)!i!} \qquad (2.11)$$

stands for a generalized Laguerre polynomial. The single-particle wavefunctions in Eq. (2.10) are similar in form to the hydrogenic bound state wavefunctions except that the argument of the Laguerre polynomial and the exponential function is replaced by a constant parameter σ rather than $2Z/n$ which varies from shell to shell. Like the pure Coulomb bound state, the degree of the Laguerre polynomial in Eq. (2.11), which corresponds to a radial quantum number, is $n - l - 1$. Furthermore, when $\sigma = 2Z/n$, the single-particle states are identical to the eigenstates of the pure Coulomb potential $-Z/r$ with the principal quantum number n. In contrast to the pure Coulomb bound states, however, the Sturmian states form a complete set, because of the completeness of the Laguerre polynomials.

2.2.1 Basis function for the ground state of a two-electron atom

We now need to construct a basis function for the entire atom from the one-electron wavefunction $|nlm\rangle_\sigma$. In the uncoupled representation, the wave-

function of the two-electron system takes the form of a simple product of the two one-electron wavefunctions

$$|n_1 l_1 m_1 n_2 l_2 m_2\rangle_\sigma = |n_1 l_1 m_1\rangle_\sigma |n_2 l_2 m_2\rangle_\sigma. \tag{2.12}$$

Since the total angular momentum of the system $\hat{L}^2$ and its z component $\hat{L}_z$ are conserved, L and M are good quantum numbers. We can construct the eigenstates of $\hat{L}^2$ and $\hat{L}_z$ based on $|n_1 l_1 m_1 n_2 l_2 m_2\rangle_\sigma$ by a Clebsch-Gordon transformation

$$\begin{aligned} |\, n_1 n_2 l_1 l_2 LM\rangle_\sigma &= \sum_{m_1}\sum_{m_2}(-1)^{l_1-l_2+M}\sqrt{2L+1}\begin{pmatrix} l_1 & l_2 & L \\ m_1 & m_2 & M \end{pmatrix} \\ &\quad \cdot |\, n_1 l_1 m_1 n_2 l_2 m_2\rangle_\sigma. \end{aligned} \tag{2.13}$$

Because we are only interested in the ^1S ground state for which $L = M = 0$, the angular momenta of the two electrons in Eq.(2.13) must be identical. Therefore, the ground state basis function is

$$\begin{aligned} |\, n_1 n_2 ll00\rangle_\sigma &= \sum_{m=-l}^{m=l} \frac{(-1)^{l-m}}{\sqrt{2l+1}} |\, n_1 lm n_2 l-m\rangle_\sigma \\ &= (-1)^l \frac{\sqrt{2l+1}}{4\pi} |\, n_1 l n_2 l\rangle_\sigma P_l(cos\theta_{12}), \end{aligned} \tag{2.14}$$

where θ_{12} is the angle between the two electrons and $|\, n_1 l n_2 l\rangle_\sigma$ is the radial part of the function in Eq. (2.12). Following the Pauli-principle, the two electrons in the atom should be indistinguishable, which requires the wavefunction of the system to be (anti) symmetrized [1]. Therefore, the correct

[1]The entire spin-orbit wavefunction is a simple product of both spin and orbital wavefunctions. For the ground state ^1S, the spin wavefunction is antisymmetric, therefore, the orbital wavefunction must be symmetric. Because there is no spin-orbit coupling for the ground state, we only discuss the orbital wavefunction here.

ground state basis set for the entire atom is

$$\mid n_1 n_2 l\rangle_\sigma = \frac{1}{\sqrt{2(1+\delta_{n_1,n_2})}}(\mid n_1 n_2 ll00\rangle_\sigma + \mid n_2 n_1 ll00\rangle_\sigma), \tag{2.15}$$

where $n_1, n_2 = 1, 2, ...$ and $l = 0, 1, ..., min(n_1, n_2)$. Because the Sturmian polynomial basis is not orthogonal

$$\begin{aligned} {}_\sigma\langle n'lm \mid nlm\rangle_\sigma &\equiv I(nn'l) \\ &= \delta_{n',n} - \sqrt{\frac{(n+l)(n-l-1)}{4n(n-1)}}\delta_{n,n'+1} \\ &\quad -\sqrt{\frac{(n+l+1)(n-l)}{4n(n+1)}}\delta_{n,n'-1}, \end{aligned} \tag{2.16}$$

the ground state basis function for the entire atom in Eq. (2.15) is also not orthogonal

$$\begin{aligned} {}_\sigma\langle n_1' n_2' l' \mid n_1 n_2 l\rangle_\sigma &= \frac{\delta_{l,l'}}{\sqrt{(1+\delta_{n_1',n_2'})(1+\delta_{n_1,n_2})}} \\ &\quad \cdot \{I(n_1 n_1' l)\cdot I(n_2 n_2' l) + I(n_1 n_2' l)\cdot I(n_2 n_1' l)\}. \end{aligned} \tag{2.17}$$

The ground state wavefunction ψ_0 is then expanded in the ground state basis set $|n_1 n_2 l\rangle_\sigma$

$$\psi_0 = \sum_{n_1 n_2 l} C_{n_1 n_2 l} |n_1 n_2 l\rangle_\sigma, \tag{2.18}$$

where $l = 0, 1, 2, ..., n_2$ is the angular momentum; $n_2 = 1, 2, ..., n_1$ is the inner electron principal quantum number; $n_1 = 1, 2, ..., N$ is the outer electron principal quantum number; and N is an integer to be decided. The total number of basis function (NBF) is determined by N,

$$NBF = \frac{1}{6}N(N+1)(N+2). \tag{2.19}$$

Let i and j each represent a set of quantum numbers, $n_{1_i} n_{2_i} l_i$ and $n_{1_j} n_{2_j} l_j$, respectively; let I_{ij} stand for the superposition matrix element $\langle i|j\rangle$; and finally let H_{ij} represent the Hamiltonian matrix element. The Schrödinger equation

$$H\psi_0 = E\psi_0$$

then becomes a matrix eigenvalue problem

$$\sum_{j=1}^{NBF} (H_{ij} - EI_{ij})C_j = 0, \tag{2.20}$$

where $i = 1, 2, ..., NBF$.

2.2.2 Matrix element in the ground state basis functions $\mid n_1 n_2 l\rangle_\sigma$

For the two electron system, the Hamiltonian is

$$H = T + V_0 + V', \tag{2.21}$$

where

$$T = \frac{\mathbf{p}_1^2}{2} + \frac{\mathbf{p}_2^2}{2}, \tag{2.22}$$

$$V_0 = -\frac{Z}{r_1} - \frac{Z}{r_2}, \tag{2.23}$$

and

$$V' = \frac{1}{r_{12}}. \tag{2.24}$$

The calculation of the Hamiltonian matrix elements can be greatly simplified by taking into account the symmetry of both the ground state basis function

and the Hamiltonian operator

$$
\begin{aligned}
{}_\sigma\langle n_1' n_2' l'|H|n_1 n_2 l\rangle_\sigma &= \frac{1}{\sqrt{(1+\delta_{n_1',n_2'})(1+\delta_{n_1,n_2})}} \\
&\cdot {}_\sigma\langle n_1' n_2' ll00|H\left[|n_1 n_2 ll00\rangle_\sigma + |n_2 n_1 ll00\rangle_\sigma\right] \quad (2.25)
\end{aligned}
$$

and by using the fact that the Sturmian single-particle functions are the eigenfunctions of the pure Coulomb potential $-Z/r$ when $\sigma = 2Z/n$, i. e.,

$$
\left(\frac{\mathbf{p}_1^2}{2} - \frac{n\sigma}{2r}\right)|nlm\rangle_\sigma = -\frac{\sigma^2}{8}|nlm\rangle_\sigma. \quad (2.26)
$$

The matrix element of the kinetic energy operator T is

$$
\begin{aligned}
{}_\sigma\langle n_1' n_2' l'|T|n_1 n_2 l\rangle_\sigma &= \frac{\sigma^2}{4}\frac{\delta_{l',l}}{\sqrt{(1+\delta_{n_1',n_2'})(1+\delta_{n_1,n_2})}} \\
&\cdot \left\{ I(n_1 n_1' l) I(n_2 n_2' l)(\delta_{n_1',n_1} + \delta_{n_2',n_2} - 1)\right. \\
&\left. + I(n_1 n_2' l) I(n_2 n_1' l)(\delta_{n_1',n_2} + \delta_{n_2',n_1} - 1)\right\}. \quad (2.27)
\end{aligned}
$$

The matrix element of the single-particle potential operator V_0 is

$$
\begin{aligned}
{}_\sigma\langle n_1' n_2' l'|V_0|n_1 n_2 l\rangle_\sigma &= \frac{\sigma Z}{2}\frac{\delta_{l',l}}{\sqrt{(1+\delta_{n_1',n_2'})(1+\delta_{n_1,n_2})}} \\
&\cdot \left\{ I(n_1 n_1' l) I(n_2 n_2' l)\left(\frac{\delta_{n_1',n_1}}{n_1} + \frac{\delta_{n_2',n_2}}{n_2}\right)\right. \\
&\left. + I(n_1 n_2' l) I(n_2 n_1' l)\left(\frac{\delta_{n_1',n_2}}{n_2} + \frac{\delta_{n_2',n_1}}{n_1}\right)\right\}. \quad (2.28)
\end{aligned}
$$

For the electron-electron interaction operator V'

$$
{}_\sigma\langle n_1' n_2' l'|V'|n_1 n_2 l\rangle_\sigma = \frac{\sigma}{4}\frac{(-1)^{l+l'}}{\sqrt{(1+\delta_{n_1',n_2'})(1+\delta_{n_1,n_2})}}\sqrt{\frac{jj'}{n_1 n_1' n_2 n_2'}}
$$

$$\cdot\sqrt{\frac{a_1!a_1'!a_2!a_2'!}{(a_1+j)!(a_1'+j')!(a_2+j)!(a_2'+j')!}}\sum_{|l-l'|}^{l+l'}\begin{pmatrix} l' & k & L \\ 0 & 0 & 0 \end{pmatrix}^2$$

$$\cdot\sum_{m_1=0}^{a_1}\frac{(-1)^{m_1}}{m_1!}\begin{pmatrix} a_1+j \\ a_1-m_1 \end{pmatrix}\sum_{m_1'=0}^{a_1'}\frac{(-1)^{m_1'}}{m_1'!}\begin{pmatrix} a_1'+j' \\ a_1'-m_1' \end{pmatrix}$$

$$\cdot\sum_{m_2=0}^{a_1}\frac{(-1)^{m_2}}{m_2!}\begin{pmatrix} a_2+j \\ a_2-m_1 \end{pmatrix}\sum_{m_2'=0}^{a_2'}\frac{(-1)^{m_2'}}{m_2'!}\begin{pmatrix} a_2'+j' \\ a_2'-m_2' \end{pmatrix}$$

$$[S(l+l'+1-k+m_2+m_2',l+l'+2+k+m_1+m_1')$$

$$-S(l+l'+2+k+m_2+m_2',l+l'+1-k+m_1+m_1')$$

$$+(l+l'+2+k+m_2+m_2')!(l+l'+1-k+m_1+m_1')!$$

$$+S(l+l'+1-k+m_1+m_2',l+l'+2+k+m_2+m_1')$$

$$-S(l+l'+2+k+m_1+m_2',l+l'+1-k+m_2+m_1')$$

$$+(l+l'+2+k+m_1+m_2')!(l+l'+1-k+m_2+m_1')!],$$

(2.29)

where

$$a_i = n_i - l - 1, \quad a_i' = n_i' - l' - 1,$$
$$j = 2l+1, \qquad j' = 2l'+1, \qquad i = 1,2,$$

and

$$S(a,b) = a!b!\sum_{s=0}^{a}\begin{pmatrix} b+s \\ s \end{pmatrix}\frac{1}{2^{b+s+1}}.$$

Eq. (2.29) is different from what Müller presented [45]. There could be a misprint in his formulas. It is important to realize that the potential energy is proportional to the variational parameter σ and the kinetic energy is proportional to σ^2. This property originates from the invariance of the

Schrödinger equation in Eq. (2.2) under the scaling transformations

$$\begin{aligned} \mathbf{r}' &= \beta^2 \mathbf{r}, \\ \mathbf{P}' &= \beta \mathbf{P}, \\ t' &= \beta^3 t, \end{aligned} \tag{2.30}$$

where the scaling parameter is $\beta = \sqrt{-E}$. Taking into account this property can significantly improve the computational efficiency of the variational method.

2.2.3 Results for helium in the Sturmian polynomial basis

We have made the variational calculation with N from 1 up to 10 corresponding to a total number of basis functions of NBF from 1 to 220. When the number of the basis functions is very small, the binding energy obtained is sensitive to the variational parameter σ. However, when the number of the basis functions is large enough ($N > 2$), the binding energy obtained is almost a constant irrespective of the variation of σ over a wide range (Fig. (2.1)). Therefore, we fix σ at 4 when $N \geq 3$. This choice for σ can also improve the behavior of the wavefunction at small distances from the nucleus (Eqs. (2.5, 2.6)).

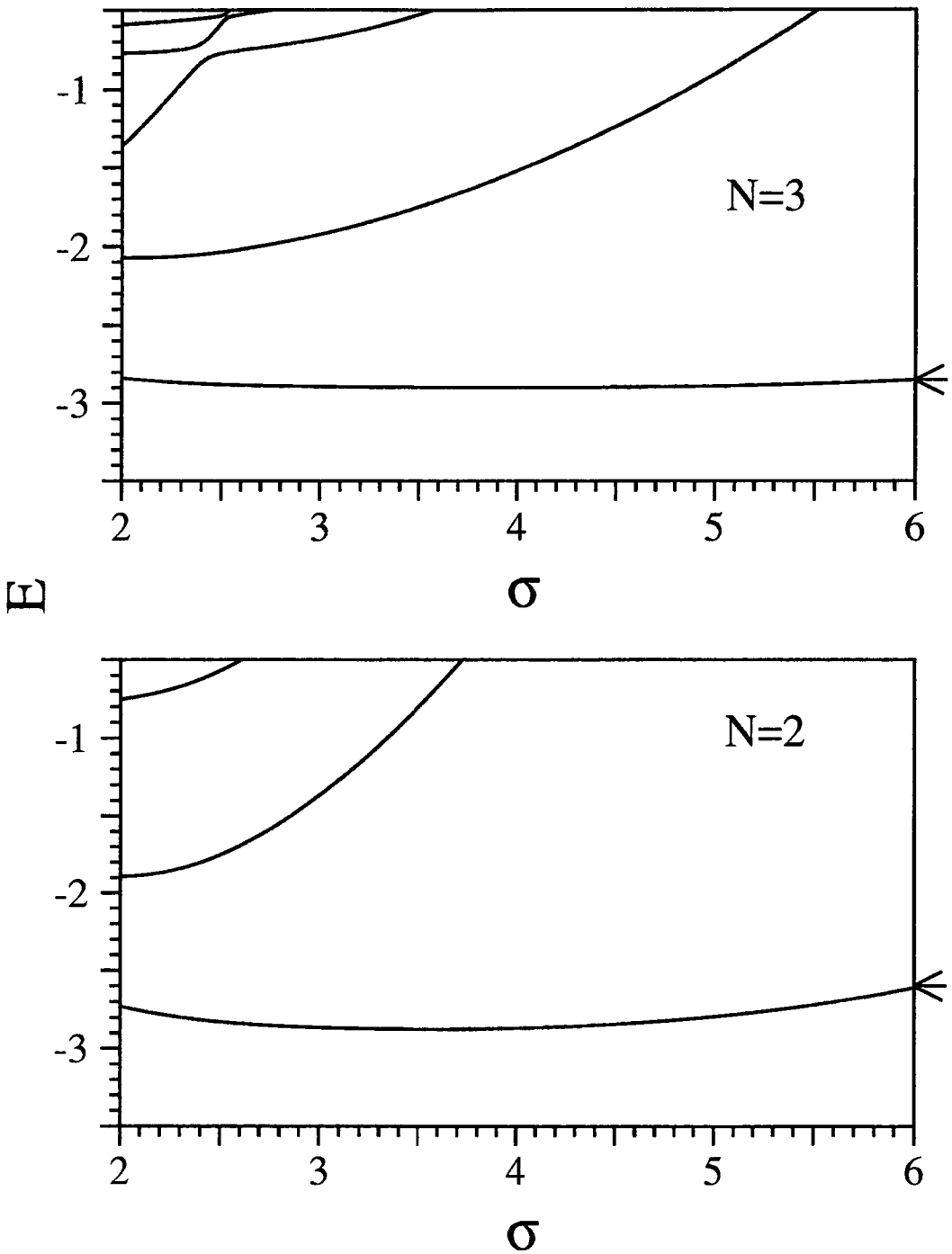

Figure 2.1: Eigenvalues of the Schrödinger equation (Eq. (2.20)) *vs* the variational parameter σ for $N = 2$ and $N = 3$. The arrow indicates the ground state energy.

Table 2.1: Binding energy $-E_0$ and its relative error with respect to the exact ground state energy vs the number of basis functions NBF.

N	NBF	$-E_0$	Relative Error (%)
1	1	2.8477	2
2	4	2.8754	1
3	10	2.8992	0.2
4	20	2.9010	0.1
5	35	2.9020	0.06
6	56	2.9025	0.04
7	84	2.9028	0.03
8	120	2.9030	0.03
9	165	2.9031	0.02
10	220	2.9032	0.02
	exact	2.903724375	

The binding energies obtained vs the number of the basis functions NBF are tabulated in Tab. (2.1). We find the energy approaches the "exact" ground state energy 2.903724375 as the number of basis functions increases. However, even with a total number of basis functions of 220, the binding energy obtained is still quite far away from the most accurate energy. The slow convergence of the binding energy is a clear indication that the Sturmian basis method is not an effective way to describe the ground state correlation. However, it is important to point out that the Sturmian basis method provides one of the best ways to describe the correlated wavefunction with single-particle basis set. Since the two-electron coordinates are separated in

the basis, the ground state wavefunction based on the basis is convenient for numerical implementation in the calculation of the transition matrix elements. In this thesis we are going to apply a Hylleraas type ground state wavefunction in the DPI calculation. We therefore skip further discussion of the properties of the ground state wavefunction in Sturmian basis and concentrate our effort on the method in Hylleraas coordinates in the next section.

2.3 Ground state in Hylleraas coordinates

The exact solution of the ground state wavefunction in the Schrödinger equation at small distance from the nucleus starts out with the linear terms

$$\psi_0 = 1 - Z(r_1 + r_2) + \frac{1}{2}r_{12} + ..., \tag{2.31}$$

which are followed by terms of the form $RlnR$, $R^{1/2}lnR$, $R^2(lnR)^2$ etc., where $R = \sqrt{r_1^2 + r_2^2}$ [46] is the hyperradius. In section 2.1 we have just discussed that the single-particle method has difficulties describing the ground state correlation. The Hylleraas coordinate basis method, however, with an explicit dependence of the basis function upon the interelectron coordinate r_{12}, provides an accurate way to calculate the ground state wavefunction. Various forms of the Hylleraas coordinate basis have been developed since the late 1950s [34, 35, 36, 37, 38, 39, 40, 41]. With three nonlinear variational parameters in the exponential factor $exp(-\beta_1 r_1 - \beta_2 r_2 - \alpha r_{12})$ of the basis function, Bonham and Kohl [40] obtained a simple ground state solution with the binding energy 2.903414. By the use of *perimetric* coordinates u, v, w,

defined by

$$\begin{aligned} u &= \epsilon(r_2 + r_{12} - r_1), \\ v &= \epsilon(r_1 + r_{12} - r_2), \\ w &= 2\epsilon(r_1 + r_2 - r_{12}) \end{aligned} \tag{2.32}$$

and the 1078 basis functions

$$|lmn\rangle_\epsilon = e^{-\frac{1}{2}(u+v+w)} L_l(u) L_m(v) L_n(w) \tag{2.33}$$

with ϵ a variational parameter and $L_l, L_m, \text{and} L_n$ normalized Laguerre polynomials, Pekeris obtained the most accurate binding energies 2.903724375 [38]. However, we are looking for a solution which is not only accurate but also simple enough for the partial wave expansion in the calculation of the DPI. We find the method developed by Schwartz [39] can meet these requirements.

2.3.1 Basis function in Hylleraas coordinates

In the method developed by Schwartz [39], the basis functions in Hylleraas coordinates are

$$|lmn\rangle_\sigma = e^{-\sigma s/2} \sigma^{l+m+n} s^l t^m u^n, \tag{2.34}$$

where σ is an adjustable parameter, $s = r_1 + r_2$, $t = r_1 - r_2$, $u = r_{12}$, $l = 0, \frac{1}{2}, 1, \frac{3}{2}$, etc., $m = 0, 2, 4$, etc., and $n = 0, 1, 2$, etc.. The single term with $l = \frac{1}{2}$ and $m = n = 0$ is omitted in order to avoid any singularity in the first derivative of the wavefunction. Each basis function is automatically symmetrized by the use of the even integers of m. Schwartz [39] showed that

the use of fractional powers of the variable s provides an effective way to represent the effect of the weak logarithmic singularity in the formal solution by Fock [46] (also see Eq. (2.31)) and has much faster convergence rate than the methods used by Pekeris [37, 38] and others [34, 36]. Moreover, the basis function in Eq. (2.34) is convenient for a partial wave expansion. According to Sack [47] and Jacobs [48], each power of r_{12} can be expanded in the form

$$r_{12}^n = \sum_l \left[\sum_m C_{nl2m} (r_<^{2m+l-n} / r_>^{2m+l-n}) \right] P_l(cos\theta_{12}) \tag{2.35}$$

with

$$C_{nlm+2} = [(n-2l-m)/(m+2)][(n-m+1)/(2l+m+3)]C_{nlm}$$

and

$$C_{nl0} = [\Gamma(-\frac{1}{2}k+l)/\Gamma(\frac{1}{2}+l)][\Gamma(\frac{1}{2}/\Gamma(-\frac{1}{2}k)]. \tag{2.36}$$

The summation over m is finite for all positive integral powers of r_{12} and only such terms appear in the current basis functions.

The trial ground state wavefunction is expanded in the basis functions

$$\psi_0(\mathbf{r}_1, \mathbf{r}_2) = \sum_{nlm} C_{nlm} |lmn\rangle_\sigma. \tag{2.37}$$

The total number of basis functions NBF used is determined by N for which $l+m+n \leq N$.

2.3.2 Matrix element in the Hylleraas coordinate basis functions

Let i and j each stand for a set of numbers, $l_i m_i n_i$ and $l_j m_j n_j$, respectively, I_{ij} represent the superposition matrix element ${}_\sigma\langle i|j\rangle_\sigma$, and H_{ij} the Hamiltonian

matrix element. For the Schrödinger equation, we have the same form as that in the Sturmian polynomial basis (Eq. (2.20)).

When we switch from Cartesian coordinates to Hylleraas coordinates , the two-electron system volume element can be expressed as

$$\begin{aligned} d\mathbf{r_1}d\mathbf{r_2} &= 8\pi^2 r_1 r_2 r_{12} dr_1 dr_2 dr_{12} \\ &= \pi^2(s^2 - t^2)u ds dt du. \end{aligned} \tag{2.38}$$

Let us define an integral

$$\begin{aligned} \int\int\int e^{-s} s^a t^b u^c ds dt du &\equiv [a, b, c] \\ &= \frac{(a+b+c+2)!}{(b+1)(b+c+2)}, \end{aligned} \tag{2.39}$$

the overlap integral becomes

$$\begin{aligned} {}_\sigma\langle l_i n_i n_i | l_j m_j n_j \rangle_\sigma &= \frac{2\pi^2}{\sigma^6} \{[l_i + l_j + 2, m_i + m_j, n_i + n_j + 1] \\ &\quad -[l_i + l_j, m_i + m_j + 2, n_i + n_j + 1]\}. \end{aligned} \tag{2.40}$$

The matrix element of the kinetic energy operator T is

$${}_\sigma\langle l_i n_i n_i | T | l_j m_j n_j \rangle_\sigma = \frac{2\pi^2}{\sigma^4} \{$$

$$\begin{aligned} &(l_i l_j - m_i m_j + l_i n_j + n_i l_j - m_i n_j - n_i m_j) \cdot [l_i + l_j, m_i + m_j, n_i + n_j + 1] \\ &-0.5(l_i + l_j + n_i + n_j) \cdot [l_i + l_j + 1, m_i + m_j, n_i + n_j + 1] \\ &-(n_i n_j + l_i n_j + n_i l_j) \cdot [l_i + l_j, m_i + m_j + 2, n_i + n_j - 1] \\ &+(n_i n_j + m_i n_j + n_i m_j) \cdot [l_i + l_j + 2, m_i + m_j, n_i + n_j - 1] \end{aligned}$$

$$
\begin{aligned}
&+0.5(l_i + l_j) \cdot [l_i + l_j - 1, m_i + m_j + 2, n_i + n_j + 1] \\
&+0.5(n_i + n_j) \cdot [l_i + l_j + 1, m_i + m_j + 2, n_i + n_j - 1] \\
&-l_i l_j \cdot [l_i + l_j - 2, m_i + m_j + 2, n_i + n_j + 1] \\
&-m_i m_j \cdot [l_i + l_j + 2, m_i + m_j - 2, n_i + n_j + 1] \\
&+0.25 \cdot [l_i + l_j + 2, m_i + m_j, n_i + n_j + 1] \\
&-0.25 \cdot [l_i + l_j, m_i + m_j + 2, n_i + n_j + 1]\}.
\end{aligned}
\tag{2.41}
$$

The matrix element of the single-particle potential operator V_0 is

$$
{}_\sigma\langle l_i n_i n_i | V_0 | l_j m_j n_j \rangle_\sigma = -\frac{8Z\pi^2}{\sigma^5}[l_i + l_j + 2, m_i + m_j, n_i + n_j + 1], \tag{2.42}
$$

and the matrix element of the electron-electron interaction operator V' is

$$
\begin{aligned}
{}_\sigma\langle l_i n_i n_i | V' | l_j m_j n_j \rangle_\sigma = \frac{2\pi^2}{\sigma^5}\{&[l_i + l_j + 2, m_i + m_j, n_i + n_j] \\
&-[l_i + l_j, m_i + m_j + 2, n_i + n_j]\}.
\end{aligned}
\tag{2.43}
$$

The Eqs. (2.39-2.43), which were originally derived for integers l, m, and n [36], are also valid for fractional values of l. It is understood, however, that the factorial $(a+b+c+2)!$ in Eq. (2.39) should be replaced by $\Gamma(a+b+c+3)$.

2.3.3 Results for helium in the basis of Hylleraas coordinates

We have made the calculation with N from 1 to 5 corresponding to a total number of basis functions NBF from 3 to 55. The binding energy and its relative error with respect to the 1078 term Pekeris energy are tabulated in Tab. (2.2).

Table 2.2: Binding energy $-E_0$ and its relative error with respect to the 1078 term Pekeris energy *vs* the number of basis functions NBF and the variational parameter σ.

N	NBF	σ	$-E_0$	Relative Error (%)
1.0	3	3.95395395	2.88865045	0.5
1.5	5	3.20620621	2.89147677	0.4
2.0	9	3.56556557	2.90349473	0.008
2.5	13	3.71271271	2.90355053	0.006
3.0	19	3.77977978	2.90368791	0.001
3.5	25	3.74874875	2.90371264	0.0004
4.0	34	3.87287287	2.90372113	0.0001
4.5	43	3.42616523	2.90372273	0.00006
5.0	55	3.94294294	2.90372407	0.00001
		exact	2.903724375	

We find the binding energy converges very rapidly as the number of the basis function NBF increases. With only 34 terms the binding energy obtained reaches 2.90372113, which converges to the 1078 term Pekeris energy with a relative error less than 0.0002%. Moreover, the wavefunction for which

the coefficients are tabulated in Tab. (2.3) satisfies the Kato cusp conditions with high accuracy. The relative errors in the cusp conditions of the 25, 34, and 55 term solutions are shown in Fig. (2.2). With 34 terms the Kato cusp conditions at the origin are satisfied with a relative error less than 0.001% pertaining to the confluence of the electron-nucleus coordinates and about 9% with regard to the confluence of the electron-electron coordinates.

Table 2.3: Normalized ground state wavefunction of helium in 34 term Hylleraas coordinate basis functions.

l	m	n	C_{lmn}	l	m	n	C_{lmn}
0	0	0	1.366082	0	2	1	5.589784×10^{-3}
0	0	1	1.930310×10^{-1}	1	2	0	-1.503759×10^{-2}
1	0	0	-2.229356×10^{-2}	0.5	0	3	1.650365×10^{-3}
0.5	0	1	-7.223280×10^{-2}	1.5	0	2	-5.209650×10^{-3}
1.5	0	0	2.613544×10^{-2}	2.5	0	1	4.694148×10^{-3}
0	0	2	-5.192320×10^{-2}	3.5	0	0	-8.534311×10^{-4}
1	0	1	9.232298×10^{-2}	0.5	2	1	-2.437572×10^{-3}
2	0	0	-1.310202×10^{-2}	1.5	2	0	4.131430×10^{-3}
0	2	0	3.618222×10^{-2}	0	0	4	1.633536×10^{-5}
0.5	0	2	4.399412×10^{-2}	1	0	3	-2.312225×10^{-4}
1.5	0	1	-6.150041×10^{-2}	2	0	2	4.972596×10^{-4}
2.5	0	0	9.868479×10^{-3}	3	0	1	-3.732132×10^{-4}
0.5	2	0	-2.464819×10^{-2}	4	0	0	6.725794×10^{-5}
0	0	3	3.499775×10^{-3}	0	2	2	-5.217095×10^{-5}
1	0	2	-2.134738×10^{-2}	1	2	1	3.622270×10^{-4}
2	0	1	2.383325×10^{-2}	2	2	0	-4.667672×10^{-4}
3	0	0	-4.134257×10^{-3}	0	4	0	-4.089245×10^{-6}

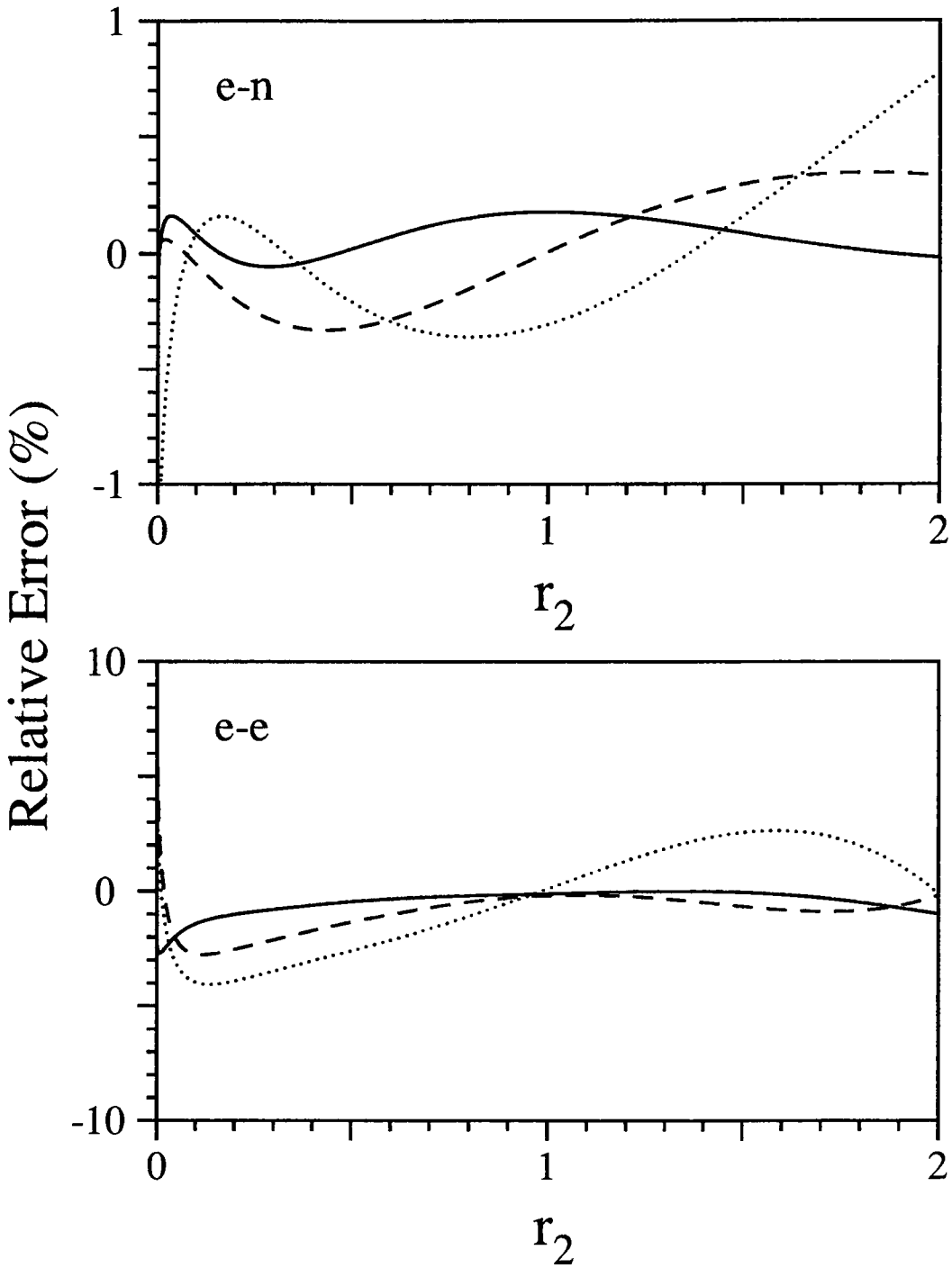

Figure 2.2: Relative errors in the Kato cusp conditions for the 25 (dotted curve), 34 (dash curve), and 55 (solid curve) term solutions of the ground state wavefunction: (e-n) one electron approaches the nucleus; and (e-e) two electrons coincide.

A contour plot of the ground state density in the 34 term solution of the Hylleraas coordinates

$$\rho(r_1, r_2) = \int \int |\psi_0(\mathbf{r_1}, \mathbf{r_2})|^2 r_1^2 d\Omega_1 r_2^2 d\Omega_2 \tag{2.44}$$

is shown in Fig. (2.3). The plot clearly indicates that the binding radius of the two electrons is about 0.7.

It is interesting to compare the correlated 34 term solution in the Hylleraas coordinates to the uncorrelated independent particle-model in Eq. (2.3). The contour plots of the effective state densities defined as

$$\rho_{eff}(r_1, r_2) = \frac{\rho(r_1, r_2)}{r_1^2 r_2^2} \tag{2.45}$$

for both cases are shown in Fig. (2.4). It is easy to see that in the Hylleraas coordinates the contour curves are pushed toward an asymmetric distribution of radial density, i. e. electron-electron repulsion favors a distribution with $r_1 < r_2$ (or $r_2 < r_1$) over the symmetric distribution $r_1 \approx r_2$. This property is consistent with the classical observation that the asymmetric orbit is much more stable than the Wannier orbit [49, 50]. The relative angles between the contour curves of the state density in Hylleraas coordinates and that of the independent-particle model are a quantitative reflection of the dynamic electron correlation.

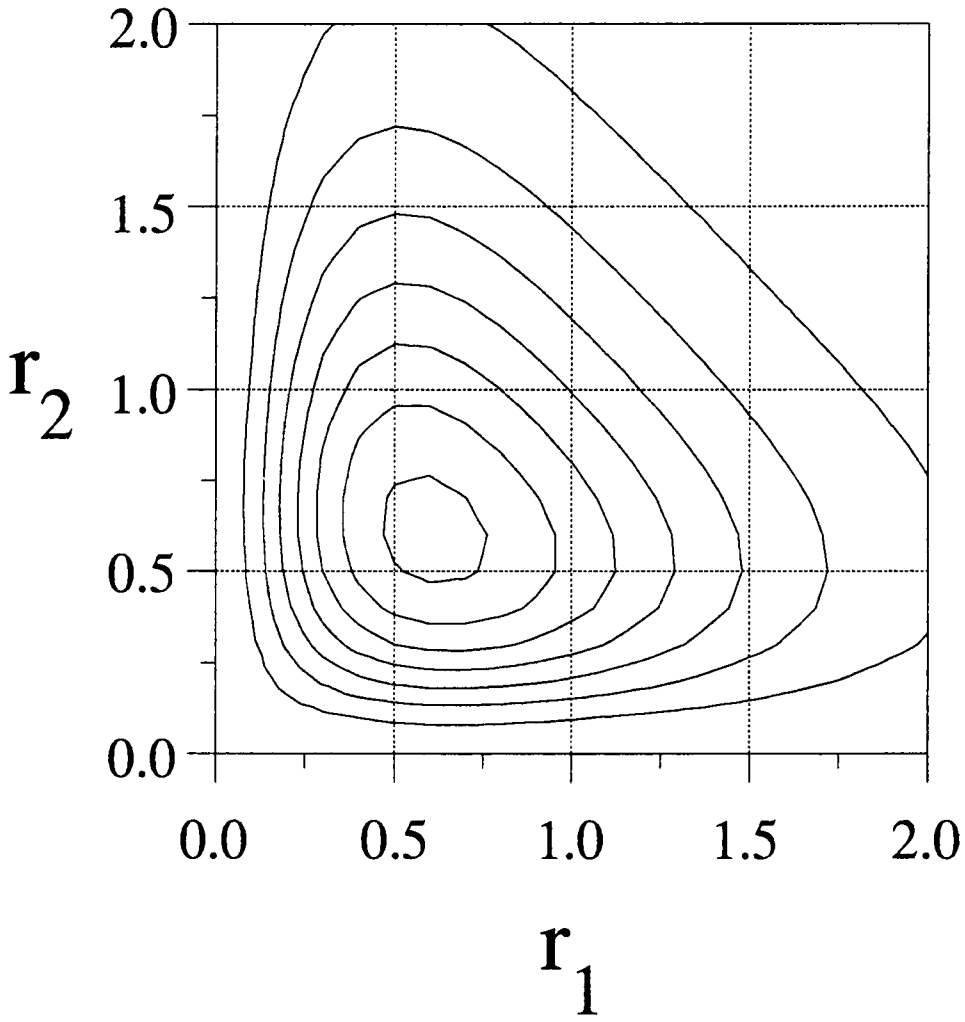

Figure 2.3: Contour plot of the ground state density $\rho(r_1, r_2)$ in the 34 term solution of the Hylleraas coordinates as a function of two electron radial coordinates. The value for each contour curve is n times 9.5×10^{-2} with n=1 for the outermost curve and n=7 for the innermost curve.

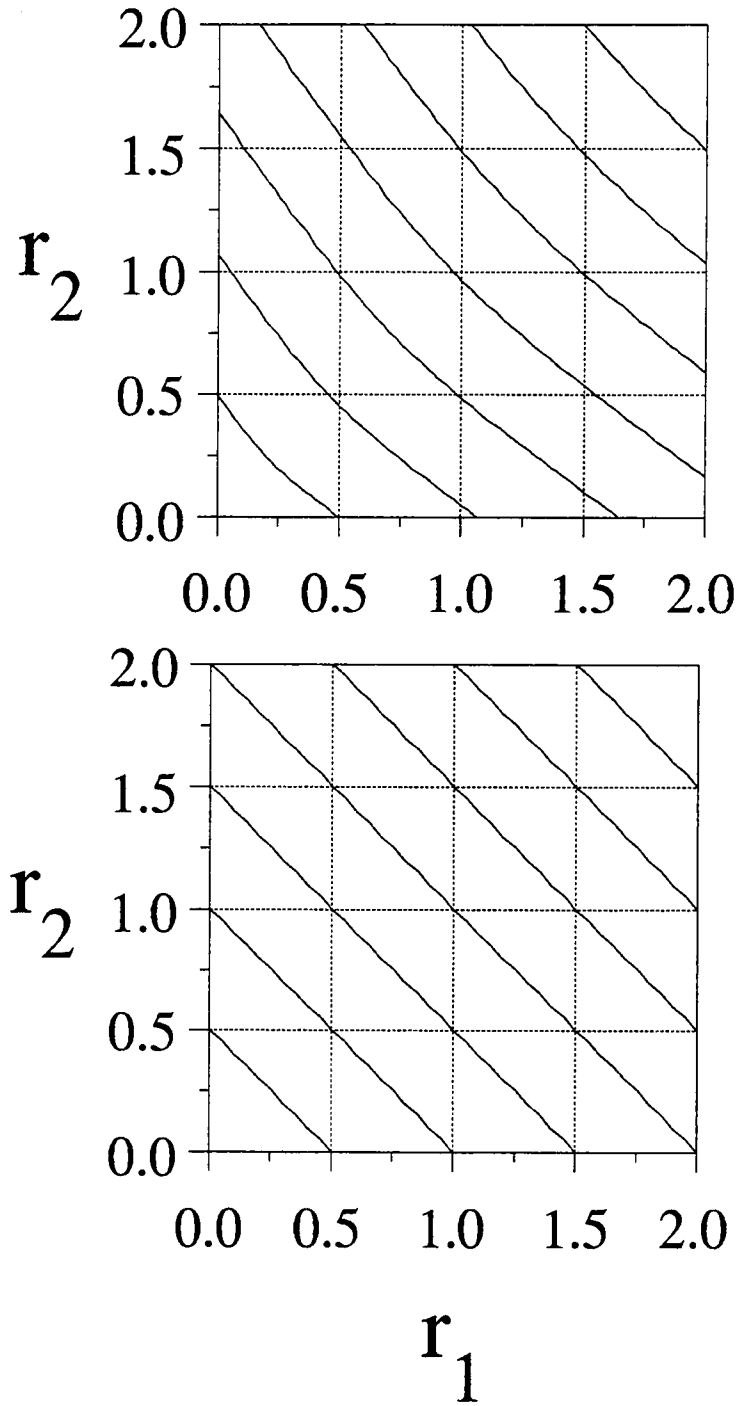

Figure 2.4: Contour plot of the effective ground state density $\rho_{eff}(r_1, r_2)$ for both the 34 term solution in the Hylleraas coordinates (upper figure) and the simple single-particle model (Eq. (2.3)) (lower panel).

Chapter 3

Final-state correlation

The study of the dynamic motion of two-continuum electrons in the field of a nucleus is one of the fundamental outstanding questions in atomic, molecular, and nuclear physics. The simple analytic form of the Coulomb potential and the small number of particles involved are in great contrast to the complexity of the process. The main difficulty arises from the infinite range of Coulomb forces which forbids free asymptotic states of charged particles. Hence, a double-continuum state remains a correlated one in the whole configuration space. This brings about fundamental as well as practical problems. Standard methods of scattering theory assume, in general, short-range forces, and therefore are not applicable to Coulomb systems. The evaluation of the transition amplitude in double photoionization requires knowledge of the double-continuum – whose exact form is unknown. Theoretical efforts have been therefore devoted to finding approximate expressions for this wavefunction. Several different forms of the double-continuum wavefunction applicable in different energy ranges and/or different configuration space have

been introduced [51, 52, 53, 54, 55, 56, 57, 58]. In this chapter, we briefly review various approximate wavefunctions available and discuss their properties and the scope of their validity. We emphasize in our study the 2C and 3C double-continuum wavefunctions, which will be used in the calculation of double photoionization.

3.1 $2C$ and $2SC$ wavefunctions

For an electron with momentum $\mathbf{k}$ in the field of a nucleus, the wavefunction ϕ_k satisfies the stationary Schrödinger equation

$$(-\frac{1}{2}\nabla^2 - \frac{Z}{r})\phi_k^{(-)}(\mathbf{r}) = E_1\phi_k^{(-)}(\mathbf{r}), \tag{3.1}$$

with the energy

$$E_1 = \frac{k^2}{2}.$$

There is an exact analytic solution of the equation, which is regular at the origin and fulfills asymptotic boundary conditions appropriate to the scattering problem. With the momentum normalization, the solution is [59, 60]

$$\phi_k^{(-)}(\mathbf{r}) = \frac{1}{(2\pi)^{3/2}}e^{-\eta\pi/2}\Gamma(1-i\eta)e^{i\mathbf{k}\cdot\mathbf{r}}\,{}_1F_1[i\eta, 1, -i(kr+\mathbf{k}\cdot\mathbf{r})], \tag{3.2}$$

where the Sommerfeld parameter is given by

$$\eta = -\frac{Z}{k}$$

and the sign "$(-)$" indicates that $\psi_k^{(-)}$ is an incoming wave. The solution of the one-electron system is the foundation of our further understanding of the many-electron systems.

For a two-electron atom or ion, the system is not separable. The traditional idea has been to break down the three-body system into two-body subsystems by ignoring the electron-electron interaction. The double-continuum state is therefore constructed as a product of the two Coulomb function (2C) resulting from the two hydrogenic subsystems

$$\psi_{2C}(\mathbf{r}_1, \mathbf{r}_2) = \frac{1}{\sqrt{2}} \left[\phi_{k_1}^{(-)}(\mathbf{r}_1) \phi_{k_2}^{(-)}(\mathbf{r}_2) + \mathbf{r}_1 \leftrightarrow \mathbf{r}_2 \right]. \tag{3.3}$$

Obviously, for high Z ($\gg 1$) atomic systems, this 2C wavefunction is a good approximate solution to the Schrödinger equation. In this case the electron-nucleus interaction dominates the three-body Coulomb potential and the electron-electron interaction is not important. For low Z systems such as He and H^-, however, the electron-electron interaction is comparable in strength to the electron-nucleus interaction and the approximation underlying the 2C wavefunction is not justified. If we make a Taylor series expansion at small distances r_1 and r_2, it is very easy to see that the $2C$ wavefunction satisfies exactly the first Kato cusp condition pertaining to the confluence of the electron-nucleus coordinates at the nucleus, however, because of its neglect of electron-electron correlation, it does not satisfy the second Kato cusp condition for the confluence of electron-electron coordinates at all.

Based on a similar idea of the possible approximate separability of the two-electron atomic system in the configuration space, Rudge and Seaton [52], Jetzke and Faisal [54], and Pan and Starace [61] have developed a practical approach to partially recover the electron-electron correlation. They have shown that the Hamiltonian H of the two-electron atomic system can

be expressed exactly as a sum of two single-electron Hamiltonians with two screened Coulomb potentials which satisfy the invariance under interchange of the two-electron coordinates

$$H = \sum_{i=1}^{2} \left[-\frac{1}{2}\nabla_i^2 + V_i \right], \tag{3.4}$$

where

$$V_i = \frac{S_i(\mathbf{r}_1, \mathbf{r}_2)}{r_i} \tag{3.5}$$

with the two-electron screening functions

$$S_i(\mathbf{r}_1, \mathbf{r}_2) = -Z + \sum_{j=1, j\neq i}^{2} \frac{\mathbf{r}_i \cdot \mathbf{r}_{ij} r_i}{r_{ij}^3}. \tag{3.6}$$

The ith screened Coulomb potential corresponds physically to the work done on the ith electron by the other electron and the nucleus. Moreover, asymptotically, in the two-electron break-up (ionization) channel, the velocities $\mathbf{k}_1$ and $\mathbf{k}_2$ must be related to their coordinates such that

$$\mathbf{r}_1 = \mathbf{k}_1 t$$

and

$$\mathbf{r}_2 = \mathbf{k}_2 t, \tag{3.7}$$

where t is the time. Therefore, the screening functions translate exactly into a *complete set* of two dynamic charges $Z_i(\mathbf{k}_1, \mathbf{k}_2)$ which depend only on the asymptotic velocities $\mathbf{k}_i$:

$$\begin{aligned} \lim_{\mathbf{r}_j \to \infty} S_i(\mathbf{r}_1, \mathbf{r}_2) &= Z_i(\mathbf{k}_1, \mathbf{k}_2) \\ &= -Z + \sum_{j=1, j\neq i}^{2} \frac{\mathbf{k}_i \cdot \mathbf{v}_{ij} k_i}{v_{ij}^3}, \end{aligned} \tag{3.8}$$

where

$$v_{ij} = |\mathbf{v}_{ij}| = |\mathbf{k}_i - \mathbf{k}_j|$$

and $i = 1, 2$. Noting that the summation of the two screened Coulomb potentials gives

$$\frac{S_1}{r_1} + \frac{S_2}{r_2} = -\frac{Z}{r_1} - \frac{Z}{r_2} + \frac{1}{r_{12}}, \tag{3.9}$$

the introduction of the effective charge Z_1 and Z_2 in place of the electron-electron interaction serves to keep the potential invariant in the asymptotic region of configuration space and the summation of the two Sommerfeld parameters are thus reduced to the well known Peterkop-Rudge-Seaton relation

$$-\frac{Z_1}{k_1} - \frac{Z_2}{k_2} = -\frac{Z}{k_1} - \frac{Z}{k_2} + \frac{1}{2k_{12}}, \tag{3.10}$$

where $\mathbf{k}_{12} = \mathbf{v}_{12}/2$. Following this, we obtain a remarkably simple result that in the asymptotic domain the two-electron system separates completely into a sum of two one-electron Coulomb Hamiltonians

$$H_{\lim_{r_1, r_2 \to \infty}} = \sum_{i=1}^{2} \left[-\frac{1}{2}\nabla_i^2 + \frac{Z_i(\mathbf{k}_1, \mathbf{k}_2)}{r_i} \right], \tag{3.11}$$

where the *complete set* of two dynamic charges, Z_i, is given by Eq. (3.8). A solution for Eq. (3.11), ψ_{2SC}, satisfying the ingoing-wave boundary condition is easily found to be the same in form as ψ_{2C} except that the nucleus charge in the one-electron Coulomb function Z is replaced by the effective charge $Z_i(\mathbf{k}_1, \mathbf{k}_2)$

$$\psi_{2SC}(\mathbf{r}_1, \mathbf{r}_2) = \psi_{2C}(\mathbf{r}_1, \mathbf{r}_2)|_{Z \to Z_i} \tag{3.12}$$

The wavefunction ψ_{2SC} with screened Coulomb charge is expected to be considerably simpler to use in practice because of the nature of separability in configuration space, however, its drawback is also obvious. From a fundamental point of view, the wavefunction does not satisfy the Kato cusp condition at the electron-electron collision point and is inconsistent with the asymptotic scattering solution at large interparticle distances, hereafter referred to as the Redmond boundary condition [62],

$$\lim_{r_1\to\infty, r_2\to\infty, r_{12}\to\infty} \psi(\mathbf{r}_1,\mathbf{r}_2) \propto e^{i\mathbf{k}_1\cdot\mathbf{r}_1 + i\mathbf{k}_2\cdot\mathbf{r}_2} e^{-i\eta_1 ln(k_1 r_1 - \mathbf{k}_1\cdot\mathbf{r}_1)} \times e^{-i\eta_2 ln(k_2 r_2 - \mathbf{k}_2\cdot\mathbf{r}_2)} e^{-i\eta_{12} ln(k_{12} r_{12} - \mathbf{k}_{12}\cdot\mathbf{r}_{12})}, \tag{3.13}$$

where the Sommerfeld parameter is

$$\eta_{12} = 1/(2k_{12}).$$

Furthermore, the range of validity is difficult to estimate. From a practical point of view the 2SC wavefunction is of limited value since the evaluation of ionization amplitudes involves integration over configuration space in domains outside the asymptotic region where the 2SC function is justified. For example, the reaction zones most important for such amplitudes at high energy are often confined to a small region around the origin where all particles are close together. Hence a proper description of the continuum state resulting from such a process requires wavefunctions whose range of validity extends beyond the asymptotic region.

3.2 $3C$ and $DS3C$ wavefunctions

In the $2C$ and $2SC$ approaches, the prominence is given to the electron-nucleus interactions and the electron-electron interaction is simply ignored or represented merely by dynamic screening due to the presence of a second electron. The six-dimensional wavefunction of the three-body continuum is expressed in the coordinates $\mathbf{r}_1$ and $\mathbf{r}_2$ of the two electrons with respect to the nucleus. No explicit dependence on the interelectron coordinate $\mathbf{r}_{12} = \mathbf{r}_1 - \mathbf{r}_2$ is included.

In the three Coulomb product (3C) approach, however, the full symmetry of the three two-body Coulomb interaction has been taken into account. In this case the three-body wavefunction is represented as a product of three two-body Coulomb wavefunctions, one for each pair of interacting particles. Each pair is considered to interact separately with a relative energy on the two-body energy shell and with electric charges unscreened by the presence of the third particle, i. e.,

$$\psi_{3C}(\mathbf{r}_1, \mathbf{r}_2) = \frac{1}{\sqrt{2}} \left[\phi^{(-)}_{\mathbf{k}_1}(\mathbf{r}_1) \phi^{(-)}_{\mathbf{k}_2}(\mathbf{r}_2) \mathrm{D}^{(-)}(\mathbf{k}_{12}, \mathbf{r}_{12}) + \mathbf{r}_1 \leftrightarrow \mathbf{r}_2 \right], \qquad (3.14)$$

where $\phi^{(-)}_{\mathbf{k}_1}(\mathbf{r}_1)$ and $\phi^{(-)}_{\mathbf{k}_2}(\mathbf{r}_2)$ are the incoming Coulomb waves of the two electrons, and $D^{(-)}(\mathbf{k}_{12}, \mathbf{r}_{12})$ is a distortion function to describe the electron-electron correlation,

$$D^{(-)}(\mathbf{k}_{12}, \mathbf{r}_{12}) = e^{-\pi\eta_{12}/2}\Gamma(1 - i\eta_{12})\, {}_1F_1[i\eta_{12}, 1, -i(k_{12}r_{12} + \mathbf{k}_{12}\mathbf{r}_{12})]. \quad (3.15)$$

The 3C wavefunction was initially introduced in the 1960s to study the excitation process in electron-hydrogen collisions [51] and in the 1980s to

investigate ionization and electron capture to the continuum in H^--H collisions [63]. In the late 1980s, the 3C wavefunction was discussed by Brauner, Briggs, and Klar and was extensively applied to the calculation of the triply-differential cross sections for ionization of the hydrogen atom by electron or positron impact [64].

Since in the asymptotic limit, the confluent hypergeometric function ${}_1F_1$ is reduced to an eikonal phase factor

$$ {}_1F_1[i\eta, 1, -i(kr + \mathbf{k}\cdot\mathbf{r})]|_{r\to\infty} = \frac{e^{\pi\eta/2}}{\Gamma(1-i\eta)} e^{-i\eta ln(kr+\mathbf{k}\cdot\mathbf{r})}, \tag{3.16} $$

the 3C wavefunction therefore satisfies the Redmond boundary condition (Eq. (3.13)) in the asymptotic region where the separation of all the Coulomb interacting particles tends to infinity. This property is of considerable importance from the viewpoint of the formal scattering theory, however, its practical value for the calculation of photoionization is quite limited since the dominant contributions to the photoionization process originate from small- to intermediate- interparticle distances. We therefore focus on the properties of the wavefunction in the *entire* coordinate space in the perturbative regime of small Sommerfeld parameters $Z/k_1 \gg 1$ where k_1 is the velocity of the fast electron. In the following we will show that the 3C wavefunction satisfies the Kato cusp conditions at the three two-body collision points and moreover, it appropriately describes the three-body final state correlation in the full coordinate space when the photon energy is high and the energy sharing between the two-electrons is asymmetric. The latter is the theoretical basis for application in double photoionization by high energy photons.

For the two-electron atomic system, assume the wavefunction in the fragmentation (double ionization) channel to have the form

$$\psi_f^{(-)}(\mathbf{r}_1,\mathbf{r}_2) = \frac{1}{\sqrt{2}}\left[\phi_{\mathbf{k}_1}^{(-)}(\mathbf{r}_1)\phi_{\mathbf{k}_2}^{(-)}(\mathbf{r}_2)\mathrm{B}^{(-)}(\mathbf{k}_{12},\mathbf{r}_{12}) + \mathbf{r}_1 \leftrightarrow \mathbf{r}_2\right], \tag{3.17}$$

where $\phi_{\mathbf{k}_1}^{(-)}(\mathbf{r}_1)$ and $\phi_{\mathbf{k}_2}^{(-)}(\mathbf{r}_2)$ are the incoming Coulomb waves of the two electrons, satisfying the single-electron Schödinger equations

$$\left(-\frac{1}{2}\nabla_i^2 - \frac{Z}{r_i}\right)\phi_{\mathbf{k}_i}^{(-)}(\mathbf{r}_i) = \frac{\mathrm{k}_i^2}{2}\phi_{\mathbf{k}_i}^{(-)}(\mathbf{r}_i) \tag{3.18}$$

with $i = 1,2$ and $B^{(-)}(\mathbf{k}_{12},\mathbf{r}_{12})$ is a function to be determined. With this ansatz and the total energy of the two electrons

$$E_{tot} = \frac{k_1^2}{2} + \frac{k_2^2}{2}, \tag{3.19}$$

the three-body Schrödinger equation for infinite nuclear mass becomes

$$\left(-\frac{1}{2}\nabla_1^2 - \frac{1}{2}\nabla_2^2 - \frac{Z}{r_1} - \frac{Z}{r_2} + \frac{1}{r_{12}}\right)\psi_f^{(-)}(\mathbf{r}_1,\mathbf{r}_2) = \mathrm{E}_{\mathrm{tot}}\psi_{\mathrm{f}}^{(-)}(\mathbf{r}_1,\mathbf{r}_2), \tag{3.20}$$

is reduced to

$$\left[-\frac{1}{2}\nabla_{\mathbf{r_{12}}}^2 + \frac{1}{2r_{12}} + (-i\mathbf{k}_{12} + \mathrm{ZM}_1 - \mathrm{ZM}_2)\cdot\nabla_{\mathbf{r_{12}}}\right] B^{(-)}(\mathbf{k}_{12},\mathbf{r}_{12}) = 0, \tag{3.21}$$

where $\mathbf{k}_{12}$ is the relative momentum (=velocity/2) and $\mathbf{M}_i$ is defined as the derivative of the logarithm of the two ${}_1F_1$ functions in $\phi_{\mathbf{k}_1}^{(-)}$ and $\phi_{\mathbf{k}_2}^{(-)}$, i. e.,

$$\mathbf{M}_i \equiv \frac{(\hat{r}_i + \hat{k}_i)}{2}\frac{{}_1F_1[1 + i\eta_i, 2, -i(k_i r_i + \mathbf{k}_i\cdot\mathbf{r}_i)]}{{}_1\mathrm{F}_1[\mathrm{i}\eta_\mathrm{i}, 1, -\mathrm{i}(\mathrm{k_i r_i} + \mathbf{k}_\mathrm{i}\cdot\mathbf{r}_\mathrm{i})]}. \tag{3.22}$$

Here $\eta_i = -Z/k_i$ with $i = 1,2$. The important observation is that $\mathbf{M}_i$ are bounded in the full configuration space (see Fig. 3.1), i. e.,

$$|\mathbf{M}_i| \lesssim 2$$

for *all* r_i and *all* angles $\theta_i = \cos^{-1}(\hat{k}_i \cdot \hat{r}_i)$. Fig. 3.1 displays the radial and angular dependence of M_i for typical values of k_i representing a fast electron (i=1) and a slow electron (i=2) in the double continua of helium at $E = 2$ keV. At high energies, the typical relative momentum between the fast and the slow electrons satisfies

$$k_{12} \gg Z. \tag{3.23}$$

Therefore, Eq. (3.21) can be simplified to

$$\left(-\frac{1}{2}\nabla^2_{\mathbf{r_{12}}} + \frac{1}{2r_{12}} - i\mathbf{k}_{12} \cdot \nabla_{\mathbf{r_{12}}}\right) B^{(-)}(\mathbf{k}_{12}, \mathbf{r}_{12}) = 0. \tag{3.24}$$

The solution of this equation is nothing but the distortion factor to a plane wave due to the electron-electron interaction,

$$B^{(-)}(\mathbf{k}_{12}, \mathbf{r}_{12}) = \mathrm{D}^{(-)}(\mathbf{k}_{12}, \mathbf{r}_{12}). \tag{3.25}$$

Consequently, $\psi_f^{(-)}(\mathbf{r}_1, \mathbf{r}_2)$ in Eq. (3.17) becomes identical to the 3C wavefunction (Eq. (3.14)). Taking into account that the energy distribution in the double photoionization is extremely asymmetric at high energies, the condition of Eq. (3.23) is then reduced to

$$E \gg Z^2. \tag{3.26}$$

The 3C function is therefore the appropriate three-body final state wavefunction in the *full* coordinate space provided that the photon energy is high and the energy sharing is asymmetric.

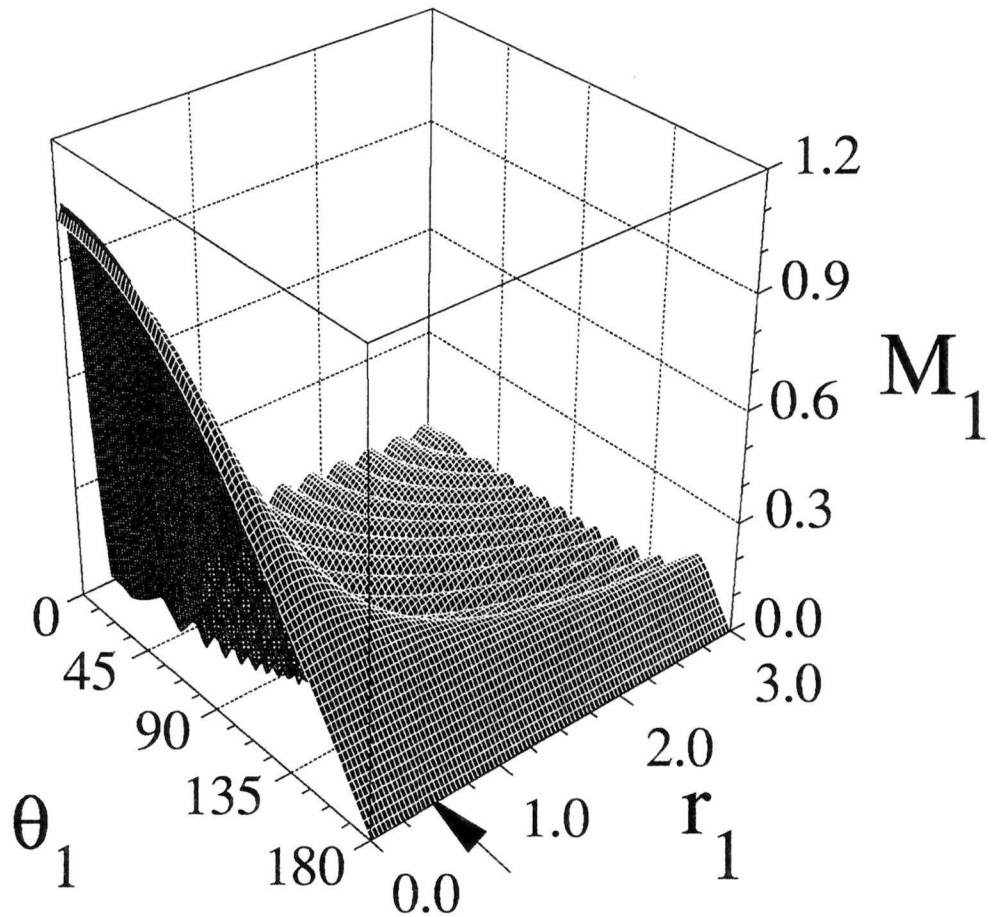

Figure 3.1: Behavior of $|\mathrm{M}_i(r_i, \theta_i)|$ as a function of radial r_i and angular θ_i coordinates in the double continua of helium at $E_{tot} = 2$ keV with an asymmetric energy distribution: fast electron $E_1 = 1950$ eV (M_1) and slow electron $E_2 = 50$ eV (M_2). Arrow indicates dominant region for the dipole matrix element.

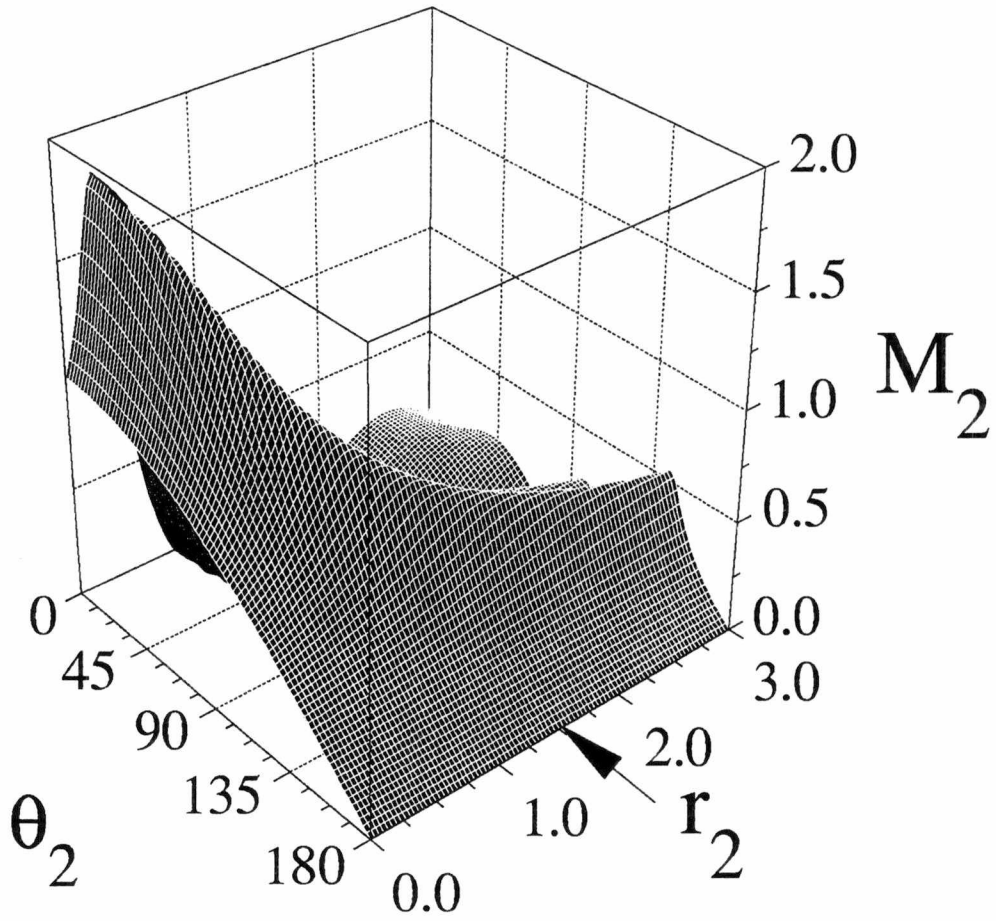

Fig. (3.1) continued.

At small interparticle distances, the 3C wavefunction can be expanded in a Taylor series

$$\begin{aligned}\psi_{3C}(\mathbf{r}_1,\mathbf{r}_2) \propto [\ & 1+\eta_1(k_1 r_1+\mathbf{k}_1\cdot\mathbf{r}_1)\\ & +1+\eta_2(k_2 r_2+\mathbf{k}_2\cdot\mathbf{r}_2)\\ & +1+\eta_{12}(k_{12} r_{12}+\mathbf{k}_{12}\cdot\mathbf{r}_{12})+...]\\ = \Big[\ & 1-Z(r_1+\hat{\mathbf{k}}_1\cdot\mathbf{r}_1)\\ & +1-Z(r_2+\hat{\mathbf{k}}_2\cdot\mathbf{r}_2)\\ & +1+\frac{1}{2}(r_{12}+\hat{\mathbf{k}}_{12}\cdot\mathbf{r}_{12})+...\Big], \end{aligned} \tag{3.27}$$

where $\hat{\mathbf{k}}_i$ is the unit vector of the momentum and i refers to 1, 2 and 12. Because the average of $\hat{\mathbf{k}}_i\cdot\mathbf{r}_i$ on a constant sphere vanishes, i. e.,

$$\langle\hat{\mathbf{k}}_1\cdot\mathbf{r}_1\rangle=\langle\hat{\mathbf{k}}_2\cdot\mathbf{r}_2\rangle=\langle\hat{\mathbf{k}}_{12}\cdot\mathbf{r}_{12}\rangle=0, \tag{3.28}$$

the 3C wavefunction thus satisfies the Kato cusp conditions at the three two-body collision points exactly. This is crucial for the photoionization shake-off process since it is governed by the behavior of the wavefunctions at small interparticle distances. So we conclude that the 3C wavefunction appropriately describes the final state correlation to the order of Z/k_1 and is expected, together with an accurate initial state wavefunction, to provide an effective calculation for the double photoionization in the high energy range.

In the low energy range, however, the validity of the 3C wavefunction is not justified. In fact, when the 3C wavefunction is applied to the calculation of the total cross section in double photoionization [26] and to the description of the angular distributions of ionized electrons for electron impact and

photoionization [64, 65], it suffers from several deficiencies. The most serious of these concerns the absolute value of the cross sections obtained for low total energy of the continuum electrons. In this case the absolute values are much too low. The reason can be traced to the appearance of the two-body normalization factor in the 3C wavefunction. The normalization factor corresponding to repulsive electron-electron interaction goes exponentially to zero as the total energy of the two electrons goes to zero. This exponential decrease causes the magnitude of the cross section also to decrease exponentially, a behavior which is at variance with the Wanier threshold law and with experiment. To correct the deficiency Berakdar and Briggs [66] applied an approach similar to that of Rudge and Seaton [52] and Peterkop [53] by introducing effective Sommerfeld parameters in the two-body factors of the 3C wavefunction. The new Sommerfeld parameters, η_1', η_2', and η_{12}', are a linear function of the original three Sommerfeld parameters, η_1, η_2, and η_{12},

$$\eta_i' = \sum_j A_{ij}\eta_j, \tag{3.29}$$

where $i = 1$, 2 and 12, and the nine coefficients A_{ij} are introduced corresponding to the modification of a particular two-body Coulomb interaction by the presence of the third particle. The determination of the coefficients is based on the Peterkop-Rudge-Seaton relation

$$\eta_1' + \eta_2' + \eta_{12}' = \eta_1 + \eta_2 + \eta_{12} \tag{3.30}$$

and the consideration of the simple collinear configuration for which the

nucleus lies in the middle of the two electrons and the potential

$$\begin{aligned} V &= -\frac{Z}{r_1} - \frac{Z}{r_2} + \frac{1}{r_{12}} \\ &= -\frac{Z-\frac{1}{4}}{r_1} - \frac{Z-\frac{1}{4}}{r_2}, \end{aligned} \tag{3.31}$$

i. e., the electron-electron interaction is subsumed completely by an effective electron-nucleus interaction with an effective nucleus charge of $Z-1/4$. There are still an infinite number of ways of choosing the three new Sommerfeld parameters. They found with the choice of

$$\eta_1' = -\frac{4Z - sin\theta}{4k_1},$$
$$\eta_2' = -\frac{4Z - sin\theta}{4k_2},$$

and

$$\eta_{12}' = \frac{1 - sin^2\theta}{2k_{12}} \tag{3.32}$$

with $\theta = cos^{-1}(\hat{\mathbf{k}}_1 \cdot \hat{\mathbf{k}}_2)/2$, the triply-differential cross section for ionization of helium by electron-impact is in good agreement with the *absolute* experiment data when the outgoing electrons share energy equally. However, no results for the total cross section and for the differential cross section with asymmetric energy sharing were reported. The 3C wavefunction with "dynamic screening" represented by the Sommerfeld parameters is designated DS3C.

We have just mentioned the collinear configuration for which the nucleus is between the two electrons and the electron-electron interaction is subsumed completely by an effective electron-nucleus interaction, i. e.,

$$V = -\frac{Z_1}{r_1} - \frac{Z_2}{r_2} \tag{3.33}$$

with

$$Z_1 = Z - \frac{1}{4} \text{ and } Z_2 = Z - \frac{1}{4}. \tag{3.34}$$

In the asymptotic region $r_1 \gg r_2$ or $r_2 \gg r_1$, the electron-electron interaction in completely decoupled. The potential of the two electron system is reduced to the summation of the two hydrogenic ones (Eq. (3.33)) and

$$\lim_{r_1 \gg r_2} Z_1 = Z - 1, \; Z_2 = Z, \tag{3.35}$$

$$\lim_{r_2 \gg r_1} Z_1 = Z, \qquad Z_2 = Z - 1. \tag{3.36}$$

Based on the Eqs. (3.33-3.36), different forms of DS3C wavefunction were introduced [67, 56, 55] with the "dynamic screening" represented by the three new Sommerfeld parameters which are functions of variables in configuration space. Except in the asymptotic regions and in the collinear configuration, the validity of the various forms of the DS3C wavefunction is unknown. In addition, it is extremely difficult to calculate the total cross section of double photoionization, which we are interested in, with the DS3C wavefunction including the relative momentum and/or the coordinates in the Sommerfeld parameters, we skip further discussion of the properties of the DS3C wavefunctions.

Chapter 4

Double photoionization of helium with 2C wavefunction as the approximate final-state wavefunction

In this chapter, we will study the double and single photoionization of helium and their ratio by using the correlated 34-term ground-state wavefunction in the representation of Hylleraas coordinates and the uncorrelated 2C final-state wavefunction. Detailed calculations are performed in acceleration, velocity, and length gauges and the results are displayed and compared with the experiment data. The limitations of the present work are discussed.

4.1 Double photoionization of helium

The main task now is to evaluate the dipole matrix elements in Eqs. (1.5-1.8) with the ground-state wavefunction (Eq. (2.37)) and the 2C final-state wavefunction (Eq. (3.3).) Let us first simplify the calculations by taking into

account the symmetry of the dipole operator and the initial- and final-state wavefunctions. For the dipole matrix element

$$T = \langle \psi_f(\mathbf{r}_1, \mathbf{r}_2) | d(\mathbf{r}_1, \mathbf{r}_2) | \psi_0(\mathbf{r}_1, \mathbf{r}_2) \rangle,$$

where the initial-state wavefunction $\psi_0(\mathbf{r}_1, \mathbf{r}_2)$, the final-state wavefunction $\psi_f(\mathbf{r}_1, \mathbf{r}_2)$, and the dipole operator $d(\mathbf{r}_1, \mathbf{r}_2)$ in three gauges are satisfying the exchange symmetry, i. e.,

$$\psi_0(\mathbf{r}_1, \mathbf{r}_2) = \psi_0(\mathbf{r}_2, \mathbf{r}_1),$$

$$d(\mathbf{r}_1, \mathbf{r}_2) = d(\mathbf{r}_2, \mathbf{r}_1),$$

and

$$\psi_f(\mathbf{r}_1, \mathbf{r}_2) = \frac{1}{\sqrt{2}} \left[\phi_f(\mathbf{r}_1, \mathbf{r}_2) + \phi_f(\mathbf{r}_2, \mathbf{r}_1) \right].$$

The matrix element

$$\begin{aligned} T &= \frac{1}{\sqrt{2}} [\langle \phi_f(\mathbf{r}_1, \mathbf{r}_2) | d(\mathbf{r}_1, \mathbf{r}_2) | \psi_0(\mathbf{r}_1, \mathbf{r}_2) \rangle + \langle \phi_f(\mathbf{r}_2, \mathbf{r}_1) | d(\mathbf{r}_1, \mathbf{r}_2) | \psi_0(\mathbf{r}_1, \mathbf{r}_2) \rangle] \\ &= \frac{1}{\sqrt{2}} [\langle \phi_f(\mathbf{r}_1, \mathbf{r}_2) | d(\mathbf{r}_1, \mathbf{r}_2) | \psi_0(\mathbf{r}_1, \mathbf{r}_2) \rangle + \langle \phi_f(\mathbf{r}_1, \mathbf{r}_2) | d(\mathbf{r}_2, \mathbf{r}_1) | \psi_0(\mathbf{r}_2, \mathbf{r}_1) \rangle] \\ &= \sqrt{2} \langle \phi_f(\mathbf{r}_1, \mathbf{r}_2) | d(\mathbf{r}_1, \mathbf{r}_2) | \psi_0(\mathbf{r}_1, \mathbf{r}_2) \rangle. \end{aligned} \tag{4.1}$$

So the dipole matrix element between the symmetrized initial- and final-state wavefunctions is identical to that between the symmetrized initial-state wavefunction and the unsymmetrized final-state wavefunction multiplied by a factor of $\sqrt{2}$. The argument is valid for all three gauges and also for single photoionization, which will be discussed in the next section.

4.1.1 Partial wave analysis

We now perform the evaluation of the matrix element in Eq. (4.1) by a partial wave analysis. The unsymmetrized final-state wavefunction is now a product of two Coulomb wavefunctions

$$\phi_f(\mathbf{r}_1,\mathbf{r}_2) \equiv \phi_{2C}(\mathbf{r}_1,\mathbf{r}_2) = \phi^{(-)}_{\mathbf{k}_1}(\mathbf{r}_1)\phi^{(-)}_{\mathbf{k}_2}(\mathbf{r}_2), \tag{4.2}$$

where the Coulomb waves $\phi^{(-)}_{\mathbf{k}_i}(\mathbf{r}_i)$ (i=1,2), which are the exact solutions of the hydrogenic system with central charge Z, can be expanded in terms of partial waves $\varphi^Z_{k_i lm}(\mathbf{r}_i)$ with well defined quantum numbers l and m. The spherical Coulomb waves have the form

$$\varphi^Z_{k_i lm}(\mathbf{r}_i) = R^Z_{k_i l}(r_i)Y_{lm}(\hat{\mathbf{r}}_i), \quad (i=1,2) \tag{4.3}$$

with

$$R^Z_{k_i l}(r_i) = \frac{1}{r}\left[\frac{2}{\pi k_i}\right]^{1/2} \frac{2^l e^{-\pi\eta_i/2}|\Gamma(1+l-i\eta_i)|}{\Gamma(2l+2)} \rho_i^{l+1} e^{-i\rho_i} \cdot {}_1F_1[1+l-i\eta_i, 2l+2, 2i\rho_i] \tag{4.4}$$

and

$$\rho_i = k_i r_i, \quad \eta_i = -Z/k_i.$$

Note that the spherical Coulomb waves are energy normalized according to

$$\langle\varphi^Z_{k_i lm}(\mathbf{r}_i)|\varphi^Z_{k'_i l'm'}(\mathbf{r}_i)\rangle = \delta(E_i - E'_i)\delta_{ll'}\delta_{mm'}$$

with

$$E_i = \frac{k_i^2}{2},$$

when the central charge Z is the same for both wavefunctions. The expansion of the one-electron Coulomb wave in terms of spherical wave reads

$$\phi_{\mathbf{k}_i}(\mathbf{r}_i) = \sum_{l=0}^{\infty} \sum_{m=-l}^{l} i^l e^{i\sigma_l(\eta_i)} Y^*_{lm}(\hat{\mathbf{k}}_i) \varphi^Z_{k_i lm}(\mathbf{r}_i), \tag{4.5}$$

where the Coulomb phase shift is given by

$$\sigma_l(\eta_i) = arg\Gamma(1 + l - i\eta_i).$$

Replacing the one-electron orbits appearing in Eq. (4.2) by Eq. (4.5) leads to

$$\begin{aligned}\phi_{2C}(\mathbf{r}_1, \mathbf{r}_2) = \sum_{l_1 m_1} \sum_{l_2 m_2} & i^{l_1+l_2} e^{i[\sigma_{l_1}(\eta_1)+\sigma_{l_2}(\eta_2)]} Y^*_{l_1 m_1}(\hat{\mathbf{k}}_1) Y^*_{l_2 m_2}(\hat{\mathbf{k}}_2) \\ & \cdot R^Z_{k_1 l_1}(r_1) R^Z_{k_2 l_2}(r_2) Y_{l_1 m_1}(\hat{\mathbf{r}}_1) Y_{l_2 m_2}(\hat{\mathbf{r}}_2).\end{aligned} \tag{4.6}$$

Because the total angular momentum L^2 and its z component L_z are conserved, it is customary to introduce the bipolar harmonics $y^{l_1 l_2}_{LM}(\hat{\mathbf{r}}_1, \hat{\mathbf{r}}_2)$, the eigenstates of L^2 and L_z

$$Y_{l_1 m_1}(\hat{r}_1) Y_{l_2 m_2}(\hat{r}_2) = \sum_{LM} y^{l_1 l_2}_{LM}(\hat{\mathbf{r}}_1, \hat{\mathbf{r}}_2) \langle LM | l_1 m_1 l_2 m_2 \rangle, \tag{4.7}$$

where $\langle LM | l_1 m_1 l_2 m_2 \rangle$ denotes the Clebsch-Gordan coefficients. We therefore have

$$\begin{aligned}\phi_{2C}(\mathbf{r}_1, \mathbf{r}_2) = \sum_{l_1 m_1} \sum_{l_2 m_2} & i^{l_1+l_2} e^{i[\sigma_{l_1}(\eta_1)+\sigma_{l_2}(\eta_2)]} Y^*_{l_1 m_1}(\hat{\mathbf{k}}_1) Y^*_{l_2 m_2}(\hat{\mathbf{k}}_2) \\ & \cdot \sum_{LM} R^Z_{k_1 l_1}(r_1) R^Z_{k_2 l_2}(r_2) \langle LM | l_1 m_1 l_2 m_2 \rangle y^{l_1 l_2}_{LM}(\hat{\mathbf{r}}_1, \hat{\mathbf{r}}_2).\end{aligned} \tag{4.8}$$

The form of the final-state wavefunction is now very convenient for proceeding further in the evaluation of the dipole matrix elements: since the

ground state is spherically symmetric, the dipole operator selects only the P_0 part (L=1, M=0) in the infinite expansion over L and M. Moreover, the selection rules for the Clebsch-Gordan coefficients $\langle LM|l_1m_1l_2m_2\rangle$ suppress all the bipolar harmonics except those of the form y_{10}^{ll+1} and y_{10}^{l+1l}. As a consequence, the P_0 part of $\phi_{2C}(\mathbf{r}_1,\mathbf{r}_2)$ which is relevant for DPI is given by

$$\phi_{2C}(\mathbf{r}_1,\mathbf{r}_2) = \sum_{l_1m_1}\sum_{l_2m_2} i^{l_1+l_2}e^{i[\sigma_{l_1}(\eta_1)+\sigma_{l_2}(\eta_2)]}Y^*_{l_1m_1}(\hat{\mathbf{k}}_1)Y^*_{l_2m_2}(\hat{\mathbf{k}}_2)$$
$$\cdot\langle 10|l_1m_1l_2m_2\rangle\delta_{l_1,l_2\pm1}\delta_{m_1+m_2,0}\Phi^{ZZ}_{k_1l_1k_2l_2}(\mathbf{r}_1,\mathbf{r}_2), \qquad (4.9)$$

where

$$\Phi^{ZZ}_{k_1l_1k_2l_2}(\mathbf{r}_1,\mathbf{r}_2) = y_{10}^{l_1l_2}(\hat{\mathbf{r}}_1,\hat{\mathbf{r}}_2)R^Z_{k_1l_1}(r_1)R^Z_{k_2l_2}(r_2).$$

Inserting now the relevant part of the final-state wavefunction (Eq. (4.9)) into the dipole matrix elements T in Eq. (4.1) and integrating over the four angles $\hat{\mathbf{k}}_1$ and $\hat{\mathbf{k}}_2$ in the six-fold differential equations, which are proportional to $|T|^2$, leads to the formulae for the energy distribution of the cross sections

$$\frac{d\sigma_a^{++}}{dE_2} = \frac{4\pi^2Z^2}{cE^3}\sum_{l_1}\sum_{l_2=l_1\pm1}\left|\langle\Phi^{ZZ}_{k_1l_1k_2l_2}(\mathbf{r}_1,\mathbf{r}_2)|\frac{z_1}{r_1^3}+\frac{z_2}{r_2^3}|\psi_0(\mathbf{r}_1,\mathbf{r}_2)\rangle\right|^2, \qquad (4.10)$$

$$\frac{d\sigma_v^{++}}{dE_2} = \frac{4\pi^2}{cE}\sum_{l_1}\sum_{l_2=l_1\pm1}\left|\langle\Phi^{ZZ}_{k_1l_1k_2l_2}(\mathbf{r}_1,\mathbf{r}_2)|\frac{\partial}{\partial z_1}+\frac{\partial}{\partial z_2}|\psi_0(\mathbf{r}_1,\mathbf{r}_2)\rangle\right|^2, \qquad (4.11)$$

and

$$\frac{d\sigma_l^{++}}{dE_2} = \frac{4\pi^2E}{c}\sum_{l_1}\sum_{l_2=l_1\pm1}\left|\langle\Phi^{ZZ}_{k_1l_1k_2l_2}(\mathbf{r}_1,\mathbf{r}_2)|z_1+z_2|\psi_0(\mathbf{r}_1,\mathbf{r}_2)\rangle\right|^2. \qquad (4.12)$$

Noting that the energy is conserved, the total energy shared by the two photoelectrons satisfies

$$E_1 + E_2 \equiv E_{tot} = E + E_0. \tag{4.13}$$

The probability that the first electron has energy E_1 and the second electron has energy E_2 is

$$\frac{d\sigma^{++}}{dE_2}(E_1, E_2) \propto \sum_{l_1 l_2} \left| \langle y_{10}^{l_1 l_2}(\hat{\mathbf{r}}_1, \hat{\mathbf{r}}_2) R^Z_{k_1 l_1}(r_1) R^Z_{k_2 l_2}(r_2) | d(\mathbf{r}_1, \mathbf{r}_2) | \psi_0(\mathbf{r}_1, \mathbf{r}_2) \rangle \right|^2 \tag{4.14}$$

with

$$y_{10}^{l_1 l_2}(\hat{\mathbf{r}}_1, \hat{\mathbf{r}}_2) = \sum_{m_1 m_2} Y_{l_1 m_1}(\hat{\mathbf{r}}_1) Y_{l_2 m_2}(\hat{\mathbf{r}}_2) \langle l_1 m_1 l_2 m_2 | 10 \rangle. \tag{4.15}$$

The energy distribution in the three gauges when the first electron has energy E_2 and the second electron has energy E_1 is

$$\begin{aligned}
\frac{d\sigma^{++}}{dE_2}(E_2, E_1) &\propto \sum_{l_1 l_2} \left| \langle y_{10}^{l_1 l_2}(\hat{\mathbf{r}}_1, \hat{\mathbf{r}}_2) R^Z_{k_2 l_1}(r_1) R^Z_{k_1 l_2}(r_2) | d(\mathbf{r}_1, \mathbf{r}_2) | \psi_0(\mathbf{r}_1, \mathbf{r}_2) \rangle \right|^2 \\
&= \sum_{l_2 l_1} \left| \langle y_{10}^{l_2 l_1}(\hat{\mathbf{r}}_2, \hat{\mathbf{r}}_1) R^Z_{k_2 l_2}(r_2) R^Z_{k_1 l_1}(r_1) | d(\mathbf{r}_2, \mathbf{r}_1) | \psi_0(\mathbf{r}_2, \mathbf{r}_1) \rangle \right|^2 \\
&= \sum_{l_1 l_2} \left| \langle y_{10}^{l_1 l_2}(\hat{\mathbf{r}}_1, \hat{\mathbf{r}}_2) R^Z_{k_1 l_1}(r_1) R^Z_{k_2 l_2}(r_2) | d(\mathbf{r}_1, \mathbf{r}_2) | \psi_0(\mathbf{r}_1, \mathbf{r}_2) \rangle \right|^2 \\
&= \frac{d\sigma^{++}}{dE_2}(E_1, E_2),
\end{aligned} \tag{4.16}$$

which is identical to the case when the first electron has energy E_1 and the second electron has energy E_2. So the energy distribution has U shape symmetry along the axis $E_2 = E_1 = E_{tot}/2$. Obviously, this exchange symmetry is the direct requirement of the Pauli principle in the Hilbert space.

Since the ground state wavefunction in the representation of Hylleraas coordinates can also be expanded in partial wave form

$$\psi_0(\mathbf{r}_1,\mathbf{r}_2)=\sum_l \phi_l^0(r_1,r_2)P_l(cos\theta_{12}), \tag{4.17}$$

the evaluation of the matrix elements in Eqs. (4.10,4.11,4.12) can be carried out easily. For the acceleration gauge

$$\langle\Phi^{ZZ}_{k_1l_1k_2l_2}(\mathbf{r}_1,\mathbf{r}_2)|\frac{z_1}{r_1^3}+\frac{z_2}{r_2^3}|\psi_0(\mathbf{r}_1,\mathbf{r}_2)\rangle$$

$$=-4\pi\sqrt{\frac{2(2l_1+1)(2l_2+1)}{3}}\begin{pmatrix}1 & l_1 & l_2\\ 0 & 0 & 0\end{pmatrix}$$
$$\cdot\int dr_1 R^Z_{k_1l_1}(r_1)\int dr_2 R^Z_{k_2l_2}(r_2)\left[\frac{r_2^2\phi^0_{l_2}(r_1,r_2)}{2l_2+1}+\frac{r_1^2\phi^0_{l_1}(r_2,r_1)}{2l_1+1}\right]. \tag{4.18}$$

For the length gauge

$$\langle\Phi^{ZZ}_{k_1l_1k_2l_2}(\mathbf{r}_1,\mathbf{r}_2)|z_1+z_2|\psi_0(\mathbf{r}_1,\mathbf{r}_2)\rangle$$

$$=-4\pi\sqrt{\frac{2(2l_1+1)(2l_2+1)}{3}}\begin{pmatrix}1 & l_1 & l_2\\ 0 & 0 & 0\end{pmatrix}$$
$$\cdot\int dr_1 r_1^2 R^Z_{k_1l_1}(r_1)\int dr_2 r_2^2 R^Z_{k_2l_2}(r_2)\left[\frac{r_1\phi^0_{l_2}(r_1,r_2)}{2l_2+1}+\frac{r_2\phi^0_{l_1}(r_2,r_1)}{2l_1+1}\right]. \tag{4.19}$$

For the velocity gauge

$$\langle\Phi^{ZZ}_{k_1l_1k_2l_2}(\mathbf{r}_1,\mathbf{r}_2)|\frac{\partial}{\partial z_1}+\frac{\partial}{\partial z_2}|\psi_0(\mathbf{r}_1,\mathbf{r}_2)\rangle$$

$$= -4\pi\sqrt{\frac{2(2l_1+1)(2l_2+1)}{3}}\begin{pmatrix} 1 & l_1 & l_2 \\ 0 & 0 & 0 \end{pmatrix}$$
$$\cdot \int dr_1 r_1^2 R^Z_{k_1 l_1}(r_1) \int dr_2 r_2^2 R^Z_{k_2 l_2}(r_2) \left[\frac{\phi^v_{l_2}(r_1,r_2)}{2l_2+1} + \frac{\phi^v_{l_1}(r_2,r_1)}{2l_1+1}\right], \tag{4.20}$$

where

$$\phi^v_{l'}(r_1,r_2) = \sum_{lmn} C_{lmn} e^{-\sigma(r_1+r_2)/2} \sigma^{l+m+n}$$
$$\cdot \left\{-\frac{\sigma}{2}(r_1+r_2)^l (r_2-r_1)^m + l(r_1+r_2)^{l-1}(r_2-r_1)^m \right.$$
$$\left. -m(r_1+r_2)^l (r_2-r_1)^{m-1} \right\} R^0_{nl'}(r_1,r_2) \tag{4.21}$$

and $R^0_{nl'}(r_1,r_2)$ is the partial wave expansion coefficients of r_{12}^n, i. e.,

$$r_{12}^n = \sum_{l'} R^0_{nl'}(r_1,r_2) P_{l'}(cos\theta_{12}). \tag{4.22}$$

Integrating over the energy E_2 in Eqs. (4.10,4.11,4.12) leads to the total cross sections

$$\sigma^{++} = \int_0^{E_{tot}/2} \frac{d\sigma}{dE_2} dE_2. \tag{4.23}$$

4.1.2 Results and discussion

A formalism similar to the one given in the last subsection was first applied to the calculation of the total cross sections for the double photoionization of helium by Byron and Joachain (BJ) [30]. BJ obtained a "Hylleraas type" ground-state wavefunction with three "relative partial waves" corresponding to the ss, pp, and dd couplings of the electrons. Their 45-parameter wavefunction gives a binding energy of 2.9020, which indicates that 96.9% of the

correlation energy is accounted for. However, possibly because of the limitation of the computing facilities at that time, BJ truncated the dd part of the ground-state wavefunction in their evaluation. BJ obtained the total cross sections for double ionization in the velocity and length forms. The results of both gauges differ sharply, for example, the ratio at the peak position $\sigma_l^{++}/\sigma_v^{++} \approx 1.8$, although theoretically the calculations are equivalent if both ψ_0 and ψ_f are exact solutions of the Schrödinger equation.

The same formalism was revisited by Rouzo and Cappello (RC) [11] for the analysis of the photoelectrons with respect to energies and angles and for the calculation of total cross sections. Using a multi-configuration self-consistent field (MCSCF) type ground-state wavefunction with four "relative partial waves" corresponding to the ss, pp, dd, and ff couplings, RC obtained a ground state with binding energy of 2.90289 for which about 98% of the correlation energy is taken into account. Implementing the calculation fully with the ground-state wavefunction, RC arrived at their total cross sections in both velocity and length forms. They found the dd wave contributes to the ground state wavefunction with only a small weighting ($\leq 0.02\%$), however, it contributes to the correlation energy much more significantly (up to 5%). Moreover, the dd wave enhances the total cross section in the length form significantly while it reduces the cross section in the velocity gauge slightly. As a consequence, unfortunately, the ratio of the cross sections at peak positions between the two gauges $\sigma_l^{++}/\sigma_v^{++}$, which should be 1 ideally, is worsened in comparison to the incomplete calculation by BJ and took a

new value of 2.6.

We are now reporting on our results for all three gauges with the 34-term ground-state wavefunction in the representation of Hylleraas coordinate for which the coefficients are given in Tab. (2.3). Note that present ground-state wavefunction with binding energy 2.903721 has much high accuracy than those in the calculations of both BJ and RC. Moreover, the inclusion of the term r_{12}^n in the ground-state wavefunction corresponds to an infinite number of "relative partial wave" couplings in the MCSCF model because the expansion of r_{12}^n has infinite number of partial waves when n is odd.

We implement the calculation fully with all the contributing partial waves (≤ 5) included. The total cross sections in the three gauges are tabulated in Tab. 4.1 and displayed in Fig. (4.1). The acceleration gauge gives the smallest values at all photon energies, while the length form provides the largest ones. The peak positions of the cross sections for acceleration, velocity, and length gauges are approximately at photon energies of 100, 100, and 120 eV, respectively, and the corresponding ratios are

$$\sigma_l^{++} : \sigma_v^{++} : \sigma_a^{++} \approx 2.5 : 1 : 0.6. \tag{4.24}$$

In the high energy range ($E \geq 1$ keV), the partial wave approach for velocity and length gauges becomes much more difficult. The integration in evaluating the dipole matrix element needs small step sizes as a result of the highly oscillatory feature in the 2C Coulomb function. Furthermore, the velocity and length gauges require the integration to be extended to a large configuration region away from the nucleus. However, the calculation

Table 4.1: Cross sections (in cm^2) for double photoionization of helium with 2C final state as a function of incident photon energy. σ_a^{++}, σ_v^{++}, and σ_l^{++} indicate the results for the three gauges in acceleration, velocity, and length forms.

E(eV)	σ_a^{++}	σ_v^{++}	σ_l^{++}
80	5.17×10^{-22}	6.93×10^{-22}	1.13×10^{-21}
82	1.36×10^{-21}	1.86×10^{-21}	3.16×10^{-21}
86	2.44×10^{-21}	3.45×10^{-21}	6.32×10^{-21}
90	3.01×10^{-21}	4.39×10^{-21}	8.58×10^{-21}
95	3.30×10^{-21}	4.99×10^{-21}	1.05×10^{-20}
100	3.35×10^{-21}	5.22×10^{-21}	1.18×10^{-20}
110	3.10×10^{-21}	5.11×10^{-21}	1.30×10^{-20}
120	2.71×10^{-21}	4.69×10^{-21}	1.32×10^{-20}
140	1.99×10^{-21}	3.70×10^{-21}	1.23×10^{-20}
160	1.45×10^{-21}	2.84×10^{-21}	1.09×10^{-20}
180	1.08×10^{-21}	2.19×10^{-21}	9.38×10^{-21}
200	8.15×10^{-22}	1.70×10^{-21}	8.03×10^{-21}
250	4.39×10^{-22}	9.50×10^{-22}	5.42×10^{-21}
300	2.59×10^{-22}	5.65×10^{-22}	3.74×10^{-21}
400	1.10×10^{-22}	2.34×10^{-22}	1.92×10^{-21}
500	5.56×10^{-23}	1.13×10^{-22}	1.09×10^{-21}
600	3.15×10^{-23}	6.14×10^{-23}	6.69×10^{-22}
1000	6.24×10^{-24}	1.03×10^{-23}	1.55×10^{-22}

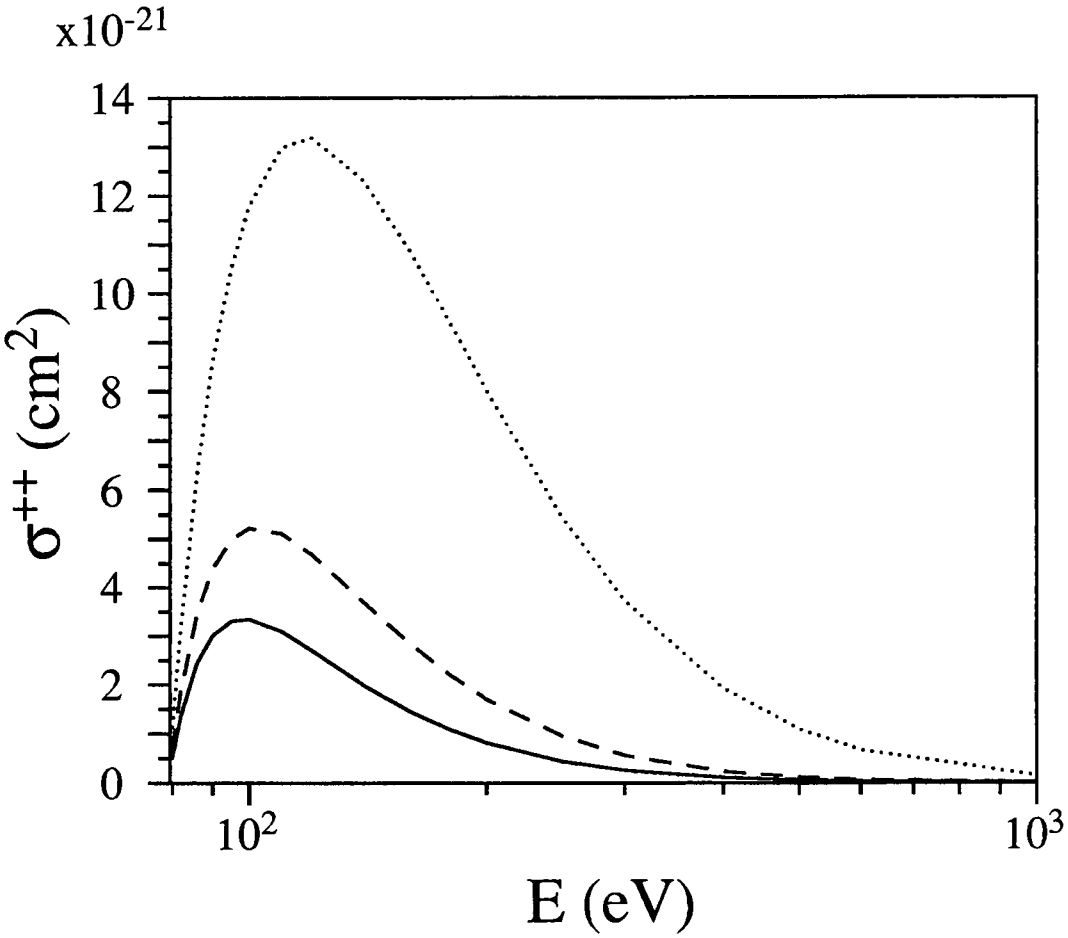

Figure 4.1: Total cross section for double photoionization of helium with a 2C final state as a function of incident photon energy in the acceleration (solid curve), velocity (dash curve), and length (dotted curve) gauges.

in acceleration gauge is much more convenient because the main contribution to the dipole matrix element is confined to a small regime in configuration space. In this gauge, the total cross sections at 2, 4, 8, and 16 keV are 6.52×10^{-25}, 6.56×10^{-26}, 6.36×10^{-27}, and 6.02×10^{-28} cm^2, respectively.

In Fig. (4.2), the electron energy distribution $d\sigma_a^{++}/dE_2$ is given for photon energies 100, 120, 200, and 500 eV. These are the acceleration-gauge results with the 34-term ground-state wavefunction and with the 2C ($Z = 2$) Coulomb waves. As explained in last subsection, these plots have the proper symmetry along the axis $E_2 = E_{tot}/2$ which are consistent with the prediction by RC but different from the results from the earlier version of the formalism by BJ. Obviously, the formulas derived by BJ do not satisfy the exchange symmetry in Hilbert space, therefore, it is not suitable for a discussion of the energy distribution. From Fig. (4.2), it is apparent that the energy distribution tends to become flat as the threshold region ($E \geq 79$ eV) is approached. This trend is in accordance with the WRP theory which predicts that, near threshold, there is a constant probability irrespective of the fraction of the available energy each electron carries off. On the contrary, highly energetic photons favor the unequal sharing of the excess energy between the two photoelectrons. For instance, with 500 eV photons, the probability of the event when one electron takes most of the available energy ($E_1 \simeq 420eV$) while the other escapes slowly is about 100 times greater than the probability for having both electrons ejected with the same energy $E_{tot}/2 \simeq 210$ eV.

At high photon energies $E \geq 1$ keV, the differential cross section $d\sigma_a/dE_2$

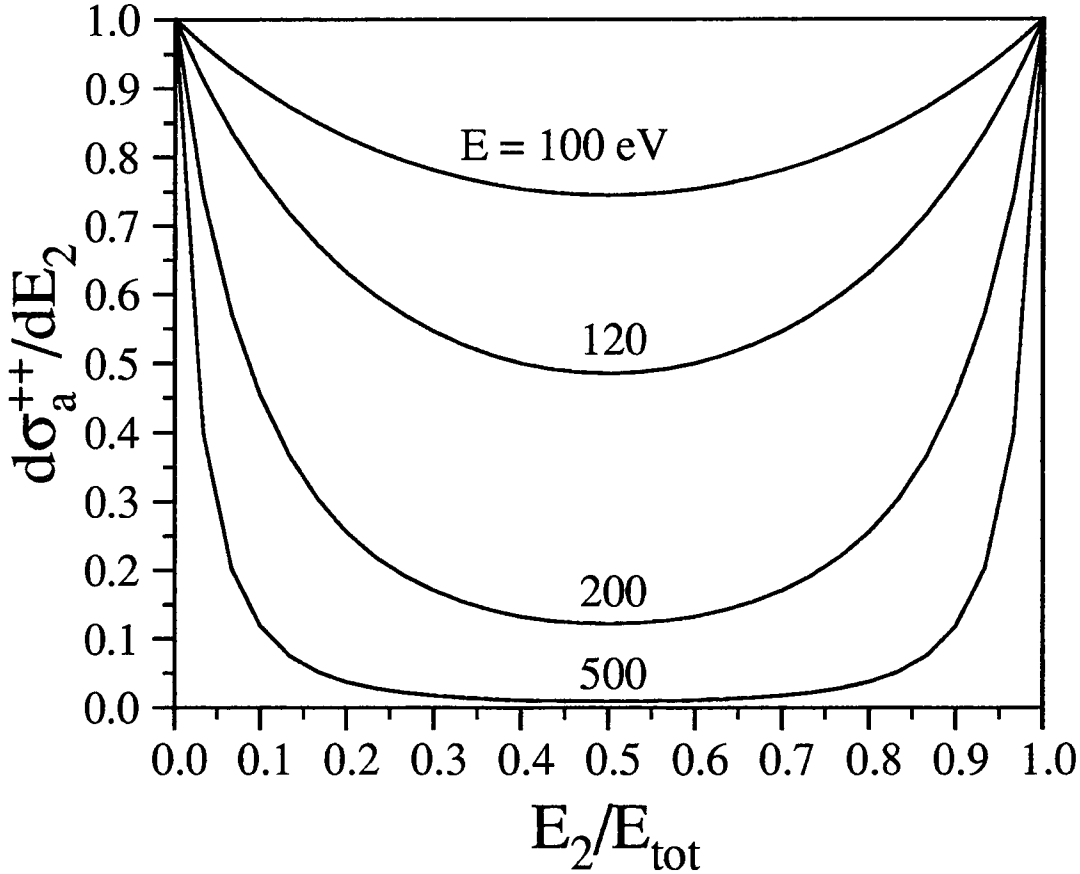

Figure 4.2: Energy distribution $d\sigma_a^{++}/dE_2$ with a 2C final state in the acceleration gauge as a function of the ratio E_2/E_{tot}, where E_2 is the energy of one electron and E_{tot} is the total energy available for both electrons. The distributions have been normalized to 1 for $E_2 = 0$. For the DPI of helium by 100, 120, 200, and 500 eV photons, E_{tot} takes the values 21, 41, 121, and 421 eV, and the actual maxima (for $E_2 = 0$) are 3.74×10^{-4}, 2.03×10^{-4}, 4.36×10^{-5}, and 2.69×10^{-6}, respectively.

with asymmetric energy sharing ($E_2 \ll E_1$) dominates the contribution to the total cross section. For example, with 1000 eV photons, the probability of the event when one electron takes most of the available energy ($E_1 \simeq 920eV$) while the other escapes slowly is about 1000 times greater than the probability for having both electrons ejected with the same energy $E_{tot}/2 \simeq 460$ eV. For such an energy configuration ($E_2 \ll E_1$), the contribution to the differential cross section $d\sigma_a/dE_2$ comes predominantly from the contribution of the first part in the matrix element (Eq. (4.18)) with the dipole operator z_1/r_1^3 and the contribution from the second part with the dipole operator z_2/r_2^3 is essentially negligible. Moreover, in terms of the partial wave analysis, the major contribution comes from the case of $l_1 = 1$ and $l_2 = 0$. Therefore, in the high energy range, the double photoionization is dominated by a mechanism that one of the electrons interacts with the high-energy photon directly and receives the angular momentum of the photon and most of the photon energy, while the other electron escapes through relaxation. This mechanism is called "shakeoff" mechanism.

4.2 Single photoionization of helium

Since it is more convenient for the experimentalist to measure the double-to-single ratio rather than to measure the absolute cross sections themselves, most experiments only quote the ratios. For comparison with measurements, we have to calculate the total cross sections for single photoionization and the ratios. We employ the uncorrelated wavefunction which is a product

of an incoming Coulomb function with central charge Z_1 and a hydrogenic bound state wavefunction with central charge Z as the final state

$$\psi_f(\mathbf{r}_1, \mathbf{r}_2) = \frac{1}{\sqrt{2}} \left[\phi_f(\mathbf{r}_1, \mathbf{r}_2) + \phi_f(\mathbf{r}_2, \mathbf{r}_1)\right],$$

where

$$\phi_f(\mathbf{r}_1, \mathbf{r}_2) = \phi^{(-)}_{\mathbf{k}_1}(\mathbf{r}_1)\varphi^Z_{n_2 l_2 m_2}(\mathbf{r}_2)$$

with

$$\varphi^Z_{n_2 l_2 m_2}(\mathbf{r}_2) = R^Z_{n_2 l_2}(r_2) Y_{l_2 m_2}(\hat{\mathbf{r}}_2).$$

Note that a different central charge Z_1 for the continuum electron $\phi^{(-)}_{\mathbf{k}_1}$ is implicitly introduced whose value will be discussed later. For the ground state, we employ the 34-term Hylleraas type wavefunction. Following the general formalism in Eqs. (1.9-1.11) and the discussion in the previous section of this chapter (Eq. (4.1)), we will, in this section, evaluate the total cross sections of single ionization in acceleration, velocity, and length gauges.

4.2.1 Partial wave analysis

As in the case of double photoionization, the Coulomb function $\phi^{(-)}_{\mathbf{k}_1}$ in the unsymmetrized final state wavefunction ϕ_f can be expanded in partial waves $\varphi^{Z_1}_{k_1 l_1 m_1}$ (Eq. (4.3)) with well defined quantum numbers l_1 and m_1. The two one-electron harmonics $Y_{l_i m_i}(\hat{\mathbf{r}}_i)$ $(i = 1, 2)$ can be coupled to form a bipolar harmonics $y^{l_1 l_2}_{LM}(\hat{\mathbf{r}}_1, \hat{\mathbf{r}}_2)$, which are the eigenstates of the total angular momentum L^2 and its z component L_z. Keeping only P_0 part $(L = 1, M =$

0), because of the dipole selection rule, we get the relevant expression for SPI

$$\phi_f(\mathbf{r}_1,\mathbf{r}_2) = \sum_{l_1 m_1} i^{l_1} e^{i\sigma_{l_1}(\eta_1)} Y^*_{l_1 m_1}(\hat{\mathbf{k}}_1)$$
$$\cdot\langle 10|l_1 m_1 l_2 m_2\rangle \delta_{l_1,l_2\pm 1}\delta_{m_1+m_2,0}\Phi^{Z_1 Z}_{k_1 l_1 n_2 l_2}(\mathbf{r}_1,\mathbf{r}_2), \qquad (4.25)$$

where

$$\Phi^{Z_1 Z}_{k_1 l_1 k_2 l_2}(\mathbf{r}_1,\mathbf{r}_2) = y^{l_1 l_2}_{10}(\mathbf{r}_1,\mathbf{r}_2) R^{Z_1}_{k_1 l_1}(r_1) R^{Z}_{n_2 l_2}(r_2).$$

Inserting now the relevant part of the final-state wavefunction (Eq. (4.25)) into the dipole matrix element T (Eq. (4.1)) and integrating over the angles $\hat{\mathbf{k}}_1$ in Eqs. (1.9-1.11) leads to the formulas for the branching contributions $\sigma^+(n_2)$ to the total cross sections σ^+ from each energy subshell n_2 and the total cross sections in the three gauges. For the acceleration gauge

$$\sigma^+_a(n_2) = \frac{4\pi^2 Z^2}{cE^3} \sum_{l_2} \sum_{l_1=l_2\pm 1} \left| \langle \Phi^{Z_1 Z}_{k_1 l_1 n_2 l_2}(\mathbf{r}_1,\mathbf{r}_2)| \frac{z_1}{r_1^3} + \frac{z_2}{r_2^3} |\psi_0(\mathbf{r}_1,\mathbf{r}_2)\rangle \right|^2, \qquad (4.26)$$

$$\sigma^+_a = \sum_{n_2} \sigma^+_a(n_2). \qquad (4.27)$$

For the velocity gauge

$$\sigma^+_v(n_2) = \frac{4\pi^2}{cE} \sum_{l_2} \sum_{l_1=l_2\pm 1} \left| \langle \Phi^{Z_1 Z}_{k_1 l_1 n_2 l_2}(\mathbf{r}_1,\mathbf{r}_2)| \frac{\partial}{\partial z_1} + \frac{\partial}{\partial z_2} |\psi_0(\mathbf{r}_1,\mathbf{r}_2)\rangle \right|^2, \qquad (4.28)$$

$$\sigma^+_v = \sum_{n_2} \sigma^+_v(n_2). \qquad (4.29)$$

For the length gauge

$$\sigma^+_l(n_2) = \frac{4\pi^2 E}{c} \sum_{l_2} \sum_{l_1=l_2\pm 1} \left| \langle \Phi^{Z_1 Z}_{k_1 l_1 n_2 l_2}(\mathbf{r}_1,\mathbf{r}_2)| z_1 + z_2 |\psi_0(\mathbf{r}_1,\mathbf{r}_2)\rangle \right|^2, \qquad (4.30)$$

$$\sigma^+_l = \sum_{n_2} \sigma^+_l(n_2). \qquad (4.31)$$

The formulas for the calculation of the cross sections to the excited final states ("satellites") $\sigma^+(n_2)$ are similar in form to those for the calculation of the energy distribution in double photoionization (Eqs. (4.10,4.11,4.12)) except for one of the spherical Coulomb function $R^Z_{k_2 l_2}$ which is replaced by a hydrogenic bound-state wavefunction $R^Z_{n_2 l_2}$. Following the procedure for double photoionization, the evaluation of the matrix element in Eqs. (4.26,4.28,4.30) can be pursued which leads to the same forms as the Eqs. (4.18,4.20,4.19) with the following replacement:

$$R^Z_{k_1 l_1}(r_1) \rightarrow R^{Z_1}_{k_1 l_1}(r_1) \tag{4.32}$$

$$R^Z_{k_2 l_2}(r_2) \rightarrow R^Z_{n_2 l_2}(r_2). \tag{4.33}$$

The satellite ratios $R_i(n_2)$ which measure the branching contributions $\sigma^+(n_2)$ to the total cross sections σ^+ from each energy subshell n_2 in the three gauges are defined by

$$R_i(n_2) = \frac{\sigma_i^+(n_2)}{\sigma_i^+(1)}, \quad (i = a, v, l). \tag{4.34}$$

4.2.2 Results and discussion

For singly ionized helium, the electron in the bound state experiences only the central charge of the nucleus ($Z = 2$). However, the escaping electron is moving in the field of the nucleus screened by the bound electron. The effective charge Z_1 felt by the continuum electron should lie in between 1 and 2. We therefore made two separate calculations with $Z_1 = 1$ and $Z_1 = 2$ in the acceleration, velocity, and length gauges. The total cross sections for

single ionization are given in Tab. (4.2) and are compared with experimental data [19] in Fig. (4.3). For $Z_1 = 1$, the acceleration gauge gives the smallest values at all photon energies, while the length form provides the largest ones. For $Z_1 = 2$, the order of the results in the three gauges is reversed. The experimental results are always located between those from the same gauge with $Z_1 = 1$ and $Z_1 = 2$. It is expected that a properly chosen effective charge between 1 and 2 in the Coulomb function $\phi^{(-)}_{\mathbf{k}_1}$ for the escaping electron can lead to converged results for the three gauges and the experimental data.

It is interesting to note that the experimental data are much closer to the results from the acceleration and velocity gauges than those from the length gauge and this feature becomes even more striking (Fig. (4.3)) at high energies. Dalgarno and Sadeghpour [31] have shown that for large photon energies the error in the length form of the dipole matrix element remains unaltered whereas in the velocity and acceleration forms the error drops as E^{-1} and E^{-2}, respectively, when an approximate wavefunction is applied. Our results confirm the prediction by Dalgarno and Sadeghpour. Moreover, it seems that the acceleration gauge can achieve better results even at low energies.

We also obtain the branching contributions $\sigma^+(n_2)$ to the total cross sections σ^+ from each energy subshell n_2 in the three gauges. The satellite ratios $R_a(n_2)$ $(n_2 = 2, 3)$ in the acceleration gauge with $Z_1 = 1$ are displayed in Fig. (4.4) and are compared with the measurement by Wehlitz *et al* [68]. At low photon energies there is a large difference between the calculation and

Table 4.2: Total cross sections (in cm^2) for single photoionization of helium with a 2C final state as a function of incident photon energy. σ_a^+, σ_v^+, and σ_l^+ indicate the results for three gauges in acceleration, velocity, and length forms and $Z_1 = 1$ and $Z_1 = 2$ denote the effective central charges used in the Coulomb function $\phi_{\mathbf{k}_1}^{(-)}$ representing the escaping electron.

	$Z_1 = 1$		
E(eV)	σ_a^+	σ_v^+	σ_l^+
80	6.03×10^{-19}	8.26×10^{-19}	2.26×10^{-18}
82	5.62×10^{-19}	7.67×10^{-19}	2.12×10^{-18}
86	4.91×10^{-19}	6.67×10^{-19}	1.87×10^{-18}
90	4.33×10^{-19}	5.85×10^{-19}	1.67×10^{-18}
95	3.74×10^{-19}	5.02×10^{-19}	1.46×10^{-18}
100	3.25×10^{-19}	4.35×10^{-19}	1.29×10^{-18}
110	2.51×10^{-19}	3.34×10^{-19}	1.03×10^{-18}
120	1.98×10^{-19}	2.63×10^{-19}	8.32×10^{-19}
140	1.30×10^{-19}	1.72×10^{-19}	5.75×10^{-19}
160	8.94×10^{-20}	1.18×10^{-19}	4.17×10^{-19}
180	6.41×10^{-20}	8.48×10^{-20}	3.13×10^{-19}
200	4.75×10^{-20}	6.28×10^{-20}	2.42×10^{-19}
250	2.50×10^{-20}	3.29×10^{-20}	1.39×10^{-19}
300	1.46×10^{-20}	1.93×10^{-20}	8.78×10^{-20}
400	6.20×10^{-21}	8.12×10^{-21}	4.30×10^{-20}
500	3.15×10^{-21}	4.10×10^{-21}	2.44×10^{-20}
600	1.80×10^{-21}	2.32×10^{-21}	1.54×10^{-20}
1000	3.62×10^{-22}	4.57×10^{-22}	4.20×10^{-21}

Tab. (4.2) continued.

E(eV)	$Z_1 = 2$ σ_a^+	σ_v^+	σ_l^+
80	8.64×10^{-19}	4.03×10^{-19}	1.71×10^{-19}
82	8.04×10^{-19}	3.79×10^{-19}	1.62×10^{-19}
86	6.99×10^{-19}	3.37×10^{-19}	1.47×10^{-19}
90	6.11×10^{-19}	3.01×10^{-19}	1.34×10^{-19}
95	5.22×10^{-19}	2.63×10^{-19}	1.20×10^{-19}
100	4.48×10^{-19}	2.32×10^{-19}	1.08×10^{-19}
110	3.39×10^{-19}	1.82×10^{-19}	8.74×10^{-20}
120	2.62×10^{-19}	1.46×10^{-19}	7.21×10^{-20}
140	1.66×10^{-19}	9.83×10^{-20}	5.11×10^{-20}
160	1.11×10^{-19}	6.93×10^{-20}	3.72×10^{-20}
180	7.82×10^{-20}	5.07×10^{-20}	2.80×10^{-20}
200	5.70×10^{-20}	3.82×10^{-20}	2.18×10^{-20}
250	2.90×10^{-20}	2.07×10^{-20}	1.23×10^{-20}
300	1.66×10^{-20}	1.24×10^{-20}	7.20×10^{-21}
400	6.83×10^{-21}	5.46×10^{-21}	3.67×10^{-21}
500	3.40×10^{-21}	2.83×10^{-21}	1.97×10^{-21}
600	1.92×10^{-21}	1.64×10^{-21}	1.16×10^{-21}
1000	3.77×10^{-22}	3.43×10^{-22}	2.76×10^{-22}

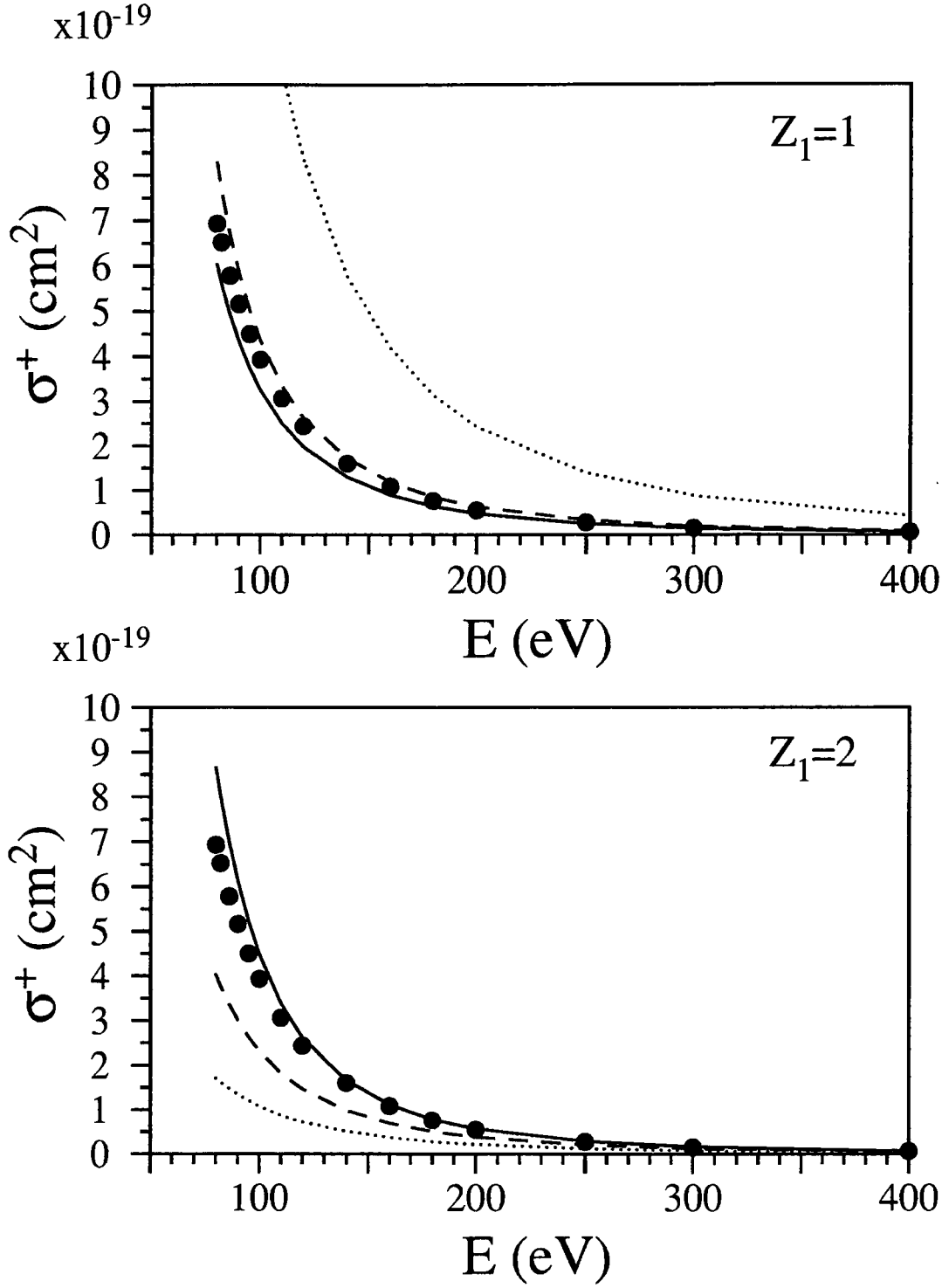

Figure 4.3: Cross sections for single photoionization of helium with 2C final state as a function of incident photon energy in the acceleration (solid curve), velocity (dash curve), and length (dotted curve) gauges compared with experimental data [69] (solid circle). $Z_1 = 1$ and $Z_1 = 2$ denote the effective central charges applied in the Coulomb function $\phi^{(-)}_{\mathbf{k}_1}$ for the escaping electron.

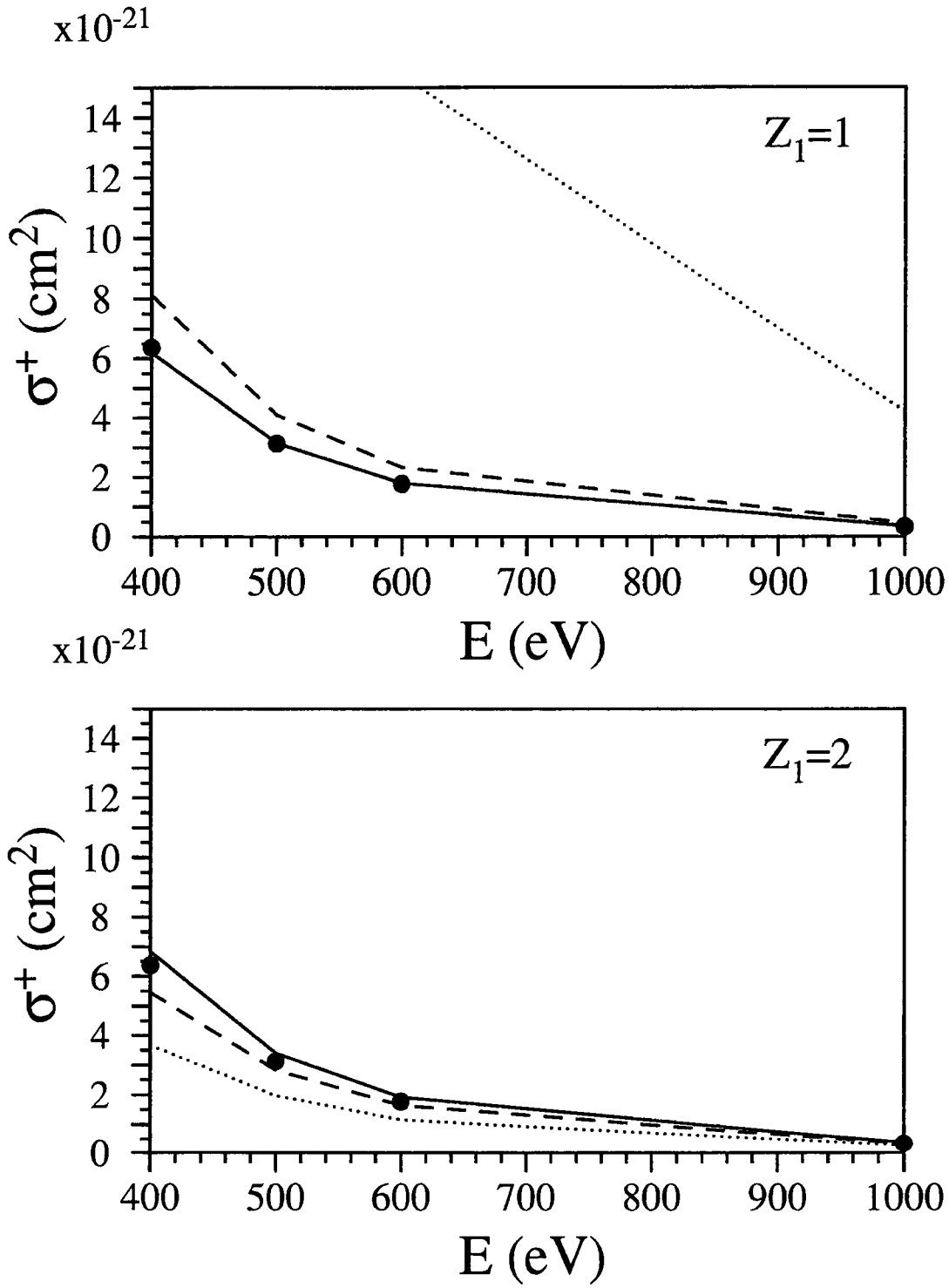

Fig. (4.3) continued for higher energies (400 eV $\leq E \leq$ 1000 eV).

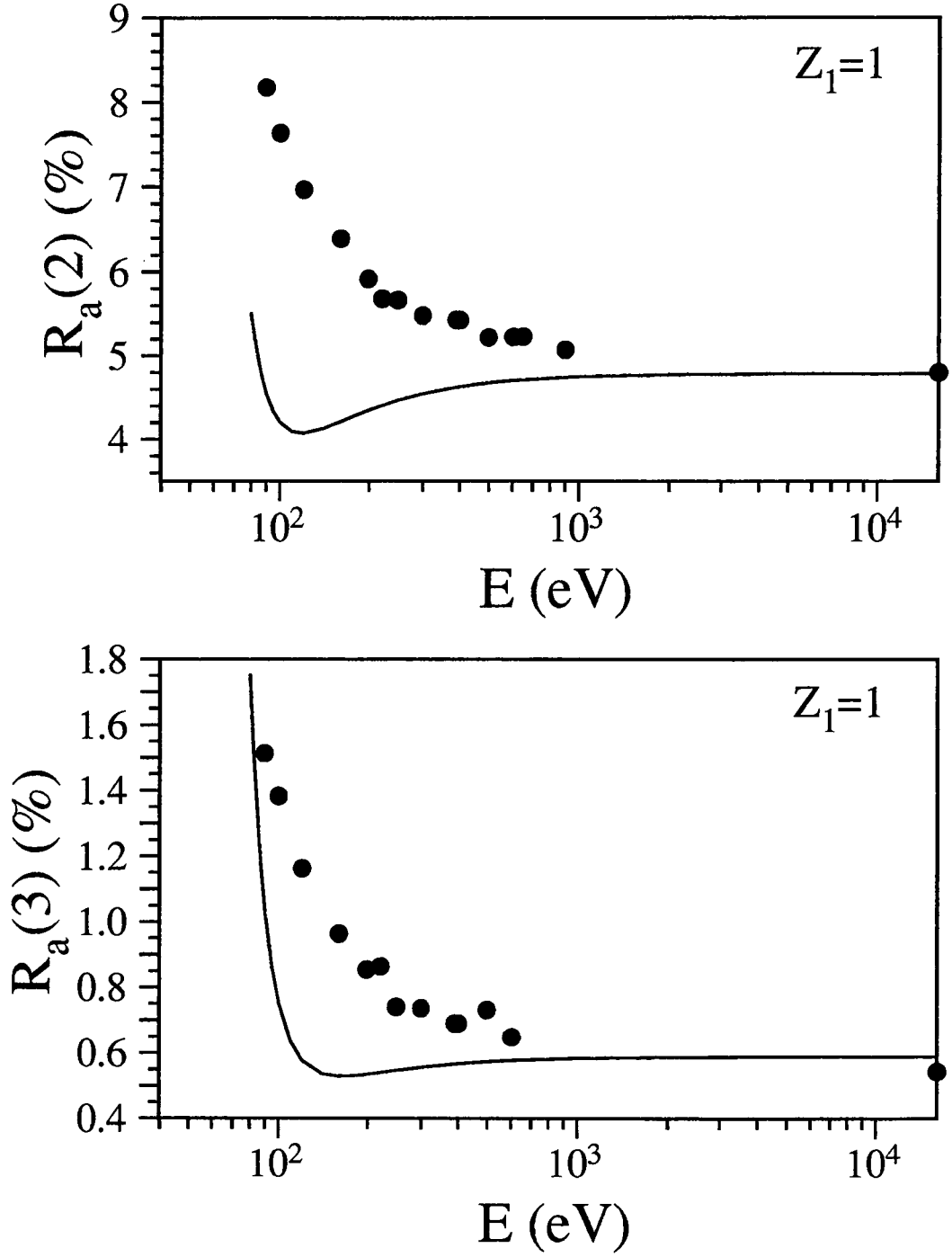

Figure 4.4: Helium satellite-to-1s ratios of $R_a(2)$ and $R_a(3)$ in present calculation (solid curve) in comparison with the measurement [68] (solid circle) at different photon energies. In the calculation the 2C final state and acceleration gauge are used.

the measurements. The deviation exists at all the photon energies although the difference is reduced in the high energy region. Only in the high-energy limit the results from both the theory and the experiment converge. Since the ground state wavefunction and the dipole approximation assumption are reliable input[1] for the calculation, the deviation of the satellites-to-1s ratio in the present calculation from the measurement demonstrates the necessity to include the electron-electron correlation in the final state wavefunction.

4.3 Ratio between the double and single photoionization of helium

We display the ratios between the double and single photoionization $R_{ph}(E)$ in the present calculation in Fig. (4.5). The total cross section for single ionization is taken from the results in Tab. (4.2) with $Z_1 = 1$. Also presented are the latest experimental data of Samson *et al* [69], and Dörner *et al* [21] in the low and intermediate energy region and Spielberger *et al* [70] in the high energy region where Compton effect is excluded. The data of Levin et al [20] cover a broad energy range from threshold to about 2 keV of photon energy. The results in the present calculation using the velocity and length gauges predict a substantial increase of the double-to-single ratio as the photon energy increases and the ratio peaks at photon energies around 300 eV. However, both the peak shapes and positions are different from those of the experiments. In the acceleration-gauge calculation, no peak in the ratio is

[1]The justification of the dipole approximation at high photon energies is presented in chapter 6.

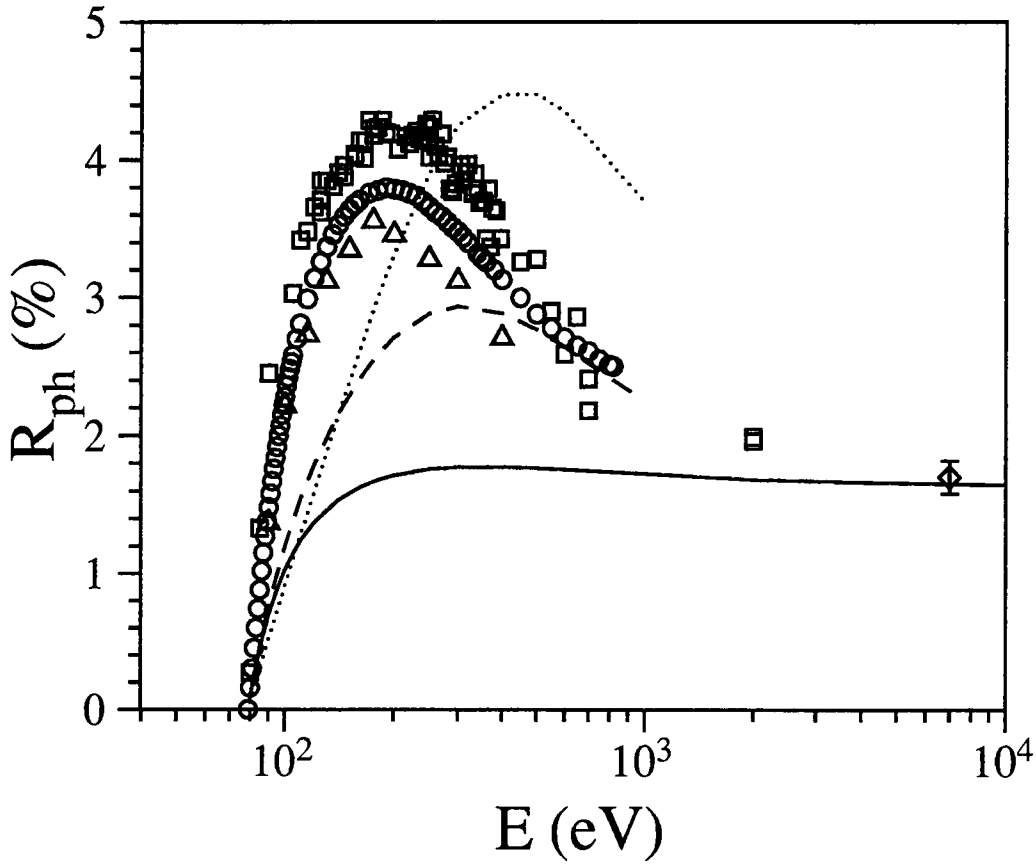

Figure 4.5: Comparison of the double-to-single ratio R_{ph} in present calculation using an uncorrelated 2C final-state wavefunction in the acceleration (solid curve), velocity (dash curve), and length (dotted curve) gauges compared with experiments. Experimental data: circles by Samson *et al* [69]; triangles by Dörner *et al* [21]; squares by Levin *et al* [20]; diamond by Spielberger *et al* [70] with Compton scattering excluded.

observed. Except in the non-relativistic high energy limit where the result in the acceleration gauge agrees with the measurements, the present calculation and the measurements deviate sharply over the entire photon energy range. The deviation illustrates the importance of the final state correlation to the evaluation of double photoionization.

Chapter 5

Double photoionization of helium with 3C wavefunction as the approximate final-state wavefunction

In the last chapter, we have discussed double photoionization of helium with a 2C wavefunction as the approximate final-state wavefunction. The results demonstrate that the 2C wavefunction without electron-electron correlation cannot predict correctly the total cross section for double photoionization or the satellite-to-1s ratio of the ionization-excitation at finite photon energies while it reproduces the total cross section for single ionization in the acceleration and velocity gauges with reasonable accuracy. However, to describe accurately the final-state correlation is a challenge to atomic physicists. At low and intermediate energies ($\leq$ 1 keV), sophisticated *ab initio* methods, such as the hyperspherical close-coupling (HSCC) [16], R-matrix [17], and complex Stumian [18] methods have been recently developed which have led to an

improved agreement with the most recent measurements [19, 20, 21]. In the region of high photon energies ($\geq$ 1 keV) several approaches have been pursued including many−body perturbation theory (MBPT) [22, 23, 24], the use of the correlated 3C wave function to represent the final state [25, 27, 28, 26] and, very recently, the use of the dipole response function [29]. In this regime, discrepancies between different theoretical predictions have remained unresolved and comparisons with experiments are complicated by the fact that in some experiments the separation of contributions from Compton scattering and from photoionization is not possible.

In this chapter we study double and single photoionization of helium and their ratio at high energies by using the accurate 34-term ground-state wavefunction in the representation of Hylleraas coordinates and the correlated 3C final-state wavefunction. We have developed a new technique for the analysis of the distortion factor in the 3C wavefunction such that the accurate evaluation of the dipole matrix element is made possible. Detailed calculations are performed in the acceleration gauge. The acceleration gauge is the best form to calculate the dipole transition amplitude at high energies [31] and the 3C wavefunction is the solution of the three-body Schrödinger equation to order Z/k_1 (Z: nuclear charge, k_1: momentum of the outgoing fast electron) in the relevant region of coordinate space where the dominant contributions to the dipole matrix element originate. Therefore, the present calculation is expected to predict the behavior of double photoionization in the high energy range with high accuracy.

5.1 Partial wave analysis

The main task now is to evaluate the dipole matrix elements in Eq. (1.6) and Eq. (1.8) with the accurate ground-state wavefunction (Eq. (2.37)) and the 3C wavefunction (Eq. (3.14)). For single ionization, it is understood that one of the Coulomb functions $\phi^{(-)}_{\mathbf{k}_2}(\mathbf{r}_2)$ for the slow electron in 3C wavefunction is replaced by the hydrogenic bound-state wavefunction $\phi_{nlm}(\mathbf{r}_2)$ with central charge Z. The dipole matrix element of single ionization in acceleration gauge

$$\begin{aligned} T = \frac{1}{\sqrt{2}} \Big[& \langle \phi^{(-)}_{\mathbf{k}_1}(\mathbf{r}_1)\phi_{n_2l_2m_2}(\mathbf{r}_2)D^{(-)}(\mathbf{k}_{12},\mathbf{r}_{12}) \mid \frac{z_1}{r_1^3} + \frac{z_2}{r_2^3} \mid \psi_0(\mathbf{r}_1,\mathbf{r}_2)\rangle \\ & + \langle \phi^{(-)}_{\mathbf{k}_1}(\mathbf{r}_2)\phi_{n_2l_2m_2}(\mathbf{r}_1)D^{(-)}(\mathbf{k}_{12},\mathbf{r}_{21}) \mid \frac{z_1}{r_1^3} + \frac{z_2}{r_2^3} \mid \psi_0(\mathbf{r}_1,\mathbf{r}_2)\rangle \Big] \\ = \sqrt{2} & \langle \phi^{(-)}_{\mathbf{k}_1}(\mathbf{r}_1)\phi_{n_2l_2m_2}(\mathbf{r}_2)D^{(-)}(\mathbf{k}_{12},\mathbf{r}_{12}) \mid \frac{z_1}{r_1^3} + \frac{z_2}{r_2^3} \mid \psi_0(\mathbf{r}_1,\mathbf{r}_2)\rangle, \end{aligned} \tag{5.1}$$

where $\mathbf{k}_{12} = \mathbf{k}_1/2$. For double photoionization, the dipole matrix element is

$$T = \sqrt{2}\langle \phi^{(-)}_{\mathbf{k}_1}(\mathbf{r}_1)\phi^{(-)}_{\mathbf{k}_2}(\mathbf{r}_2)D^{(-)}(\mathbf{k}_{12},\mathbf{r}_{12}) \mid \frac{z_1}{r_1^3} + \frac{z_2}{r_2^3} \mid \psi_0(\mathbf{r}_1,\mathbf{r}_2)\rangle, \tag{5.2}$$

where $\mathbf{k}_{12} = (\mathbf{k}_1 - \mathbf{k}_2)/2$. Since the hydrogenic states including both the bound and continuum states, thereafter denoted by $\mid k\rangle$, construct a complete set, any single particle wavefunction f can be expanded in the basis

$$\begin{aligned} \langle f \mid f\rangle &= \int \langle f \mid \mathbf{r}\rangle\langle \mathbf{r} \mid f\rangle d\mathbf{r} \\ &= \int \mid f(\mathbf{r}) \mid^2 d\mathbf{r} \\ &= \sum_k \langle f \mid k\rangle\langle k \mid f\rangle \end{aligned}$$

$$= \sum_k \int \langle f \mid \mathbf{r} \rangle \langle \mathbf{r} \mid k \rangle d\mathbf{r} \int \langle k \mid \mathbf{r}' \rangle \langle \mathbf{r}' \mid f \rangle d\mathbf{r}'$$

$$= \sum_k \left| \int \phi_k^*(\mathbf{r}) f(\mathbf{r}) d\mathbf{r} \right|^2 . \tag{5.3}$$

Therefore, the evaluation of the total cross section for double *plus* single ionization at high photon energies

$$\sigma_a^{++,+} = \frac{8\pi^2 Z^2}{cE^3} \sum_k \left| \langle \phi_{\mathbf{k}_1}^{(-)}(\mathbf{r}_1) \phi_k(\mathbf{r}_2) D^{(-)}(\mathbf{k}_{12}, \mathbf{r}_{12}) \mid d_a(\mathbf{r}_1, \mathbf{r}_2) \mid \psi_0(\mathbf{r}_1, \mathbf{r}_2) \rangle \right|^2 \tag{5.4}$$

where

$$d_a(\mathbf{r}_1, \mathbf{r}_2) = \frac{z_1}{r_1^3} + \frac{z_2}{r_2^3},$$

and $\mathbf{k}_1$ is the momentum of the fast electron, can be greatly simplified to

$$\begin{aligned} \sigma_a^{++,+} &= \frac{8\pi^2 Z^2}{cE^3} \sum_k \left| \int d\mathbf{r}_2 \phi_k^*(\mathbf{r}_2) \right. \\ &\qquad \left. \cdot \left[\int d\mathbf{r}_1 \phi_{\mathbf{k}_1}^{(-)*}(\mathbf{r}_1) D^{(-)*}(\mathbf{k}_{12}, \mathbf{r}_{12}) d_a(\mathbf{r}_1, \mathbf{r}_2) \psi_0(\mathbf{r}_1, \mathbf{r}_2) \right] \right|^2 \\ &= \frac{8\pi^2 Z^2}{cE^3} \int d\mathbf{r}_2 \left| \int d\mathbf{r}_1 \phi_{\mathbf{k}_1}^{(-)*}(\mathbf{r}_1) D^{(-)*}(\mathbf{k}_{12}, \mathbf{r}_{12}) d_a(\mathbf{r}_1, \mathbf{r}_2) \psi_0(\mathbf{r}_1, \mathbf{r}_2) \right|^2 . \end{aligned} \tag{5.5}$$

The total cross section for single ionization is

$$\sigma_a^+ = \sum_{n_2} \sigma_a^+(n_2) \tag{5.6}$$

with

$$\begin{aligned} \sigma_a^+(n_2) = \frac{8\pi^2 Z^2}{cE^3} & \sum_{l_2 m_2} \\ & \cdot \left| \langle \phi_{\mathbf{k}_1}^{(-)}(\mathbf{r}_1) \phi_{n_2 l_2 m_2}(\mathbf{r}_2) D^{(-)}(\mathbf{k}_{12}, \mathbf{r}_{12}) \mid d_a(\mathbf{r}_1, \mathbf{r}_2) \mid \psi_0(\mathbf{r}_1, \mathbf{r}_2) \rangle \right|^2 . \end{aligned} \tag{5.7}$$

The total cross section for double photoionization can therefore be obtained indirectly from the difference of $\sigma_a^{++,+}$ and σ_a^{+}

$$\sigma_a^{++} = \sigma_a^{++,+} - \sigma_a^{+}. \tag{5.8}$$

The method that uses the closure relation, which also works in the velocity and length gauges in the high energy region, is theoretically equivalent to the direct calculation. Practically, however, it is much simpler than the direct calculation because no additional integration over energy is needed. One thing which should be emphasized here is that the central charge Z for both the bound and continuum states in the set $\{|k\rangle\}$ must be the same because this is the prerequisite for the completeness of $\{|k\rangle\}$.

We now perform the evaluation of Eqs. (5.5-5.7). However, the application of the accurate Hylleraas ground-state wavefunction ψ_0 and the distortion factor $D^{(-)}$ in the 3C wavefunction to the evaluation of the cross sections is complicated by the presence of the interelectronic coordinates $\mathbf{r_{12}}$ and the relative momentum $\mathbf{k_{12}}$. Our calculation proceeds by expanding the distortion factor $D^{(-)}(\mathbf{k}_{12}, \mathbf{r}_{12})$ in terms of partial waves in the $\mathbf{r_{12}}$ coordinates. According to the integral representation for the confluent hypergeometric functions [71], the distortion factor $D^{(-)}$ has following form

$$D^{(-)}(\mathbf{k}_{12}, \mathbf{r}_{12}) = \frac{e^{-\pi\eta_{12}/2}}{\Gamma(i\eta_{12})} \int_0^1 e^{-it(k_{12}r_{12}+\mathbf{k_{12}}\cdot\mathbf{r_{12}})} t^{i\eta_{12}-1}(1-t)^{-i\eta_{12}} dt. \tag{5.9}$$

By expanding the exponential factor

$$e^{-it\mathbf{k_{12}}\cdot\mathbf{r_{12}}} = \sum_{l=0}^{\infty} (2l+1)(-i)^l j_l(tk_{12}r_{12}) P_l(cos\theta_{\hat{\mathbf{k}}_{12}\cdot\hat{\mathbf{r}}_{12}}) \tag{5.10}$$

and using

$$j_l(x) = \sqrt{\frac{\pi}{2x}} J_{l+\frac{1}{2}}(x), \tag{5.11}$$

the distortion factor becomes

$$D^{(-)}(\mathbf{k}_{12}, \mathbf{r}_{12}) = \frac{e^{-\pi\eta_{12}/2}}{\Gamma(i\eta_{12})} \sqrt{\frac{\pi}{2k_{12}r_{12}}} \sum_{l=0}^{\infty} (2l+1)(-i)^l P_l(cos\theta_{\hat{\mathbf{k}}_{12}.\hat{\mathbf{r}}_{12}}) \cdot \int_0^1 dt t^{i\eta_{12}-\frac{3}{2}} (1-t)^{-i\eta_{12}} e^{-itk_{12}r_{12}} J_{l+\frac{1}{2}}(tk_{12}r_{12}). \tag{5.12}$$

Following the integration expression used in reference [71], the integration with respect to variable t in Eq. (5.12) can be carried out and $D^{(-)}$ is presented as a summation over partial waves of $\mathbf{r_{12}}$ coordinates

$$d_l^{(-)}(\mathbf{k_{12}}, \mathbf{r_{12}}) = \frac{e^{-\pi\eta_{12}/2}\Gamma(1-i\eta_{12})}{\Gamma(i\eta_{12})} \frac{\sqrt{\pi}(2l+1)(-i)^l\Gamma(l+i\eta_{12})}{2^{l+1}l!\Gamma(l+\frac{3}{2})} \cdot (k_{12}r_{12})^l P_l(cos\theta_{\hat{\mathbf{k}}_{12}.\hat{\mathbf{r}}_{12}}) {}_1F_1[l+i\eta_{12}; 2l+2; -2ik_{12}r_{12}], \tag{5.13}$$

and

$$D^{(-)}(\mathbf{k}_{12}, \mathbf{r}_{12}) = \sum_{l=0}^{\infty} d_l^{(-)}(\mathbf{k_{12}}, \mathbf{r_{12}}). \tag{5.14}$$

The monopole term of the expression

$$d_{l=0}^{(-)}(\mathbf{k_{12}}, \mathbf{r_{12}}) = e^{-\pi\eta_{12}/2}\Gamma(1-i\eta_{12}) {}_1F_1[i\eta_{12}; 2; -2ik_{12}r_{12}] \tag{5.15}$$

is exactly the solution of the radial part of the Eq. (3.24). In the eikonal approximation the ratio of dipole–to–monopole terms

$$\frac{d_{l=1}^{(-)}(\mathbf{k_{12}}, \mathbf{r_{12}})}{d_{l=0}^{(-)}(\mathbf{k_{12}}, \mathbf{r_{12}})} \propto \eta_{12} \frac{\mathbf{k}_{12}.\mathbf{r}_{12}}{k_{12}r_{12}}, \tag{5.16}$$

is proportional to $1/k_{12}$ ($\eta_{12} = 1/(2k_{12})$), indicating the dominance of the monopole term at very high photon energies and the gradual increase of the weight of dipole and high order partial wave terms at lower energies. However, the contribution from very high order partial waves ($l > 4$) is significantly reduced by the fact that the l dependent coefficient in the expansion of Eq. (5.13) decreases in value very rapidly as l becomes very large. By an application of the addition theorem, the Legendre polynomial P_l in Eq. (5.13) takes the form

$$P_l(cos\theta_{\hat{\mathbf{k}}_{12},\hat{\mathbf{r}}_{12}}) = \frac{4\pi}{2l+1}\sum_m Y^*_{lm}(\hat{\mathbf{k}}_{12})Y_{lm}(\hat{\mathbf{r}}_{12}). \tag{5.17}$$

The spherical harmonic $Y_{lm}(\hat{r}_{12})$ as a function of the interelectronic angular coordinates $\hat{r}_{12}$ can be expanded in terms of the spherical harmonics of the two electron coordinates [1]

$$r_{12}^l Y_{lm}(\hat{r}_{12}) = \sum_{l_1=0,l_2=l-l_1}^{l} (-1)^{-l_1+m}\left[\frac{4\pi(2l+1)!(2l+1)}{(2l_1+1)!(2l_2+1)!}\right]^{1/2}$$

$$\cdot\sum_{m_1}\begin{pmatrix} l_1 & l_2 & l \\ m_1 & m_2 & -m \end{pmatrix} r_1^{l_1} r_2^{l_2} Y_{l_1 m_1}(\hat{r}_1)Y_{l_2 m_2}(\hat{r}_2). \tag{5.18}$$

The confluent hypergeometric function ${}_1F_1[l + i\eta_{12}; 2l + 2; -2ik_{12}r_{12}]$ term in the partial wave of $d_l^{(-)}$ (Eq. (5.13)) and the ground state wavefunction ψ_0 as a function of interelectron separation r_{12} can be expanded in Legendre

[1] Here $\mathbf{r}_{12}$ is defined as $\mathbf{r}_1 - \mathbf{r}_2$. If $\mathbf{r}_{12}$ is defined as $\mathbf{r}_2 - \mathbf{r}_1$, an additional sign of $(-1)^l$ is needed in Eq. (5.18)

polynomial

$$\psi_0(r_1, r_2, r_{12})\,{}_1F_1[l + i\eta_{12}; 2l + 2; -2ik_{12}r_{12}] = \sum_{l'} f_{ll'}(r_1, r_2)\; P_{l'}(cos\theta_{12}), \tag{5.19}$$

where

$$f_{ll'}(r_1, r_2) = \frac{2l' + 1}{2} \int_{-1}^{1} \psi_0(r_1, r_2, r_{12})\; {}_1F_1[l + i\eta_{12}; 2l + 2; -2ik_{12}r_{12}] P_{l'}(x) dx$$

and

$$r_{12} = \sqrt{r_1^2 + r_2^2 - 2r_1 r_2 x}.$$

Using the above expressions, the integration over angles $\hat{\mathbf{r}}_1$ and $\hat{\mathbf{r}}_2$ in the dipole matrix element can be analytically performed with the help of the following formulas [72]:

$$Y_{lm}(\hat{\mathbf{r}}) Y_{l'm'}(\hat{\mathbf{r}}) = \sum_{LM} \left[\frac{(2l+1)(2l'+1)(2L+1)}{4\pi}\right]^{1/2} \cdot \begin{pmatrix} l & l' & L \\ m & m' & M \end{pmatrix} \begin{pmatrix} l & l' & L \\ 0 & 0 & 0 \end{pmatrix} Y^*_{LM}(\hat{\mathbf{r}}), \tag{5.20}$$

$$\langle l'm' | Y_{LM} | lm \rangle = (-1)^{-m'} \left[\frac{(2l'+1)(2L+1)(2l+1)}{4\pi}\right]^{1/2} \cdot \begin{pmatrix} l' & L & l \\ -m' & M & m \end{pmatrix} \begin{pmatrix} l' & L & l \\ 0 & 0 & 0 \end{pmatrix} \tag{5.21}$$

Note that at high energies the "shakeoff" mechanism in which one of the electrons (labeled here by 1) interacts with the high-energy photon directly while the other electron (labeled by 2) escapes through relaxation dominates the total double photoionization cross section. The main contribution to the total cross section for double photoionization comes from the first term in the

matrix element with the dipole operator (z_1/r_1^3) with the contribution from the second term with the dipole operator (z_2/r_2^3) being essentially negligible. This argument works also for single ionization and is confirmed with the 2C wavefunction for high photon energies ($\geq$ 1 keV). This approximation was first discussed in the work of Andersson [73].

The single photoionization cross section can be written as

$$\sigma_a^+(n_2) = \frac{128\pi^4 Z^2}{cE^3} \frac{\pi\eta_{12}}{e^{\pi\eta_{12}} sh(\pi\eta_{12})} \sum_{l_2 m_2} \sum_{l_1} \left| \sum_l Term^+(l) \right|^2 , \tag{5.22}$$

where

$$Term^+(l=0) = (-1)^{-m_2} \sqrt{\frac{2l_1+1}{2l_2+1}} \begin{pmatrix} 1 & l_2 & l_1 \\ 0 & m_2 & -m_2 \end{pmatrix} \begin{pmatrix} 1 & l_1 & l_2 \\ 0 & 0 & 0 \end{pmatrix}$$

$$\cdot S^+(Z, k_1, l_1, n_2, l_2) \tag{5.23}$$

with

$$S^+(Z, k_1, l_1, n_2, l_2) \equiv e^{i\sigma_l(\eta_1)} \int_0^\infty dr_1 R^Z_{k_1 l_1}(r_1)$$
$$\cdot \int_0^\infty dr_2 r_2^2 R^Z_{n_2 l_2}(r_2)\ f_{l=0,l_2}(r_1, r_2) \tag{5.24}$$

and

$$Term^+\ (l>0) = Coef(l)\ k_{12}^l \sqrt{\frac{(2l_1+1)(2l_2+1)}{2l+1}} \sum_{l_1'=0}^{l} \sum_{j_2 j_1 l'}$$

$$\cdot (-1)^{-l_1'} (2j_2+1)(2j_1+1) \left[\frac{(2l+1)!(2l+1)(2l_1'+1)(2l-2l_1'+1)}{(2l_1'+1)!(2l-2l_1'+1)!} \right]^{1/2}$$

$$\cdot \begin{pmatrix} 1 & j_1 & j_2 \\ 0 & 0 & 0 \end{pmatrix} \begin{pmatrix} j_2 & l & l_1 \\ 0 & 0 & 0 \end{pmatrix} \begin{pmatrix} l_1' & j_1 & l' \\ 0 & 0 & 0 \end{pmatrix} \begin{pmatrix} l' & l-l_1' & l_2 \\ 0 & 0 & 0 \end{pmatrix}$$

$$\cdot Rad^+(Z, j_2, k_1, n_2, l_2, l, l', l_1')\ Ang(l_1, l_2, m_2, l, l_1', l', j_1, j_2). \tag{5.25}$$

In Eqs. (5.24,5.25) the following abbreviations have been used:

$$Coef(1) = \eta_{12}$$

$$Coef(2) = \frac{-i\eta_{12}(1+i\eta_{12})}{6}$$

$$Coef(3) = \frac{-\eta_{12}(1+i\eta_{12})(2+i\eta_{12})}{90}$$

$$Coef(4) = \frac{i\eta_{12}(1+i\eta_{12})(2+i\eta_{12})(3+i\eta_{12})}{2520}$$

...

$$Rad^+(Z, l_1, k_1, n_2, l_2, l, l', l_1') = e^{i\sigma_l(\eta_1)} \int_0^\infty dr_1 R^Z_{k_1 l_1}(r_1) r_1^{l_1'}$$

$$\cdot \int_0^\infty dr_2 r_2^{l-l_1'+2}\ R^Z_{n_2 l_2}(r_2)\ f_{ll'}(r_1, r_2) \tag{5.26}$$

$$Ang(l_1, l_2, m_2, l, l_1', l', j_1, j_2) = \sum_{m_1 m_1'} (-1)^{-(m_1'+m_1+m_2)}$$

$$\cdot \begin{pmatrix} l_1' & l-l_1' & l \\ m_1' & m_2-m_1-m_1' & -m_2+m_1 \end{pmatrix} \begin{pmatrix} j_2 & 1 & j_1 \\ m_1 & 0 & -m_1 \end{pmatrix}$$

$$\cdot \begin{pmatrix} j_2 & l & l_1 \\ m_1 & m_2-m_1 & -m_2 \end{pmatrix} \begin{pmatrix} l_1' & j_1 & l' \\ m_1' & m_1 & -(m_1'+m_1) \end{pmatrix}$$

$$\cdot \begin{pmatrix} l' & l-l_1' & l_2 \\ m_1'+m_1 & m_2-m_1-m_1' & -m_2 \end{pmatrix}. \tag{5.27}$$

The single *plus* double photoionization cross sections can be written as

$$\sigma_a^{++,+} = \frac{128\pi^4 Z^2}{cE^3} \frac{\pi\eta_{12}}{e^{\pi\eta_{12}} sh(\pi\eta_{12})} \sum_{l_2 m_2} \sum_{l_1} \int_0^\infty dr_2 r_2^2 \left| \sum_l Term(l) \right|^2, \tag{5.28}$$

where

$$Term(l=0) = (-1)^{-m_2} \sqrt{\frac{2l_1+1}{2l_2+1}} \begin{pmatrix} 1 & l_2 & l_1 \\ 0 & m_2 & -m_2 \end{pmatrix} \begin{pmatrix} 1 & l_1 & l_2 \\ 0 & 0 & 0 \end{pmatrix}$$

$$\cdot S(Z, k_1, l_1, l_2, r_2) \tag{5.29}$$

with

$$S(Z, k_1, l_1, l_2, r_2) \equiv e^{i\sigma_l(\eta_1)} \int_0^\infty dr_1 R^Z_{k_1,l_1}(r_1) f_{l=0,l_2}(r_1, r_2) \tag{5.30}$$

$$Term(l>0) = Coef(l)\, k_{12}^l \sqrt{\frac{(2l_1+1)(2l_2+1)}{2l+1}} \sum_{l_1'=0}^{l} \sum_{j_2 j_1 l'}$$

$$\cdot(-1)^{-l_1'}(2l-2l_1'+1)(2j_2+1)(2j_1+1)(2l_1'+1)$$

$$\cdot\begin{pmatrix} 1 & j_1 & j_2 \\ 0 & 0 & 0 \end{pmatrix}\begin{pmatrix} j_2 & l & l_1 \\ 0 & 0 & 0 \end{pmatrix}\begin{pmatrix} l_1' & j_1 & l' \\ 0 & 0 & 0 \end{pmatrix}\begin{pmatrix} l' & l-l_1' & l_2 \\ 0 & 0 & 0 \end{pmatrix}$$

$$\cdot Rad(Z,j_2,k_1,l,l',l_1',r_2)\ Ang(l_1,l_2,m_2,l,l_1',l',j_1,j_2). \tag{5.31}$$

In Eq. (5.31) we have abbreviated the radial integrals as

$$Rad(Z,l_1,k_1,l,l',l_1',r_2) = e^{i\sigma_l(\eta_1)}r_2^{l-l_1'}\int_0^\infty dr_1 r_1^{l_1'}R^Z_{k_1l_1}(r_1)\ f_{ll'}(r_1,r_2). \tag{5.32}$$

It is interesting to note that the angular part in the formulas for single ionization (Eq. (5.25)) and that for single *plus* double photoionization (Eq. (5.31)) are identical.

5.2 Results and discussion .

The 3C wavefunction was applied to the calculation of double photoionization by Anderson and Burgdörfer [25]. Anderson and Burgdörfer applied the acceleration gauge and a 20-parameter Hylleraas-type ground state wavefunction in the representation of Hart and Herzberg [34]. In their calculation the distortion factor $D^{(-)}$, which is a slow varying function of $\mathbf{r}_{12}$ for all the photon energies, is treated as a product of a plane wave $e^{-i\mathbf{k}_{12}\cdot\mathbf{r}_{12}}$ and a Coulomb function $\phi^{(-)}_{\mathbf{k}_{12}} = e^{i\mathbf{k}_{12}\cdot\mathbf{r}_{12}}D^{(-)}(\mathbf{k}_{12},\mathbf{r}_{12})$. Both are highly oscillatory function of

$\mathbf{r}_{12}$ at high energies. The functions $e^{-i\mathbf{k}_{12}\cdot\mathbf{r}_{12}}$ and $\phi^{(-)}_{\mathbf{k}_{12}}$ are expanded in the coordinates of $\mathbf{r}_{12}$. The interelectronic angle θ_{12} is transformed into the angle θ_2 by rotations.

The application of the 3C wavefunction in the double photoionization was also performed by Hino [27] in the acceleration gauge and by Teng and Shakeshaft [26] and Kornberg and Miraglia [28] in the velocity gauge. In the calculation of Hino, the closure method and partial wave analysis are employed. Only the monopole term

$$d^{(-)}_{l=0} = \frac{e^{-\pi\eta_{12}/2}\Gamma(1-i\eta_{12})}{4r_1r_2}\left\{(r_1+r_2)^2\ {}_1F_1[i\eta_{12};3;-2ik_{12}(r_1+r_2)]\right.$$
$$\left.-(r_1-r_2)^2\ {}_1F_1[i\eta_{12};3;-2ik_{12}(r_1-r_2)]\right\} \tag{5.33}$$

in the expansion of the distortion factor $D^{(-)}(\mathbf{k}_{12},\mathbf{r}_{12})$, however, was applied. In the calculation of Teng and Shakeshaft, an 8-parameter Hylleraas-type ground state wavefunction was employed. In the calculation of Kornberg and Miraglia, a 4-parameter Hylleraas-type wavefunction in the representation of Bonham and Kohn [40] was employed. In both cases the six-dimensional integral in the dipole matrix element is reduced to a two-dimensional integral by using the three denominator integral pioneered by Lewis for real parameters [74] and developed by Brauner, Briggs, and Klar for complex ones [64].

The present approach differs from previous calculations employing 3C final states [25, 27, 26, 28]. Unlike the calculation of Hino, [27] who used the monopole term only, we include all contributing multipoles in the expansion of the distortion factor $D^{(-)}(\mathbf{k}_{12},\mathbf{r}_{12})$. Furthermore, we use a different

technique, which is numerically more stable and analytically straightforward compared with the one applied by Anderson and Burgdörfer. Finally, we use a more accurate initial-state wavefunction than those used in the calculations of Teng and Shakeshaft [26] and Kornberg and Miraglia [28]. The ground-state correlation is crucial for double photoionization in the high energy region and becomes dominant in the high-energy limit.

The total cross sections for double and single photoionization and their ratio are presented in Tab. (5.1). The cross section for single photoionization as a function of photon energy between 1 and 16 keV is shown in Fig. (5.1). Also displayed are the results in the acceleration gauge from many-body perturbation theory [27], the dipole response function [29], and from the uncorrelated 2C final state wavefunction ($D^{(-)} = 1$). The experimental data by Samson *et al* [19] is also presented for comparison. The agreement between the results obtained using the uncorrelated 2C wavefunction and the correlated 3C wavefunction shows that the effect of the final state correlation on the total cross section for single ionization in the high energy range is very small when the acceleration gauge is applied. Good agreement is found with measurements and with other calculations except for the results obtained by use of the dipole response function. Here the single ionization cross section is smaller by a factor 2 than the other calculations at 1 keV.

For a detailed analysis of the high energy behavior of the escape of a single electron, we investigate the ionization-excitation process. The satellite-to-1s

Table 5.1: Total cross sections of double (σ^{++}) and single (σ^{+}) photoionization of helium and their ratio R_{ph} in the acceleration gauge using a 3C final state wavefunction *vs* the incident photon energy E.

E (keV)	σ^{+} (cm^2)	σ^{++} (cm^2)	$R_{ph}(\%)$
1.0	3.68×10^{-22}	9.67×10^{-24}	2.62
1.2	2.06×10^{-22}	5.05×10^{-24}	2.45
1.4	1.25×10^{-22}	2.92×10^{-24}	2.33
1.6	8.13×10^{-23}	1.82×10^{-24}	2.23
1.8	5.55×10^{-23}	1.20×10^{-24}	2.16
2.0	3.93×10^{-23}	8.27×10^{-25}	2.10
3.0	1.03×10^{-23}	2.00×10^{-25}	1.93
4.0	3.98×10^{-24}	7.38×10^{-26}	1.85
5.0	1.89×10^{-24}	3.41×10^{-26}	1.81
6.0	1.02×10^{-24}	1.82×10^{-26}	1.78
7.0	6.09×10^{-25}	1.07×10^{-26}	1.76
8.0	3.88×10^{-25}	6.76×10^{-27}	1.74
10.0	1.82×10^{-25}	3.13×10^{-27}	1.72
12.0	9.81×10^{-26}	1.67×10^{-27}	1.71
14.0	5.80×10^{-26}	9.85×10^{-28}	1.70
16.0	3.68×10^{-26}	6.22×10^{-28}	1.69

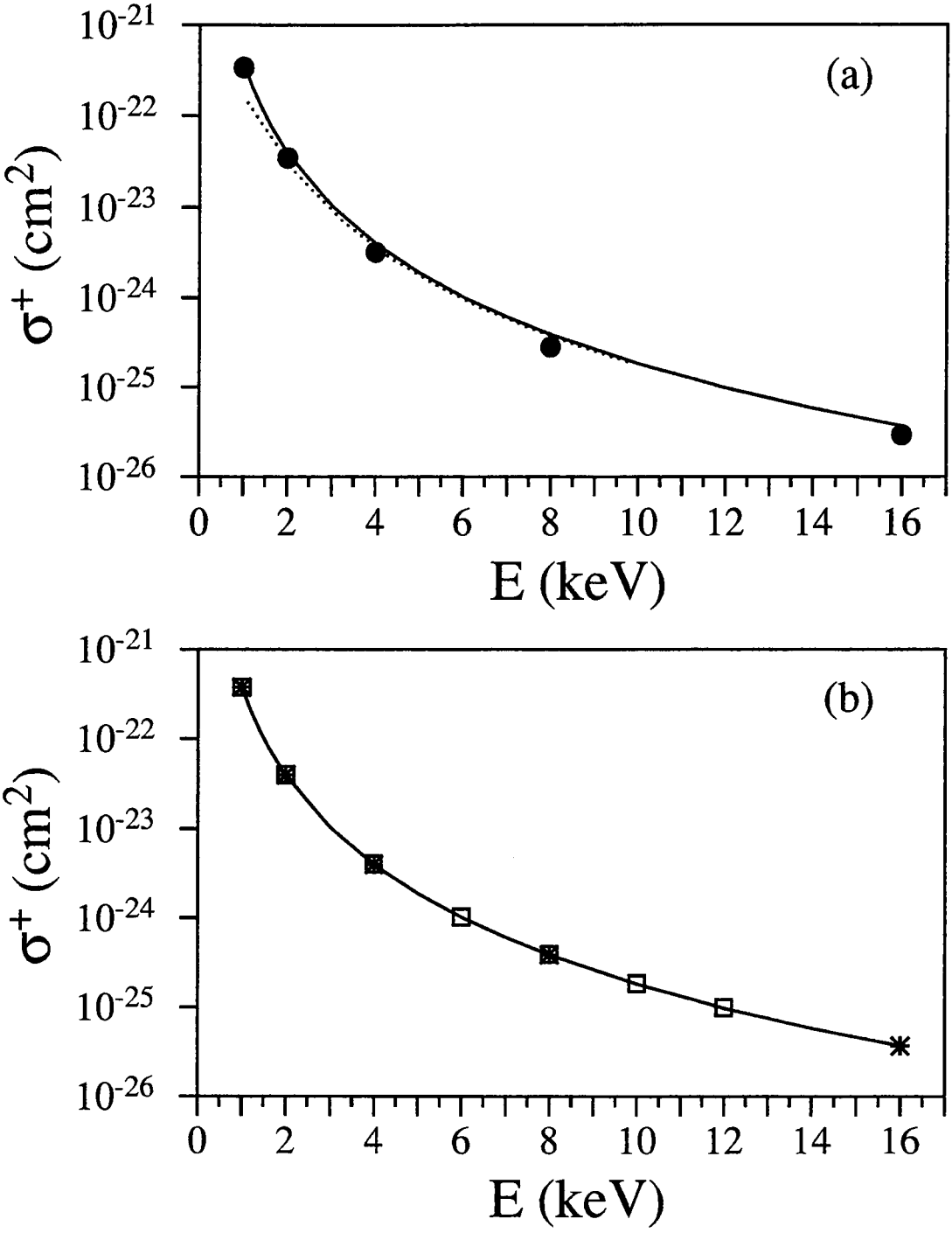

Figure 5.1: Cross sections for single ionization σ^+ with a 3C final state (solid curve) vs the photon energy E together with other results: (a) solid circles by Samson *et al* [19]; dotted curve by Forrey *et al* [29]. (b) open square by Hino *et al* [27]; the star represents the result of the current calculation using a 2C final state wavefunction.

ratio

$$R(n_2) = \frac{\sigma_a^+(n_2)}{\sigma_a^+(1)}, \tag{5.34}$$

which measures the relative contribution to the total cross section from each branch process, is shown in Fig. (5.2) for satellite $n_2 = 2$ as a function of photon energy E^{-1}. Also included are the result of the calculation using the same initial-state wavefunction but a final state wavefunction without electron-electron correlation (2C). The experimental data of Carlson *et al* [75] and Svensson *et al* [76] is also shown in the figure. The satellite-to-1s ratio R(2) obtained using a 3C final state wavefunction is seen to decrease with increasing energy while the result obtained using a 2C final state wavefunction is a constant in the high energy range. Both results approach the same asymptotic limit (E $\rightarrow \infty$), which is in agreement with the calculation of Dalgarno and Sadeghpour [31].

The double-to-single ratio R_{ph} at high energies is presented in Fig. (5.3). Included are the measurements of Levin et al. [77, 78] around 2 keV and Spielberger et al. [70] at higher energies. In the latter data set contributions from Compton scattering and from photoionization are separated and a direct comparison with photoionization calculations is possible.

In addition to the full 3C final state and the uncorrelated 2C limit we display the convergence as a function of the number of partial waves included in the distortion factor $D^{(-)}$. Taking only the monopole term into account leads to results similar to, but not identical to, Hino's calculations [27] and those emplying MBPT [23, 24]. The step-by-step inclusion of dipole and high

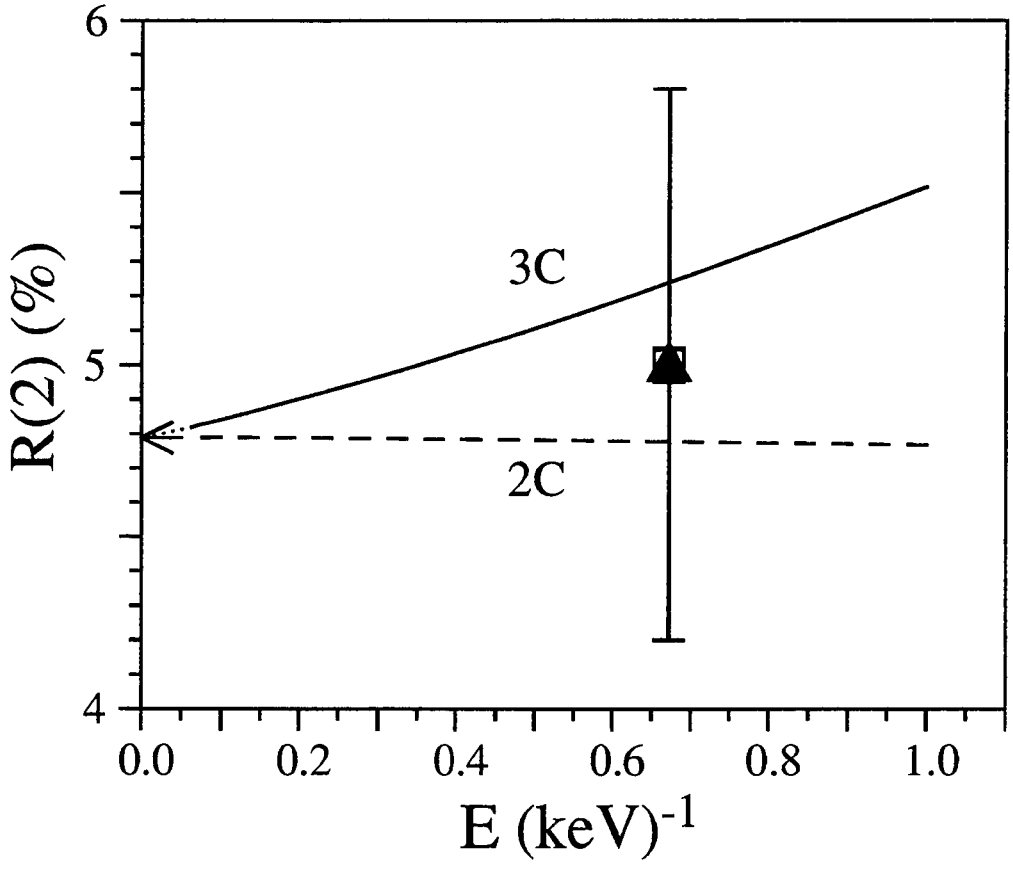

Figure 5.2: Satellite-to-1s ratio of R(2) as a function of incident photon energy E^{-1}. Solid curve: 3C results. Dashed curve: results without the final-state correlation (denoted by 2C). The asymptotic result of Dalgarno and Sadeghpour is indicated by an arrow. Experiment: solid triangle by Carlson *et al* [75]; open square by Svensson *et al* [76].

order partial waves leads to an increase in the total cross section for double photoionization. When the maximum partial wave reaches 4 the calculation has converged. The results of Teng and Shakeshaft [26] show a somewhat similar energy dependence limit but lie systematically higher. In addition to the different gauges applied, the difference comes very likely from the initial-state wavefunction. In the calculation by Teng and Shakeshaft [26] an 8-parameter ground-state wavefunction is used with relative errors in the Kato cusp conditions of about 5% for the confluence of the electron-nucleus coordinates and 35% for the confluence of the electron-electron coordinates at small interparticle separations. In the present calculation they are 0.001% and 9%, respectively.

When all contributing partial waves are summed up ($l \leq 4$) we find that the ratio is in excellent agreement with experimental data. Even more remarkable, the present results merges with the low-energy *ab initio* hyperspherical close coupling calculation at about 1 keV. The relative deviation of about 5% between the HSCC ($R = 2.48\%$) [79, 80] and the 3C function ($R = 2.62\%$) lies well within the theoretical errors of the two methods at this energy.

Figure 5.3: Comparison of ratio R_{ph} calculated using a 3C wavefunction (solid curve) with experimental data and other calculations at high energies. Experimental data: open squares by Levin *et al.* [78]; open triangles by Spielberger *et al.* [70] with Compton scattering excluded. Other calculations: (A) Previous calculations employing a 3C function (dotted curves): a: Ref. [25]; b: Ref. [27]; c: Ref. [26]. The open circles denoted by d ($l \leq 2$) and f ($l \leq 3$) show the convergence of the partial-wave expansion of the distortion factor $D^{(-)}$ in the $\mathbf{r}_{12}$ coordinate at 2 keV photon energy. The dashed curve is the present calculation including the monopole term only. The arrow at 1 keV indicates the calculated ratio by the HSCC method [79, 80]. (B) chained curve by MBPT [24]; dash-double-dotted curve by the dipole response function [29]; long-dash-short-dash curve is the result of present calculation with 2C final state. All the curves in (B) are calculated in the acceleration gauge.

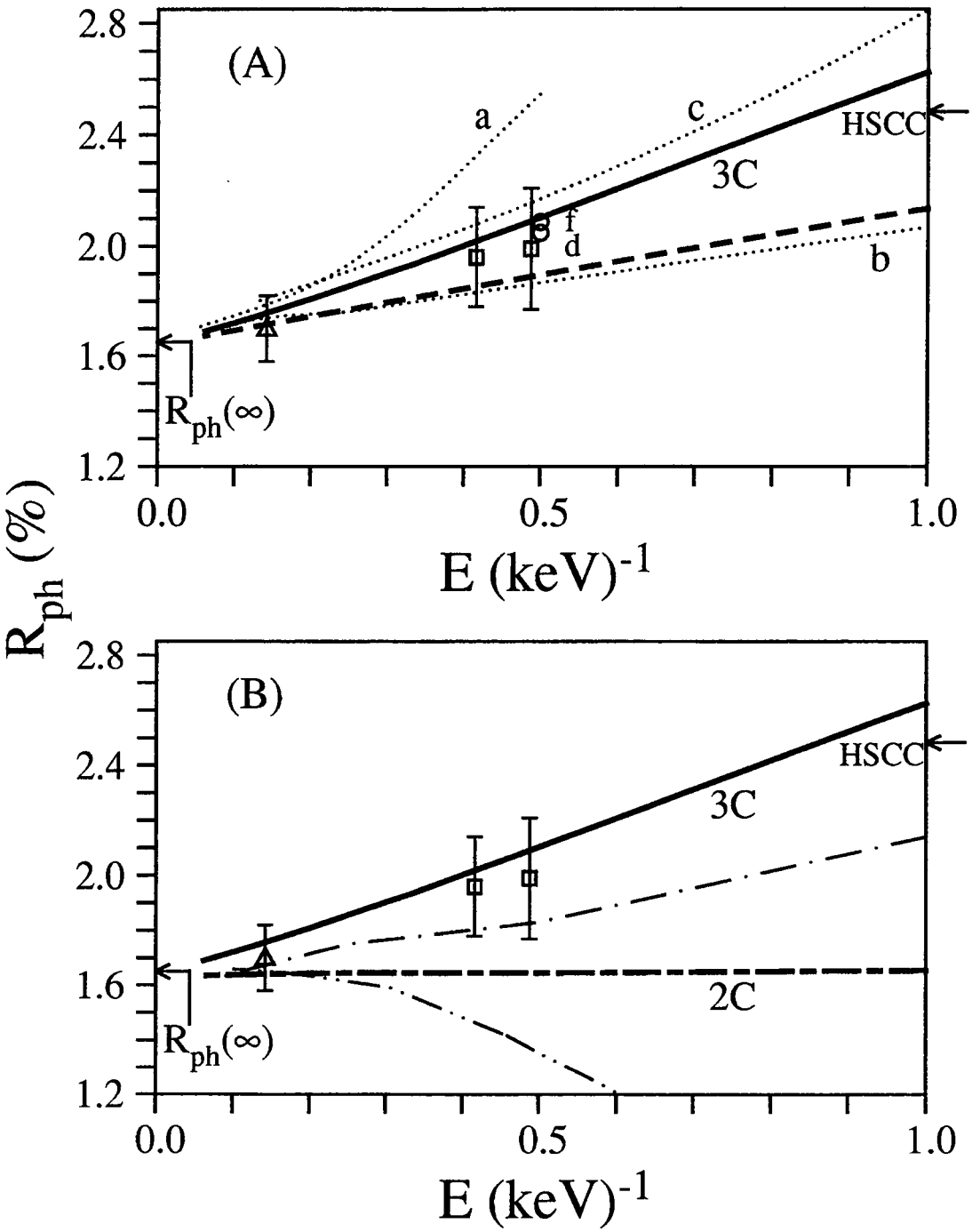
(A)
a
c
HSCC
3C
f
d
b
$R_{ph}(\infty)$
2.8
2.4
2.0
1.6
1.2
0.0
0.5
1.0
R_{ph} (%)
E (keV)$^{-1}$
(B)
HSCC
3C
2C
$R_{ph}(\infty)$
2.8
2.4
2.0
1.6
1.2
0.0
0.5
1.0
E (keV)$^{-1}$

Chapter 6

Two-electron ejection at and near the non-relativistic high-energy limit

Double ionization by a very high energy photon has been of interest since Byron and Joachim discussed it first in the late 1960s [30]. Intensive studies have subsequently been performed by Åberg [81], Brown and Gould [82], Amusia, Drukarev, Gorshkov, and Kazachkov [83], and by Ishihara, Hino, and McGuire [23]. The calculated ratios between the cross sections for double and single ionization range from 1.5% to 2.3%. Using the velocity gauge and an independent-electron final state wave function, Brown and Gould [82] calculated the dipole matrix element and obtained the asymptotic ratio of 2%. In the MBPT calculation, however, Ishihara, Hino, and McGuire [23] arrived at a value of 1.5% at 4 keV photon energy. To find the origin of the discrepancies, Dalgarno and Sadeghpour [31] analyzed the dipole matrix element in the three gauges and found that, when an approximate wave function is applied for large photon energies, the error in the length form

remains unaltered, while in the velocity and acceleration form, the error decays as E_1^{-1} and E_1^{-2}, respectively, where E_1 is the energy of the fast electron. A simple procedure to calculate the ratio based on the closure relation [84, 85] is confirmed. For one-electron ejection from helium, the cross section for ionization-excitation $\sigma_{ph}^{+}(n_2 l_2 m_2)$ is given by

$$\sigma_{ph}^{+}(n_2 l_2 m_2) = \frac{256\pi^2}{3\sqrt{2}cE^{7/2}} \left| \int \phi_{n_2 l_2 m_2}(\mathbf{r}_2)\psi_0(0,\mathbf{r}_2)\mathrm{d}\mathbf{r}_2 \right|^2, \qquad (6.1)$$

where ψ_0 is the initial state wavefunction and $\phi_{n_2 l_2 m_2}$ is the hydrogenic bound state wavefunction of the "shake-up" electron. The total cross section for single ionization is given by

$$\sigma^{+} = \sum_{n_2 l_2 m_2} \sigma_{ph}^{+}(n_2 l_2 m_2), \qquad (6.2)$$

and the cross section of single *plus* double ionization is obtained by an application of the closure relation

$$\sigma_{tot} = \int \sum_{n_2 l_2 m_2} \sigma_{ph}^{+}(n_2 l_2 m_2) = \frac{256\pi^2}{3\sqrt{2}cE^{7/2}} \int |\psi_0(0,\mathbf{r}_2)|^2 \, d\mathbf{r}_2. \qquad (6.3)$$

With the 34 term ground state wave function of helium the asymptotic ratio evaluated at 16 keV is

$$R_{ph}(\infty) = \left[\frac{\sigma_{tot} - \sigma^{+}}{\sigma^{+}} \right]_{E\to\infty} = 1.64\%, \qquad (6.4)$$

which is in agreement with the full calculation of the dipole matrix element. However, the absolute cross sections for double and single ionization deviate from those obtained using the full calculation in the non-relativistic high energy limit. Fig. (6.2) displays the ratio of the single ionization cross

section σ^+ evaluated with the asymptotic formulas (Eqs. (6.1,6.2)) to that obtained using the full calculation of the dipole matrix element (dash curve). The result approaches unity only at about 0.5 MeV, which is beyond the non-relativistic limit. In this chapter we will analyze the acceleration dipole matrix element and introduce a correction in Eqs. (6.1,6.3) which can dramatically improve the evaluation. Moreover, we extend the scope of validity of the formulas by introducing final-state correlation. The improved formulas work well for finite photon energy down to about 2 keV in the case of double photoionization.

6.1 Non-relativistic asymptotic behavior of the two-electron ejection

At very high photon energies E the singly ionized final-state ψ_f can be constructed as a product of a bound state $\phi_{n_2 l_2 m_2}$ and a plane wave $e^{i\mathbf{kr}}$

$$\psi_f(\mathbf{r}_1, \mathbf{r}_2) = \frac{\sqrt{k}}{\sqrt{2}(2\pi)^{3/2}} \left[\phi_{n_2 l_2 m_2}(\mathbf{r}_2) e^{i\mathbf{k}\mathbf{r}_1} + \phi_{\mathrm{n_2 l_2 m_2}}(\mathbf{r}_1) e^{i\mathbf{k}\mathbf{r}_2}\right], \tag{6.5}$$

where $\mathbf{r}_1$ and $\mathbf{r}_2$ are the electron coordinates, $\mathbf{k}$ is the momentum of the escaping electron, and the factor $\sqrt{k}$ indicates that the continuum wave function is energy normalized. The dipole transition matrix element $\mathbf{T}$ from the ground state ψ_0 to the singly ionized final state ψ_f in acceleration gauge is

$$\mathbf{T} = \langle \psi_0 \mid \frac{\mathbf{r}_1}{\mathrm{r}_1^3} + \frac{\mathbf{r}_2}{\mathrm{r}_2^3} \mid \psi_f \rangle^1. \tag{6.6}$$

[1] For convenience we discuss here the conjugate of the dipole transition matrix element, but the result remains unchanged for the dipole matrix element itself.

Using the symmetry properties of the wave functions and the dipole operator, Eq. (6.6) becomes

$$\mathbf{T}_s = \frac{\sqrt{2k}}{(2\pi)^{3/2}}(Term1 + Term2), \tag{6.7}$$

where

$$Term1 \equiv \int \psi_0(\mathbf{r}_1, \mathbf{r}_2)\frac{\mathbf{r}_1}{\mathrm{r}_1^3}\phi_{\mathrm{n_2 l_2 m_2}}(\mathbf{r}_2)\mathrm{e}^{\mathrm{i}\mathbf{k}\mathbf{r}_1}\mathrm{d}\mathbf{r}_1\mathrm{d}\mathbf{r}_2, \tag{6.8}$$

and

$$Term2 \equiv \int \psi_0(\mathbf{r}_1, \mathbf{r}_2)\frac{\mathbf{r}_1}{\mathrm{r}_1^3}\phi_{\mathrm{n_2 l_2 m_2}}(\mathbf{r}_1)\mathrm{e}^{\mathrm{i}\mathbf{k}\mathbf{r}_2}\mathrm{d}\mathbf{r}_1\mathrm{d}\mathbf{r}_2. \tag{6.9}$$

Noting that

$$\frac{i\mathbf{r}}{r^3} = \frac{1}{2\pi^2}\int \frac{d\mathbf{k}'}{k'^2}\mathbf{k}' e^{i\mathbf{k}'\cdot\mathbf{r}}$$

and

$$\delta(\mathbf{r}) = \frac{1}{(2\pi)^3}\int d\mathbf{k}' e^{i\mathbf{k}'\cdot\mathbf{r}}, \tag{6.10}$$

we have

$$Term1 = -\frac{i}{2\pi^2}\int \frac{d\mathbf{k}'}{k'^2}\mathbf{k}' e^{i\mathbf{k}'\cdot\mathbf{r}_1}\psi_0(\mathbf{r}_1, \mathbf{r}_2)\phi_{n_2 l_2 m_2}(\mathbf{r}_2)e^{i\mathbf{k}\cdot\mathbf{r}_1}d\mathbf{r}_1 d\mathbf{r}_2.$$

Since the ejected electron receives most of the energy from the high energy photon, we make following replacement:

$$\mathbf{k}' + \mathbf{k} = \mathbf{p}$$

$$\frac{1}{k'^2} \approx \frac{1}{k^2}(1 + \frac{2\mathbf{k}\cdot\mathbf{p}}{k^2}), \quad p < k,$$

therefore,

$$Term1 = -\frac{i}{2\pi^2}\int_{p<k}\int \frac{d\mathbf{p}}{k^2}(\mathbf{p}-\mathbf{k}+\frac{2\mathbf{k}\cdot\mathbf{p}}{k^2})e^{i\mathbf{p}\cdot\mathbf{r}_1}\psi_0(\mathbf{r}_1,\mathbf{r}_2)\phi_{n_2l_2m_2}(\mathbf{r}_2)d\mathbf{r}_1d\mathbf{r}_2.$$

Let us define a shape function

$$f_k(\mathbf{r}_1) \equiv \frac{1}{(2\pi)^3}\int_{\mathrm{p<k}} \mathrm{dp}e^{\mathrm{ip}\cdot\mathbf{r}_1}.$$

The integral of f_k can be carried out easily by making a partial wave expansion of the plane wave in which only the s wave survives. We then obtain

$$f_k(\mathbf{r}_1) = \frac{\sin(\mathrm{kr}_1)-\mathrm{kr}_1\cos(\mathrm{kr}_1)}{2\pi^2\mathrm{r}_1^3}. \tag{6.11}$$

Fig. (6.1) displays the behavior of the shape function at different photon energies. The profile becomes narrow and steep as the energy increases to keep the integrated area at unity. The width of the function is proportional to $E^{-1/2}$. In the asymptotic limit

$$\lim_{k\to\infty} f_k(\mathbf{r}) = \delta(\mathbf{r}). \tag{6.12}$$

Noting that

$$-\mathbf{k}\int_{p<k} d\mathbf{p}e^{i\mathbf{p}\cdot\mathbf{r}_1} = -\mathbf{k}8\pi^3 f_k(\mathbf{r}_1)$$

and

$$\int_{p<k} d\mathbf{p}\mathbf{p}e^{i\mathbf{p}\cdot\mathbf{r}_1} = -i8\pi^3\nabla_1 f_k(\mathbf{r}_1),$$

we find

$$\begin{aligned} Term1 \;=\; & \frac{i4\pi}{k^2}\Big\{\mathbf{k}\int f_k(\mathbf{r}_1)\psi_0(\mathbf{r}_1,\mathbf{r}_2)\phi_{\mathrm{n_2l_2m_2}}(\mathbf{r}_2)\mathrm{d}\mathbf{r}_1\mathrm{d}\mathbf{r}_2 \\ & -i\int f_k(\mathbf{r}_1)\nabla_1\psi_0(\mathbf{r}_1,\mathbf{r}_2)\phi_{\mathrm{n_2l_2m_2}}(\mathbf{r}_2)\mathrm{d}\mathbf{r}_1\mathrm{d}\mathbf{r}_2 \\ & +\frac{2i\mathbf{k}}{k^2}\int f_k(\mathbf{r}_1)\mathbf{k}\cdot\nabla_1\psi_0(\mathbf{r}_1,\mathbf{r}_2)\phi_{\mathrm{n_2l_2m_2}}(\mathbf{r}_2)\mathrm{d}\mathbf{r}_1\mathrm{d}\mathbf{r}_2\Big\} \end{aligned}$$

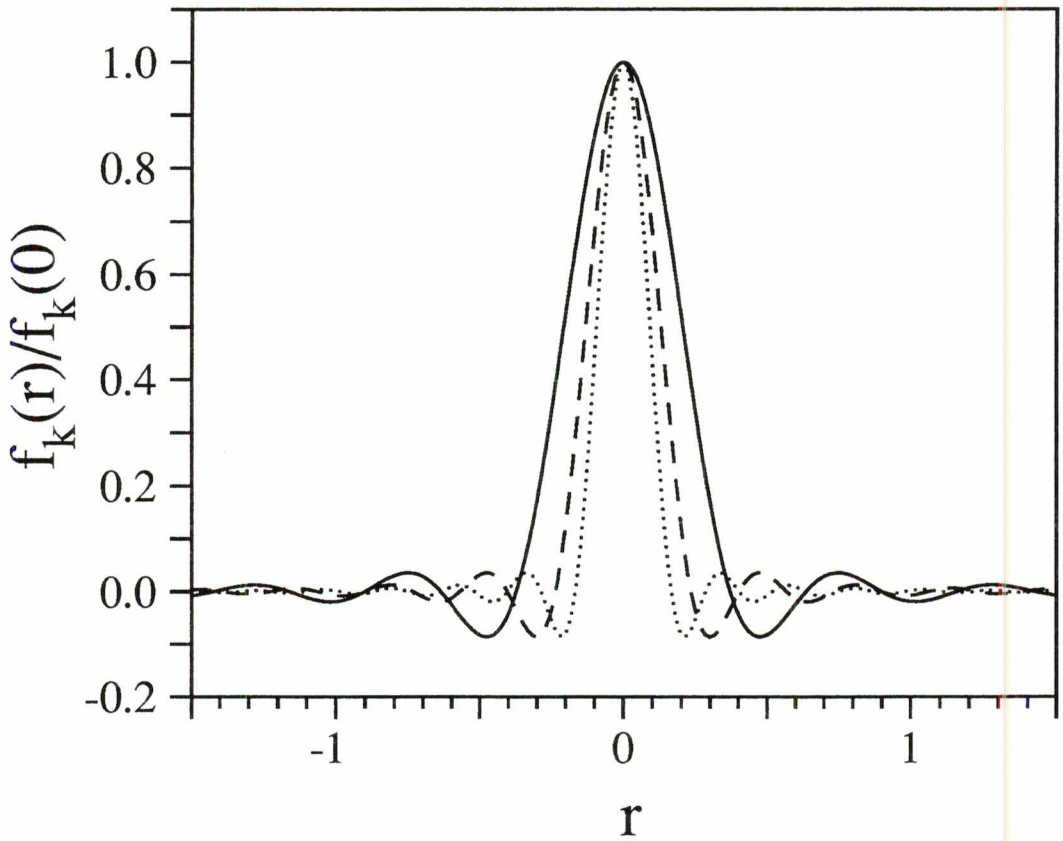

Figure 6.1: Shape function at different energies: solid curve at 2 keV; dash curve at 5 keV; and dotted curve at 10 keV. The values at the origin are 30, 119, and 336, respectively.

and

$$|\,Term1\,|^2 = \frac{(4\pi)^2}{k^2}\left\{\left|\int f_k(\mathbf{r}_1)\psi_0(\mathbf{r}_1,\mathbf{r}_2)\phi_{\mathbf{n}_2\mathbf{l}_2\mathbf{m}_2}(\mathbf{r}_2)\mathbf{dr}_1\mathbf{dr}_2\right|^2 + \frac{1}{k^2}\left|\int f_k(\mathbf{r}_1)\nabla_1\psi_0(\mathbf{r}_1,\mathbf{r}_2)\phi_{\mathbf{n}_2\mathbf{l}_2\mathbf{m}_2}(\mathbf{r}_2)\mathbf{dr}_1\mathbf{dr}_2\right|^2\right\}. \tag{6.13}$$

For $Term2$, we note that $e^{i\mathbf{k}\cdot\mathbf{r}_2}$ is a highly oscillatory function of $\mathbf{r}_2$ when k is large and $\psi_0(\mathbf{r}_1,\mathbf{r}_2)$ is a slow varying function, therefore, $Term2$ can be approximated as

$$Term2 \approx \int d\mathbf{r}_1\psi_0(\mathbf{r}_1,\langle\mathbf{r}_2\rangle)\frac{\mathbf{r}_1}{r_1^3}\phi_{n_2l_2m_2}(\mathbf{r}_1)\int d\mathbf{r}_2 e^{i\mathbf{k}\cdot\mathbf{r}_2},$$

where $\langle\mathbf{r}_2\rangle$ is the average coordinate of $\mathbf{r}_2$ such that

$$\int d\mathbf{r}_2\psi_0(\mathbf{r}_1,\mathbf{r}_2)e^{i\mathbf{k}\cdot\mathbf{r}_2} \approx \psi_0(\mathbf{r}_1,\langle\mathbf{r}_2\rangle)\int d\mathbf{r}_2 e^{i\mathbf{k}\cdot\mathbf{r}_2}.$$

Because

$$\int d\mathbf{r}_2 e^{i\mathbf{k}\cdot\mathbf{r}_2} = 0$$

for $\mathbf{k} \neq 0$, $Term2$ vanishes. Therefore, the dipole matrix element is

$$\mathbf{T}_s = \frac{\sqrt{2k}}{(2\pi)^{3/2}}\cdot Term1. \tag{6.14}$$

The branching cross section from the ground state to the single continuum state with the bound electron in a state $n_2l_2m_2$ is given by

$$\sigma^+_{ph}(n_2l_2m_2) = \frac{4\pi^2Z^2}{3cE^3}\int d\hat{k}\;|\,\mathbf{T}_s\,|^2, \tag{6.15}$$

where Z is the charge of the nucleus. Using the Eqs. (6.13,6.14) and $k \approx \sqrt{2E}$, we have

$$\sigma^{+}_{ph}(n_2 l_2 m_2) = \frac{64\pi^2 Z^2}{3\sqrt{2}cE^{7/2}} \left\{ \left| \int\int f_{k_1}(\mathbf{r}_1)\phi_{\mathrm{n_2 l_2 m_2}}(\mathbf{r}_2)\psi_0(\mathbf{r}_1,\mathbf{r}_2)\mathrm{d}\mathbf{r}_1\mathrm{d}\mathbf{r}_2 \right|^2 + \frac{1}{2E}\left| \int\int f_{k_1}(\mathbf{r}_1)\phi_{\mathrm{n_2 l_2 m_2}}(\mathbf{r}_2)\nabla_1\psi_0(\mathbf{r}_1,\mathbf{r}_2)\mathrm{d}\mathbf{r}_1\mathrm{d}\mathbf{r}_2 \right|^2 \right\}. \tag{6.16}$$

The total cross section for single ionization is given by the incoherent superposition of individual ionization-excitation cross sections

$$\sigma^{+} = \sum_{n_2 l_2 m_2} \sigma^{+}_{ph}(n_2 l_2 m_2). \tag{6.17}$$

Similarly, by an application of the closure relation

$$\int \sum_{n_2 l_2 m_2} \mid n_2 l_2 m_2\rangle\langle n_2 l_2 m_2 \mid = 1,$$

the cross section for double *plus* single ionization can be obtained

$$\begin{aligned} \sigma_{tot} &= \int \sum_{n_2 l_2 m_2} \sigma^{+}_{ph}(n_2 l_2 m_2) \\ &= \frac{64\pi^2 Z^2}{3\sqrt{2}cE^{7/2}} \left\{ \int \left| \int f_{k_1}(\mathbf{r}_1)\psi_0(\mathbf{r}_1,\mathbf{r}_2)\mathrm{d}\mathbf{r}_1 \right|^2 d\mathbf{r}_2 \right. \\ &\quad \left. + \frac{1}{2E}\int \left| \int f_{k_1}(\mathbf{r}_1)\nabla_1\psi_0(\mathbf{r}_1,\mathbf{r}_2)\mathrm{d}\mathbf{r}_1 \right|^2 d\mathbf{r}_2 \right\}. \end{aligned} \tag{6.18}$$

The cross section for double ionization σ^{++} and the ratio R_{ph} are therefore determined:

$$\sigma^{++} = \sigma_{tot} - \sigma^{+} \tag{6.19}$$

$$R_{ph} = \sigma^{++}/\sigma^{+}. \tag{6.20}$$

At infinite photon energy (beyond the non-relativistic limit), the second term in Eqs. (6.16,6.18) becomes negligible compared to the first term and the shape function f_k changes into a δ function (Eq. 6.12). In this limit, the Eqs. (6.16,6.18) transform into the formulas confirmed by Dalgarno and Sadeghpour (Eqs. (6.1,6.3)). At finite photon energies, however, the shape function f_k in Eqs. (6.16,6.18) specifies the reaction zone of the photon-atom interaction which is localized within a distance of $\sim E^{-1/2}$ around the nucleus.

At finite photon energies, in addition to the double-to-single cross section ratio, the absolute cross sections can be well described by Eqs. (6.16-6.18) when only the first term in Eqs. (6.16, 6.18) is applied. Fig. (6.2) displays the ratio of the single ionization cross section σ^{+} evaluated with the first term in Eq. (6.16) and Eq. (6.17) to that obtained using the full calculation of the dipole matrix element (solid curve). The improvement over the procedure of Dalgarno and Sadeghpour is significant at 16 keV. Moreover, the first term in Eq. (6.16) and Eq. (6.17) permits the extrapolation down to about 10 keV with only a small error ($\lesssim 4\%$). The second term in Eqs. (6.16,6.18) contributes only a very small amount to the total cross sections, however, it does signal the E^{-1} behavior of the ratio near the asymptotic limit.

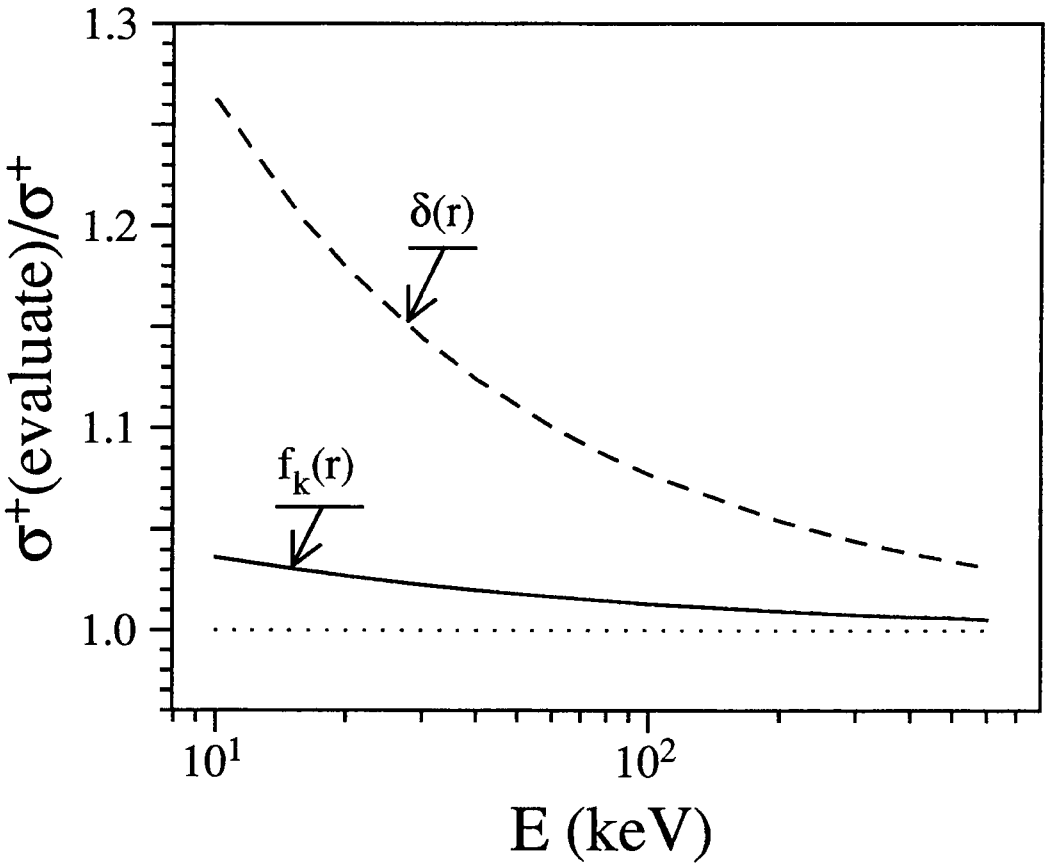

Figure 6.2: Ratios of the single ionization cross section evaluated with the asymptotic formulas to that obtained using the full calculation of the dipole matrix element: solid curve: the first term of Eq. (6.16) and Eq. (6.17); dashed curve: Eqs. (6.1,6.2).

6.2 Two-electron ejection near the non-relativistic high-energy limit

In last section we analyzed the acceleration dipole matrix element and introduced a shape function in Eqs. (6.1,6.3). The improved formulas can predict accurately not only the double-to-single ratio but also the absolute cross sections at the non-relativistic limit. In this section we extend the validity of the formulas down to a few keV by introducing final state correlation.

For single ionization, the correlated final state wavefunction is

$$\psi_f(\mathbf{r}_1,\mathbf{r}_2) = \frac{\sqrt{k}}{\sqrt{2}(2\pi)^{3/2}}\left[\phi_{n_2l_2m_2}(\mathbf{r}_2)e^{i\mathbf{k}\mathbf{r}_1}D^{(-)}(\mathbf{r}_1,\mathbf{r}_2) + \mathbf{r}_1 \leftrightarrow \mathbf{r}_2\right], \qquad (6.21)$$

where $D^{(-)}(\mathbf{r}_1,\mathbf{r}_2)$ is a distortion factor to be determined. In chapter 3 and chapter 5 we have shown that the 3C wavefunction appropriately describes the final state correlation to the order of Z/k_1 where k_1 is the momentum of the fast electron. In the partial wave expansion of the 3C wavefunction the leading contribution has also shown to arise from the s wave. Therefore we choose $D^{(-)}(\mathbf{r}_1,\mathbf{r}_2) \equiv d^{(-)}_{l=0}(\mathbf{r}_1,\mathbf{r}_2)$ to describe approximately the final state correlation.

Following the discussion of the last section, we obtain the cross section for single ionization

$$\sigma^+ = \sum_{n_2l_2m_2}\frac{64\pi^2Z^2}{3\sqrt{2}cE^{7/2}} \cdot\left\{\left|\int\int f_{k_1}(\mathbf{r}_1)\phi_{n_2l_2m_2}(\mathbf{r}_2)\psi_0(\mathbf{r}_1,\mathbf{r}_2)d^{(-)}_{l=0}(\mathbf{r}_1,\mathbf{r}_2)d\mathbf{r}_1d\mathbf{r}_2\right|^2\right.$$

$$+\frac{1}{2E}\left|\int\int f_{k_1}(\mathbf{r}_1)\phi_{n_2l_2m_2}(\mathbf{r}_2)\nabla_1[\psi_0(\mathbf{r}_1,\mathbf{r}_2)\mathrm{d}^{(-)}_{l=0}(\mathbf{r}_1,\mathbf{r}_2)]\mathrm{d}\mathbf{r}_1\mathrm{d}\mathbf{r}_2\right|^2\Bigg\}. \tag{6.22}$$

and that for single *plus* double ionization

$$\sigma_{tot}=\frac{64\pi^2Z^2}{3\sqrt{2}cE^{7/2}}\left\{\int\left|\int f_{k_1}(\mathbf{r}_1)\psi_0(\mathbf{r}_1,\mathbf{r}_2)\mathrm{d}^{(-)}_{l=0}(\mathbf{r}_1,\mathbf{r}_2)\mathrm{d}\mathbf{r}_1\right|^2 d\mathbf{r}_2\right.$$
$$\left.+\frac{1}{2E}\int\left|\int f_{k_1}(\mathbf{r}_1)\nabla_1[\psi_0(\mathbf{r}_1,\mathbf{r}_2)\mathrm{d}^{(-)}_{l=0}(\mathbf{r}_1,\mathbf{r}_2)]\mathrm{d}\mathbf{r}_1\right|^2 d\mathbf{r}_2\right\}. \tag{6.23}$$

The cross section for double ionization and the ratio R_{ph} are therefore determined (Eqs. (6.19,6.20)). Fig. (6.3) displays the double-to-single cross section ratio evaluated with only the first term in Eqs. (6.22,6.23)[2]. Also shown are the acceleration-gauge results of MBPT [24] and the very recent ones obtained using a dipole response function [29]. The experiment data of Levin et al. [77, 78] around 2 keV and Spielberger *et al* [70] at higher energies are also included for comparison. The results obtained with the present very simple method agree quite well with those of the MBPT calculation and with the measurements. It displays, however, much better behavior than that of the recently introduced dipole response function.

[2]The contribution from the second term is very small but the evaluation is complicated, therefore, we skip the evaluation.

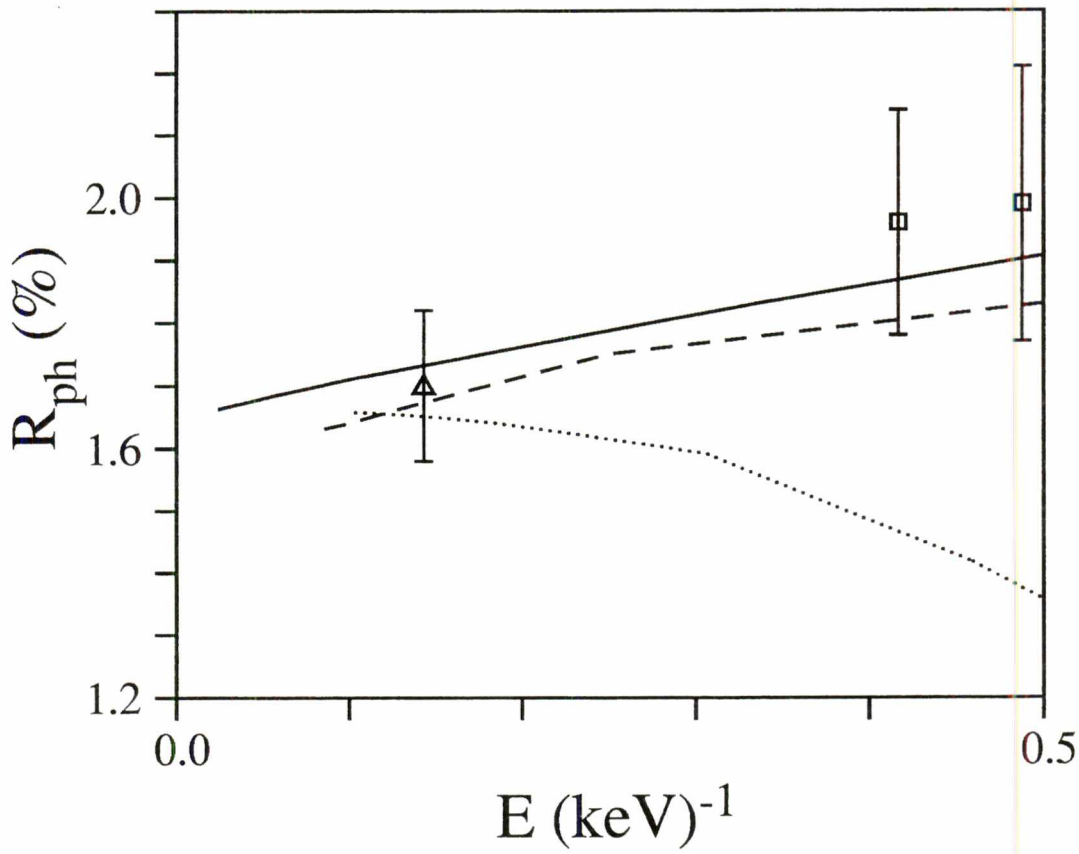

Figure 6.3: Double-to-single cross section ratio evaluated using the first terms in Eqs. (6.22,6.23) (solid curve) together with other results. Experimental data: open squares by Levin *et al.* [78]; open triangles by Spielberger *et al.* [70] with Compton scattering excluded. Other calculations: dash curve by MBPT [24]; dotted curve by use of the dipole response function [29].

6.3 Contribution of retardation to the total cross sections

In the calculation of the ratio $R_{ph} = \sigma^{++}/\sigma^{+}$, a non-relativistic formulation and the dipole approximation are commonly used. However, at high photon energies, we are no longer in a regime where the dipole approximation is necessarily valid. It becomes necessary to investigate the influence of retardation and the higher order photon multipoles on the photoeffect ratio.

For single photoionization, it is known that cross sections that do not neglect retardation differ from the dipole results by quantities of the order $(v/c)^2$ [86, 87], where v is the momentum of the ejected electron. It should be mentioned that the corrections of this order result from the application of both the relativistic Dirac formulation [86] and the non-relativistic formulation [87].

The effect of retardation on double photoionization has also been investigated [87, 88, 89]. It has been shown [87], based on the non-relativistic formulation, that retardation accounts for only 0.4% of the total cross section σ^{++} for helium at a photon energy of 1 keV; retardation accounts for 4.8% of the total cross section at 12 keV, i.e., the dipole approximation accounts for 95.2% of the contribution, which is accurate enough for the present theoretical investigations. Moreover, the cross section for double photoionization behaves similarly as that for single photoionization,

$$\frac{\sigma^{++}_{ret}}{\sigma^{++}_{dip}} = 1 + \left(\frac{v_m}{c}\right)^2 \tag{6.24}$$

where v_m is the maximum momentum of an electron. Note the fact that the shake-off mechanism dominates the contribution to the total cross section σ^{++} in the high energy regime, the above results are understandable. The mechanism specifies that in the case of double photoionization one of the electrons takes almost all of the photon energy while the other electron, which can be taken as non-relativistic escapes, independent of the incident photon energy, via relaxation. Therefore, even though the total energy of the two electrons is in the relativistic energy region, Eq. (6.24) is still expected to be applicable. The fact that corrections of the same order appear in both the single and double photoionization cross sections justifies the use of the dipole approximation in the evaluation of the double-to-single ratio at high photon energies.

Chapter 7

One- and two-electron detachment of H^- by high-energy photons

In chapter 5 and chapter 6, we have discussed the electron-electron correlation in He and investigated double photoionization cross section using an accurate ground state wavefunction and a correlated 3C wavefunction. Similar to He, H^- is also an ideal prototype system for the study of the electron-electron correlation because of its simplicity. Unlike He, however, the electron-electron repulsion almost matches in strength the electron-nucleus attraction. The potential is

$$\begin{aligned} V &= -\frac{1}{r_1} - \frac{1}{r_2} + \frac{1}{r_{12}} \\ &= -\frac{1}{r_<} + \frac{r_<}{r_>^2} + ..., \end{aligned} \tag{7.1}$$

i. e., the electron moving in the outer region of the configuration space only experiences the effect of a dipole-term field which is of short range. As a consequence, the two electrons are bound in the only two bound states with

each for singlet and triplet states, respectively. Moreover, one-electron detachment of H^- leaves behind a neutral atom. When a high-energy photon interacts with this two-electron system, usually one electron is emitted with high energy while the other is ionized through an electron-electron shake-off process. For H^-, the fast electron is influenced by the short-range potential rather than a Coulombic one. Therefore, photodetachment of H^- is expected to display dynamic features different from those of He. Up to now, limited attention has been devoted to investigating the double emission process of H^- [90, 91, 92, 93, 94]. Most of the studies have concentrated on the behavior of the two-electron escape near threshold[90, 91, 92], in part due to its astrophysical importance. For the higher energy range (up to $\sim$ 100 eV), Broad and Reinhardt made the first calculation over twenty years ago[93] using a multichannel J-matrix technique with an L^2 basis set. Very recently, the eigenchannel R-matrix method with a local finite element basis set was applied by Meyer, Greene, and Esry [95]. The results of Meyer, Greene, and Esry agree approximately with the prediction of Broad and Reinhardt in peak position of the ratio between the double- and single-electron detachment, but sharply differ in magnitudes. Moreover, R_{ph} for H$-$ is systematically higher than the corresponding value for He. In the non-relativistic high-energy limit, Dalgarno and Sadeghpour [31] obtained an asymptotic ratio $R_{ph}(\infty)$ of 1.51%. In the high but finite photon energy region, no reliable calculation is currently available to our knowledge. We report here on the first reliable calculation for photon energies above 1 keV. The method applied to H$-$ is

similar to that used for He. We calculate the binding energy and ground state wavefunction in the Hylleraas coordinate basis set and apply the 3C wavefunction for the double continuum state. We find that the electron-electron correlations in both the initial and the final states are crucial for the photodetachment process of H^- at high energies.

7.1 Ground state wavefunction of H^-

The procedure for obtaining the ground state wavefunction of H^- is the same as that for He, however, the convergence rates for both systems are different. We therefore have examined the binding energies and the wavefunctions obtained with different numbers of basis functions NBF.

With $\sigma = 1.524248$ and $NBF = 43$ we obtain the binding energy of 0.527681, compared to the "exact" energy 0.527751 [37]. In Tab. (7.1) we tabulate the coefficients of the wavefunction. The relative errors in the cusp conditions of the 43-term Hylleraas wavefunction as a function of the radial coordinate are shown in Fig. 7.1. We find that the Kato cusp conditions are satisfied with a relative error of less than 3% pertaining to the confluence of the electron-nucleus coordinates and less than 1% for the confluence of the interelectronic coordinates.

The contour plot of the joint probability density $\rho(r_1, r_2)$ as a function of the two-electron radial coordinates is shown in Fig. 7.2. The characteristic binding radii corresponding to the peak position of ρ are found to be $r_1 \approx r_2 \approx 1.5$, which is about twice as that of He. Furthermore, its density

Table 7.1: Normalized ground state wavefunction of H^- in 43 term Hylleraas coordinate basis functions.

l	m	n	C_{lmn}	l	m	n	C_{lmn}
0	0	0	7.157047×10^{-2}	2.5	0	1	-1.418312×10^{-3}
0	0	1	2.370987×10^{-2}	3.5	0	0	2.688384×10^{-4}
1	0	0	-1.266266×10^{-2}	0.5	2	1	1.837742×10^{-3}
0.5	0	1	-3.431578×10^{-3}	1.5	2	0	-3.483315×10^{-4}
1.5	0	0	5.725485×10^{-3}	0	0	4	-1.113159×10^{-6}
0	0	2	-7.922958×10^{-3}	1	0	3	9.402090×10^{-5}
1	0	1	2.564644×10^{-3}	2	0	2	-3.448736×10^{-4}
2	0	0	-1.816601×10^{-3}	3	0	1	2.337865×10^{-4}
0	2	0	4.011924×10^{-3}	4	0	0	-4.489179×10^{-5}
0.5	0	2	1.017276×10^{-2}	0	2	2	-1.395440×10^{-5}
1.5	0	1	-5.292501×10^{-3}	1	2	1	-5.653002×10^{-4}
2.5	0	0	1.223378×10^{-3}	2	2	0	1.753835×10^{-4}
0.5	2	0	-9.057300×10^{-5}	0	4	0	-2.276712×10^{-5}
0	0	3	5.047268×10^{-4}	0.5	0	4	4.187238×10^{-7}
1	0	2	-6.335449×10^{-3}	1.5	0	3	-8.515944×10^{-6}
2	0	1	4.028368×10^{-3}	2.5	0	2	2.199329×10^{-5}
3	0	0	-7.801937×10^{-4}	3.5	0	1	-1.451680×10^{-5}
0	2	1	-1.945814×10^{-3}	4.5	0	0	2.876307×10^{-6}
1	2	0	-7.373061×10^{-5}	0.5	2	2	5.481879×10^{-6}
0.5	0	3	-3.758691×10^{-4}	1.5	2	1	5.436521×10^{-5}
1.5	0	2	2.109831×10^{-3}	2.5	2	0	-2.045828×10^{-5}
				0.5	4	0	1.193330×10^{-5}

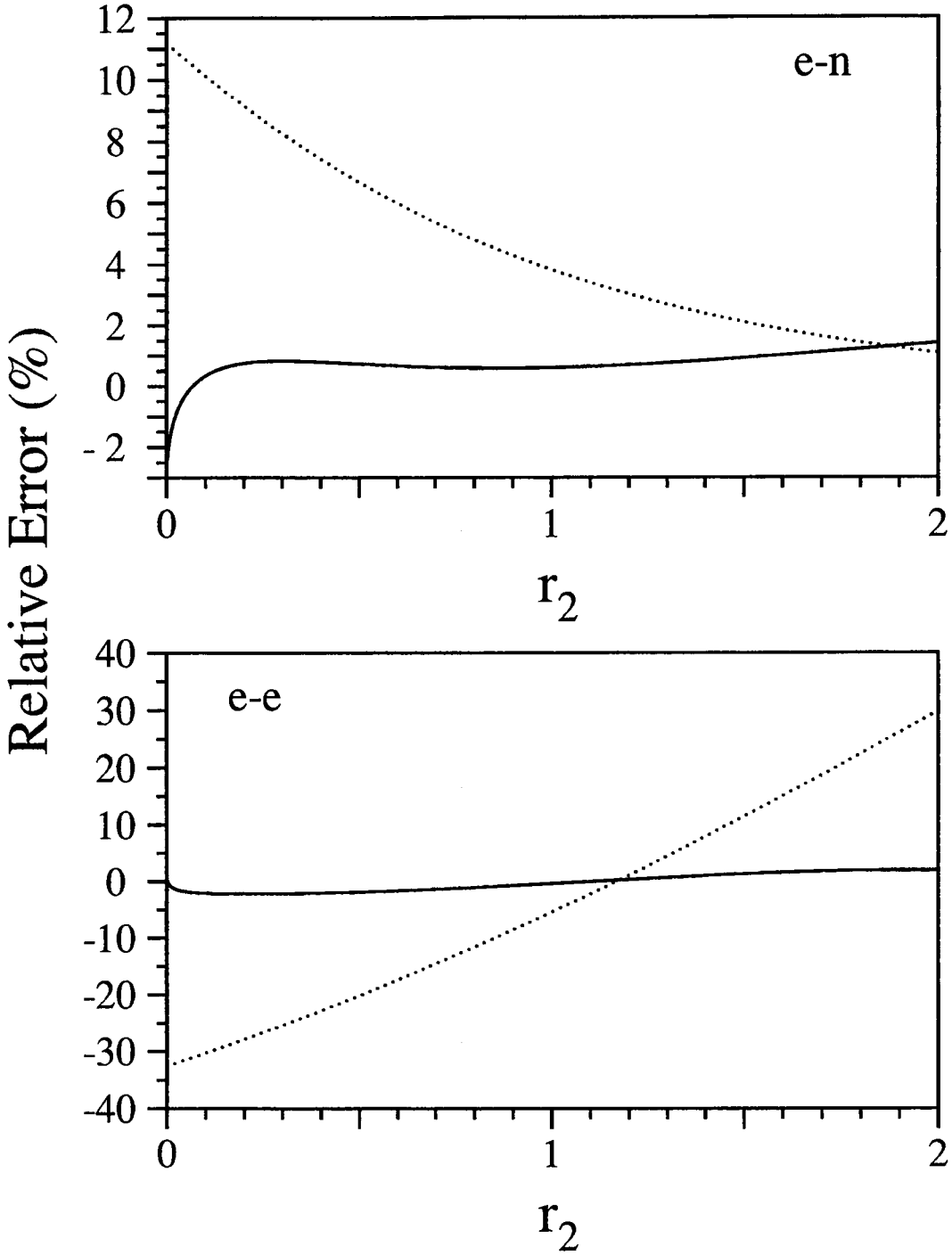

Figure 7.1: Relative errors in the Kato cusp conditions for the 43-term solution of the ground state wavefunction for H− (solid curve) compared to those obtained using the 20 term representation of Hart and Herzberg[34] (dotted curve). The upper plot shows the confluence of electron and nucleus (e-n) and the lower plot shows the confluence of the two electrons (e-e).

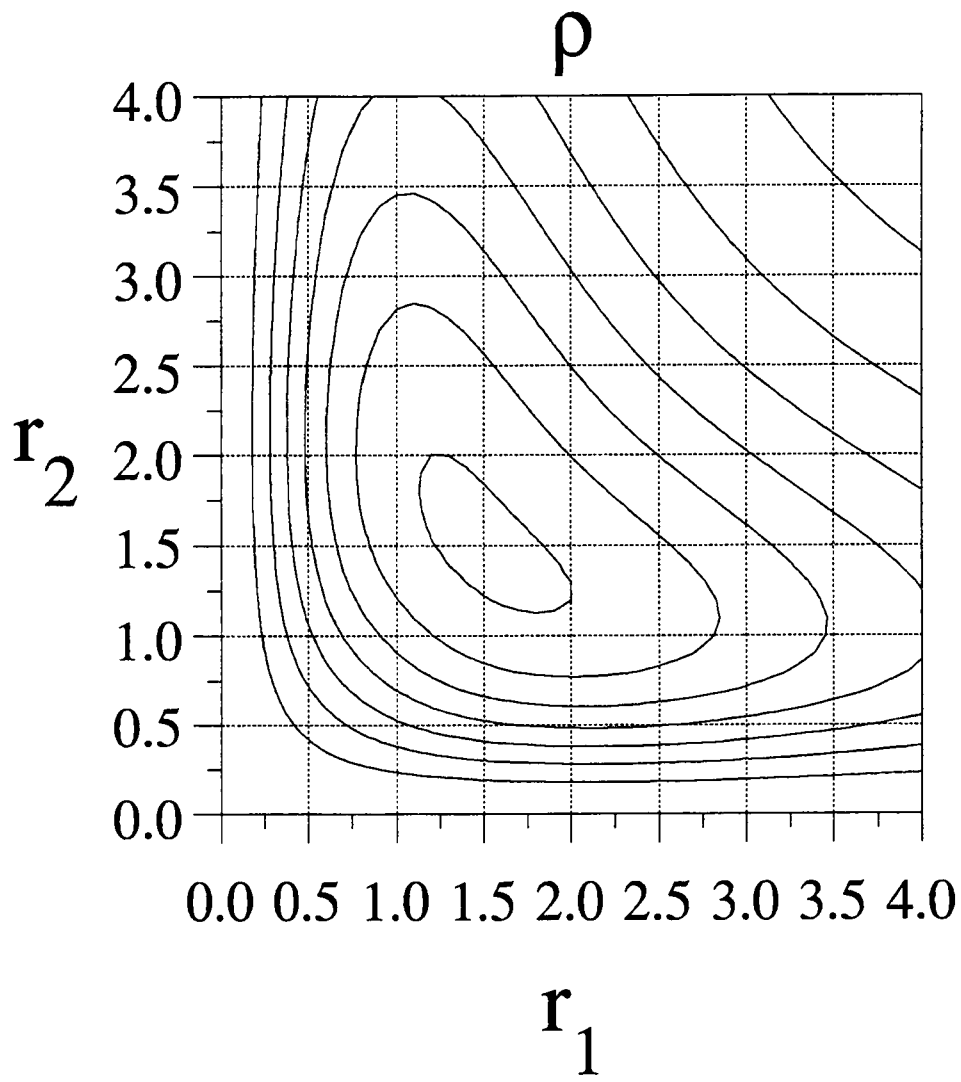

Figure 7.2: Contour plot of the joint density $\rho(r_1, r_2)$ of the ground state of H− as a function of the two electron radial coordinates. The value for each contour curve is n times 1.05×10^{-2} with n=1 for the outest curve and n=7 for the inner most curve.

distribution is strongly shifted away from the diagonal (i. e. the $r_1 \approx r_2$ line). This property has significant implications for the differences of ionization-excitation and double photoionization in the H− and He systems.

7.2 Final state wavefunction of H^-

For the final state, we employ the 3C wavefunction with

$$\eta_1 = -\frac{1}{k_1},$$
$$\eta_2 = -\frac{1}{k_2},$$

and

$$\eta_{12} = \frac{1}{2k_{12}}. \tag{7.2}$$

In chapter 3 we showed that the 3C wavefunction satisfies the cusp conditions for any two-electron systems in both the electron-nucleus and electron-electron coordinates near the origin. This is crucial for the shake-off process which is governed by the behavior of the wavefunction at small interparticle distances. In addition, we argued that the 3C wavefunction is the appropriate solution for He in the perturbative regime of small Sommerfeld parameters $Z/k_1 \gg 1$ where k_1 is the velocity of the fast electron. The justification for this assumption comes from the fact that the residual terms in the Schrödinger equation, $\mathbf{M}_i$ (i=1,2), are bound in the full configuration space and in the dominant region contributing to dipole matrix element of double photoionization, $|\mathbf{M}_i| \lesssim 1$.

The assumption remains valid for the H^- system. Fig. 7.3 displays the radial and angular dependence of M_i for typical values of k_i representing a fast electron (i=1) and a slow electron (i=2) in the double photodetachment continua of H^- at an energy $E_1 + E_2 = 1$ keV. Therefore, following the discussion in chapter 3, the 3C function is still the appropriate three-body final state wavefunction for H^- to leading order in $1/k_1$ in the full coordinate space at high photon energies ($E_1 + E_2 \gg 1$).

7.3 Results for both single and double photodetachment of H^-

We employ the acceleration gauge in the evaluation of the total cross sections for one- and two-electron photon detachment at high photon energies. This gauge places the dominant weight on the final-state wavefunction at small distances from the nucleus. Our calculation proceeds by expanding the distortion factor $D^{(-)}(\mathbf{k}_{12}, \mathbf{r}_{12})$ in terms of partial waves in $\mathbf{r_{12}}$ coordinates. All the contributing partial waves are included until convergence is reached (up to a g wave). The cross section for the ejection of a single electron is obtained by summing over all bound states $H(n_2 l_2 m_2)$ and the angular momenta of the continuum electron $(k_1 l_1 m_1)$

$$\sigma^+ = \sum_{l_1 m_1} \sum_{n_2 l_2 m_2} \sigma^+_{ph}(k_1 l_1 m_1, n_2 l_2 m_2) \tag{7.3}$$

with $l_1 = l_2 \pm 1$ and $m_1 + m_2 = 0$.

The cross section for single- *plus* double-electron detachment, σ_{tot}, at high energies is summed over all bound and continuum states of the residual

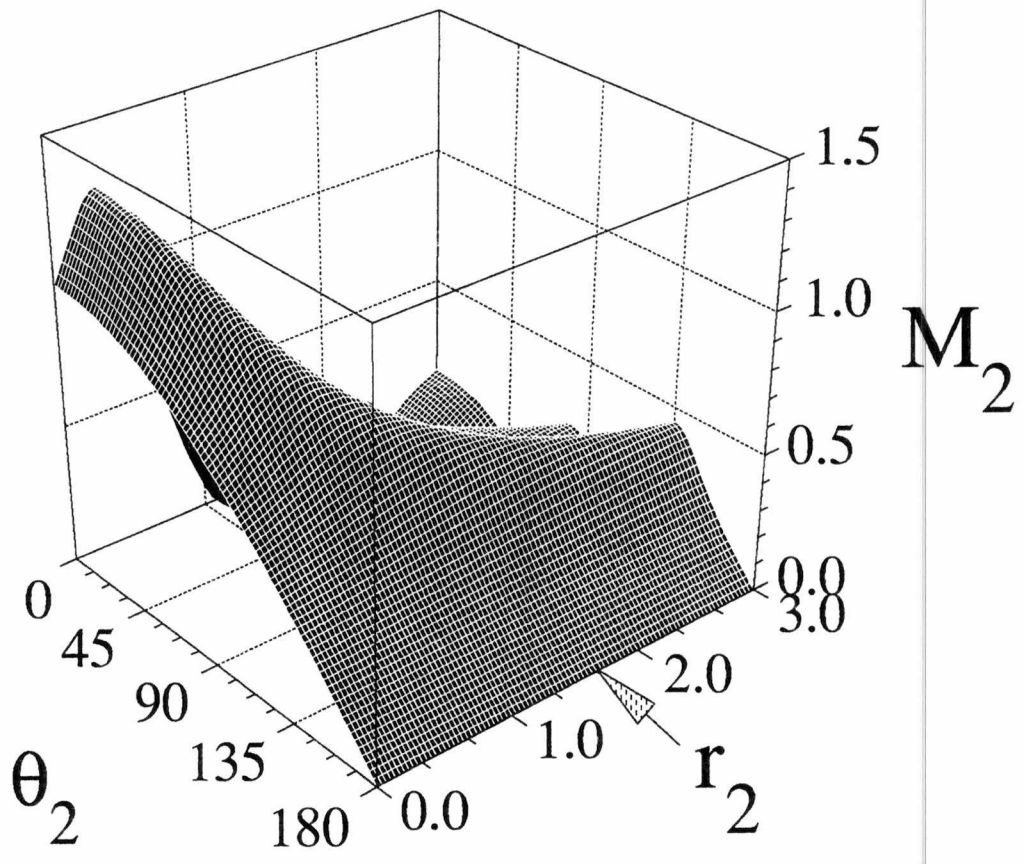

Figure 7.3: Behavior of $|\mathrm{M}_i(r_i, \theta_i)|$ as a function of radial r_i and angle θ_i coordinates at energy $E_{tot} = 1$ keV with an asymmetric energy distribution: fast electron $E_1 = 950$ eV (M_1) and slow electron $E_2 = 50$ eV (M_2). Arrow indicates dominant region of the dipole matrix element.

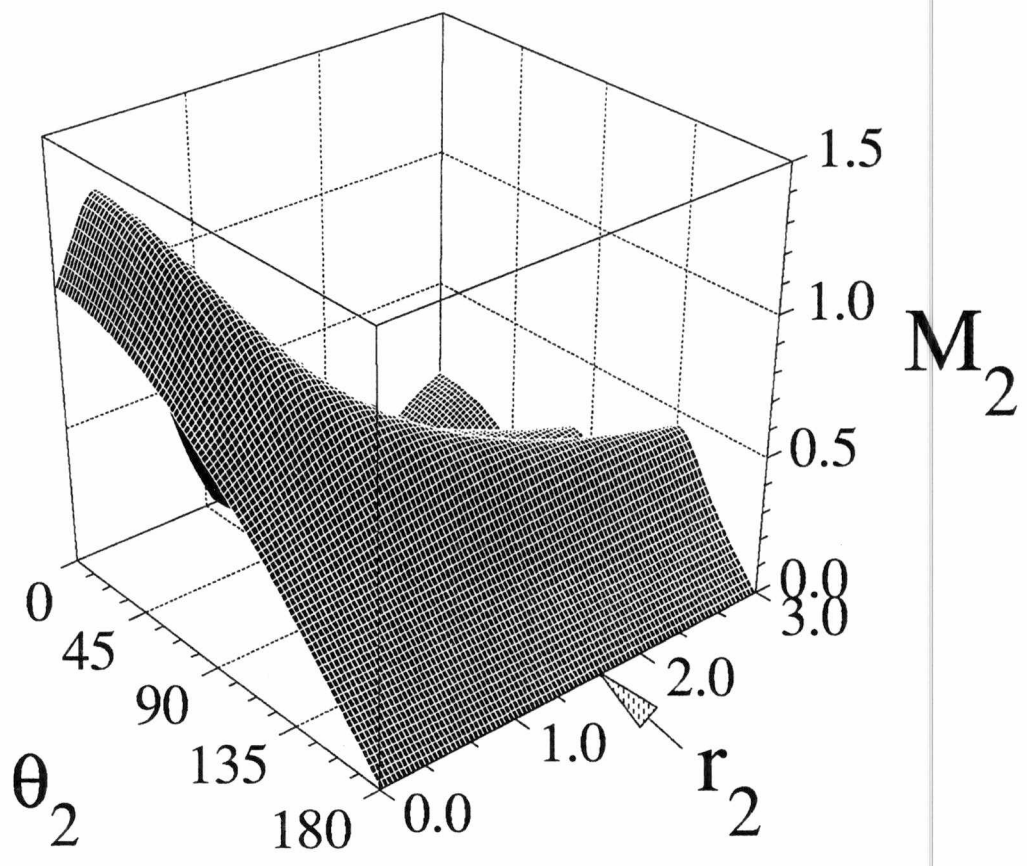

Fig. (7.3) continued.

electron and its evaluation is facilitated by the closure relation. We therefore obtain the cross section for double ionization

$$\sigma^{++} = \sigma_{tot} - \sigma^{+} \tag{7.4}$$

and the ratio

$$R_{ph} = \sigma^{++}/\sigma^{+}. \tag{7.5}$$

For a detailed analysis of the high energy behavior for one-electron detachment and its effect on two-electron ejection we study detachment-excitation, i. e., the branching cross sections

$$\sigma^{+}(n_2) = \sum_{l_1 m_1} \sum_{l_2 m_2} \sigma^{+}_{ph}(k_1 l_1 m_1, n_2 l_2 m_2). \tag{7.6}$$

In contrast to He, for which only $\sigma^{+}(1s)$ dominates the single-electron ejection process [97] (also see chapter 5), the satellite cross section $\sigma^{+}(n_2 = 2)$ for H^- also contributes significantly to one-electron ejection. The prominent role of excitation to $H(n_2 = 2)$ results from the fact that the binding radius of the ground state of H^- (Fig. 7.2) lies in between the binding radii of both states $H(1s)$ and $H(n_2 = 2)$. Therefore, the ground state wavefunction of H^- has a strong overlap with the wavefunction of $H(1s)$ and $H(n_2 = 2)$ which are favored in the shake-off process. The satellite ratio $R(2) = \sigma^{+}(n_2 = 2)/\sigma^{+}(1s)$ is approximately $\simeq 0.65$ and is only weakly dependent on the photon energy (Fig. 7.4). In contrast, the corresponding ratio for $n_2 = 3$ is a factor of $\simeq 120$ smaller. We have also calculated the single- and double-detachment cross sections using the same initial-state

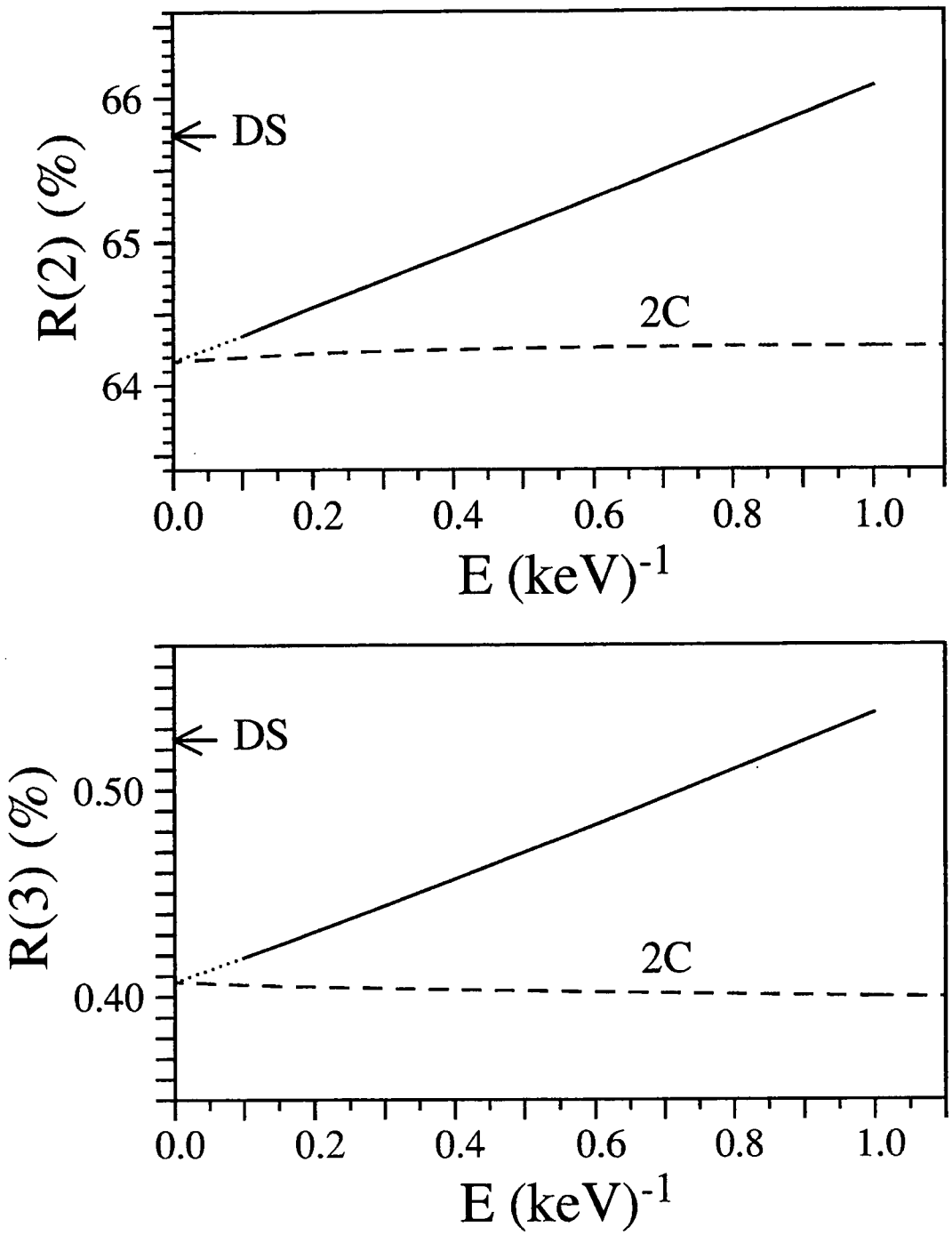

Figure 7.4: Satellite-to-1s ratios $R(n_2)$ for $n_2 = 2, 3, 4, 5, 6$, and 7 & up as a function of incident photon energy. Solid curves: 3C results. Dashed curves: results without the final-state correlation (denoted by 2C). The results of R(2) and R(3) obtained in the calculation of Dalgarno and Sadeghpour[31] are indicated by arrows (denoted by DS).

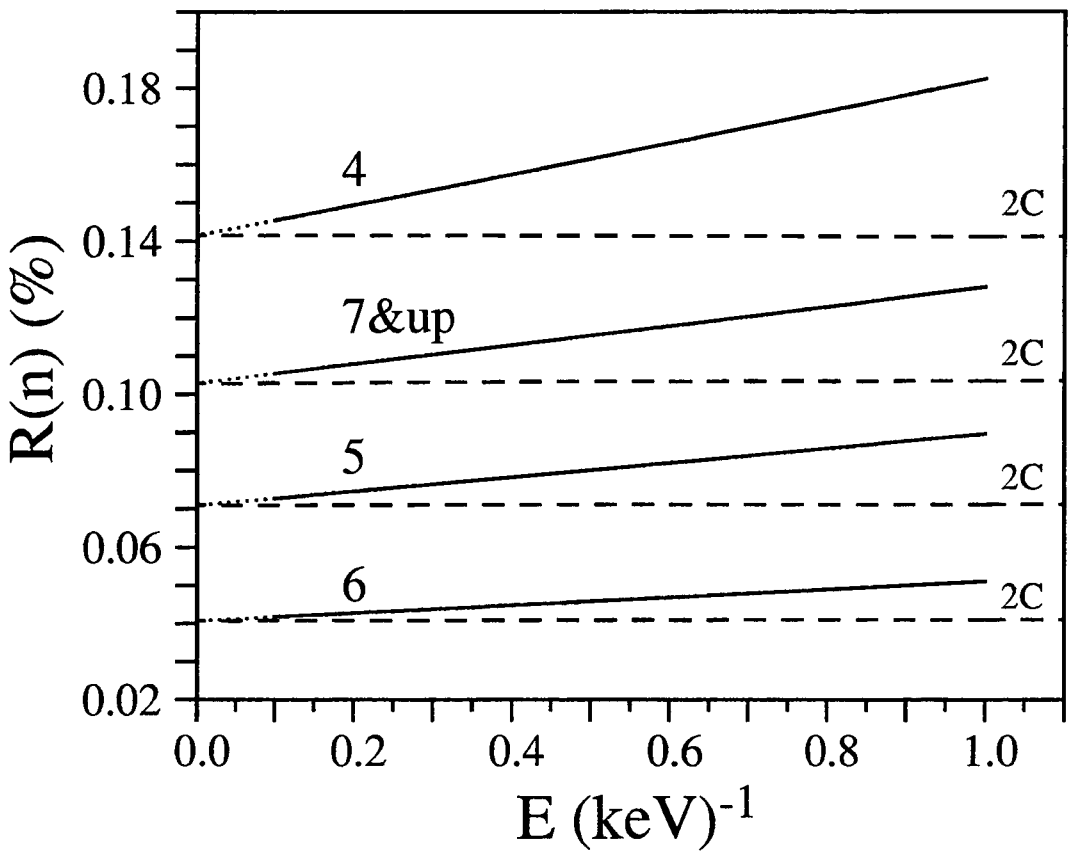

Fig. (7.4) continued for $R(n_2)$, n_2 = 4, 5, 6, and 7 & up.

wavefunction but a final-state wavefunction without electron-electron correlation (i.e., taking $D^{(-)} = 1$ in the final state wavefunction) The satellite-to-1s ratios $R(n_2)$ thus obtained are constants at high energies as can be seen in the figure (denoted by 2C). We note some minor discrepancies in $R(2)$ and $R(3)$ between the present result and the result of Dalgarno and Sadeghpour [31] in the asymptotic limit ($E \to \infty$). These deviations come from the different level of accuracy of the initial-state wavefunctions. In the calculation of Dalgarno and Sadeghpour the 20-parameter correlated representation of the ground state of Hart and Herzberg [34] is applied. Although the binding energy obtained agrees with the exact value to within 0.02%, the relative errors in the Kato cusp conditions of the ground state wavefunction (Fig. 7.1) is about 11% for the confluence of the electron-nucleus coordinates and 35% for the confluence of the electron-electron coordinates at the nucleus. In the present calculation these conditions are satisfied at a higher level of accuracy.

The total cross sections for double- and single-electron detachment and their ratio as a function of incident photon energy between 1 and 10 keV are presented in Tab. 7.2.

The cross sections for single- and double-electron detachment in the energy range calculated using the 3C wavefunction can be approximately represented by

$$\sigma^{+}(E) \approx \frac{15.18 - 6.51/E}{E^{7/2}} \qquad (10^{-24} \text{ cm}^2), \tag{7.7}$$

and

$$\sigma^{++}(E) \approx \frac{0.229 - 0.052/E}{E^{7/2}} \qquad (10^{-24} \text{ cm}^2), \tag{7.8}$$

Table 7.2: Total cross sections of double- (σ^{++}) and single-electron ejection (σ^{+}) and their ratio R_{ph} *vs* photon energy E.

E (keV)	σ^{+} (cm^2)	σ^{++} (cm^2)	R_{ph}(%)
1.0	1.15×10^{-23}	2.15×10^{-25}	1.87
1.2	6.25×10^{-24}	1.13×10^{-25}	1.81
1.4	3.73×10^{-24}	6.57×10^{-26}	1.76
1.6	2.38×10^{-24}	4.11×10^{-26}	1.73
1.8	1.60×10^{-24}	2.73×10^{-26}	1.70
2.0	1.12×10^{-24}	1.89×10^{-26}	1.68
3.0	2.84×10^{-25}	4.60×10^{-27}	1.62
4.0	1.06×10^{-25}	1.69×10^{-27}	1.59
5.0	4.96×10^{-26}	7.81×10^{-28}	1.57
6.0	2.66×10^{-26}	4.16×10^{-28}	1.56
8.0	9.89×10^{-27}	1.53×10^{-28}	1.55
10.0	4.59×10^{-27}	7.07×10^{-29}	1.54

respectively, where E is in keV. The ratio, $R_{ph} = \sigma^{++}/\sigma^{+}$, displays a linear dependence on the inverse of E within this energy interval,

$$R_{ph}(E) \approx 1.50 + 0.30/E(\text{keV}) \qquad (\%), \tag{7.9}$$

as shown in Fig. 7.5 while the ratio becomes almost constant if the final-state correlation is neglected (denoted by 2C). Our calculations with and without final-state correlation reach the same asymptotic limit of $R_{ph}(\infty) = 1.50\%$ which is marginally lower than the value of 1.51% obtained by Dalgarno and Sadeghpour [31] (denoted by DS), presumably due to the aforementioned difference in the cusp condition in the initial state.

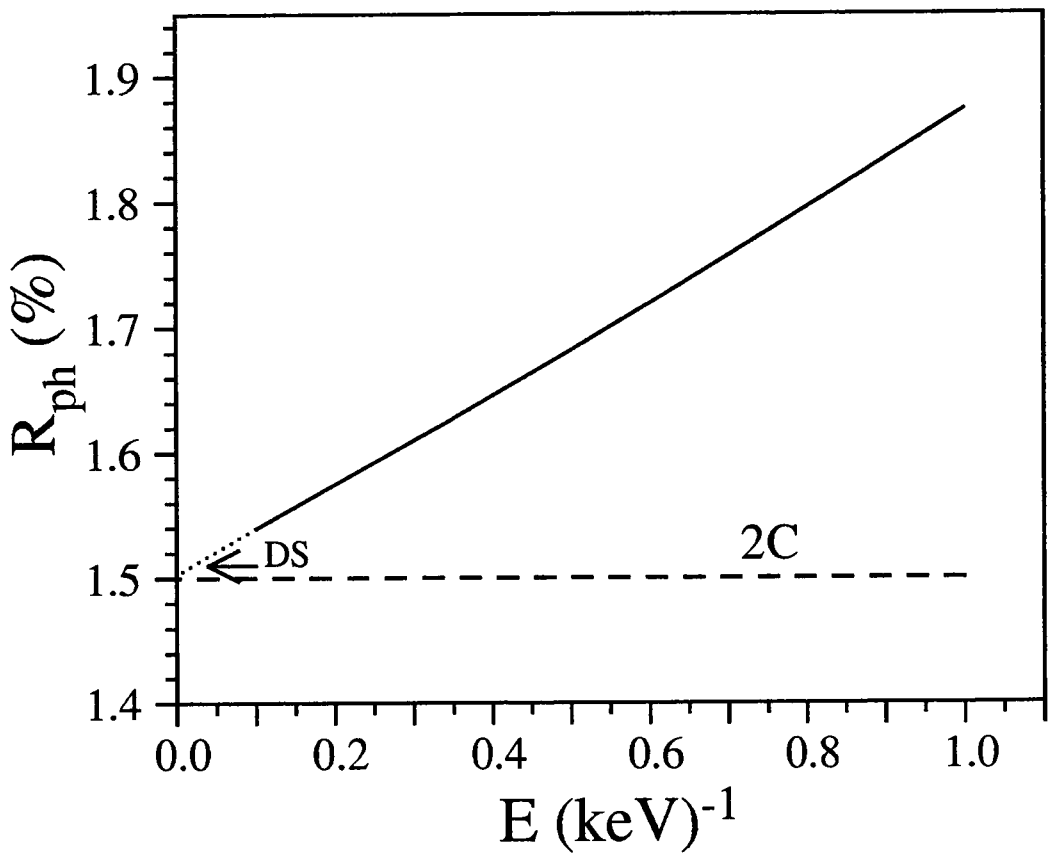

Figure 7.5: Ratio $R_{ph} = \sigma^{++}/\sigma^{+}$ between double and single detachment cross sections for H− as a function of E^{-1}. Solid curve: 3C result. Dash curve: result without the final-state correlation (denoted by 2C). The asymptotic value of Dalgarno and Sadeghpour [31] is indicated by arrow (denoted by DS).

It is interesting to note that R_{ph} for H^- is systematically lower than that for He in the high-energy range[80, 96] although one might expect otherwise because of the stronger role of electron-electron correlation[95]. A qualitative explanation involves the picture of the initial state represented by two non-equivalent electrons $(1s, 1s')$. At high photon energies the inner $1s$ electron is ejected with high energy while the outer, loosely bound electron $1s'$ is shaken off. The outer $1s'$ electron strongly overlaps with both the $2s$ and $1s$ orbitals of neutral hydrogen but has little overlap with the hydrogenic continuum. Therefore, double ionization is less likely for H^- than for He.

In summary, we have studied the single- and double-electron photodetachment of H^- at photon energies in the 1 keV to 10 keV range using an accurate Hylleraas initial-state wavefunction and a correlated 3C final-state wavefunction. In the high-energy limit, the double electron ejection is dominated only by the initial-state correlation, resulting in an asymptotic limit of $R_{ph}(\infty) = 1.50\%$. At the high but finite energies studied here, the final-state correlation is found to be important, giving rise to an E^{-1} high-energy behavior for the ratio R_{ph}. It is hoped that the present result will be experimentally tested in the near future.

Chapter 8

Conclusions

We have investigated the double ionization and ionization-excitation of He and H^- by high energy photons ($\geq$ 1 keV) using an accurate Hylleraas-type initial state wavefunction and a correlated 3C final state wavefunction. We have shown that the 3C wavefunction, which describes the three-body final state to leading order in Z/k_1 in the full configuration space and which satisfies the Kato cusp conditions exactly at the three two-body collision points, is the correct wavefunction to represent the double continuum in the high energy region. A new technique for the analysis of the distortion factor $D^{(-)}$ in the 3C wavefunction has been developed which can lead to an accurate evaluation of the transition probabilities. We have also studied double photoionization using the same initial state wavefunction but a final-state wavefunction without electron-electron correlation (2C). For He our calculation shows that the double-to-single ratio is 2.62 % at 1 keV with the 3C final state wavefunction and approaches the same asymptotic value of $R_{ph}(\infty) = 1.65\%$ with and without final state correlation. This result is

in excellent agreement with experimental data. For H^- we have made the first reliable calculation at high photon energies. Using the aforementioned correlated final state wavefunction we arrive at an E^{-1} high-energy behavior for the ratio $R_{ph}(E)$ with an asymptotic limit of $R_{ph}(\infty) = 1.50\%$, in agreement with Dalgarno and Sadeghpour [31]. We also obtained a finite energy correction of $a_{-1}E^{-1}$ (%) with $a_{-1} = 0.30$ keV. We have also pointed out that the interaction between the high but finite energy photon and an atomic system is localized in a region within a distance of $\sim E^{-1/2}$ about the nucleus instead of a point at the center. We introduced a shape function into the formulas suggested by Kabir and Salpeter [84] and by Dalgarno and Stewart [85]. This correction can dramatically improve the evaluation of the absolute cross sections for the double and single ionization processes at high but non-relativistic photon energies. Moreover, we include final-state correlation into the formulas. The results obtained with this simple method agree quite well with those of MBPT and with the measurements at the high photon energies. They display much better behavior than that obtained using the recently introduced dipole response function.

Bibliography

Bibliography

[1] G. H. Wannier, The threshold law for single ionization of atoms or ions by electrons, *Phys. Rev.* **90**, *817 (1953).*

[2] A. R. P. Rau, *Phys. Rev. A* **4**, *207 (1971).*

[3] R. Peterkop, WKB approximation and threshold law for electron-atom ionization, *J. Phys. B* **4**, *513 (1971).*

[4] F. H. Read, *Electron impact ionization*, edited by T. D. Märk and G. H. Dunn (Springer, Berlin, 1985).

[5] J. B. Donahue, P. A. M. Gram, M. V. Hynes, R. W. Hamm, C. A. Frost, H. C. Bryant, K. B. Butterfield, D. A. Clark, and W. W. Smith, Observation of two-electron photoionization of the H^- ion near threshold, *Phys. Rev. Lett.* **48**, *1538 (1982).*

[6] Y. K. Bae and J. R. Peterson, Near-threshold measurements of K^- two-electron photoionization cross sections, *Phys. Rev. A* **37**, *3254 (1988).*

[7] R. I. Hall, A. G. McConkey, L. Avaldi, K. Ellis, M. A. M. A. Macdonald, G. Dawber, and G. C. King, Threshold photo-double ionization

processes in helium studied by a photoelectron/photoion coincidence technique, *J. Phys. B* **25**, *1195 (1992).*

[8] P. Lablanquie, J. Mazeau, L. Andric, P. Selles, and A. Huetz, Effect of electron energy sharing on the double photoionization of helium near threshold, *Phys. Rev. Lett.* **20**, *2192 (1995).*

[9] H. Kossmann, V. Schmidt, and T. Andersen, Test of Wannier threshold laws: double-photoionization cross section in helium, *Phys. Rev. Lett.* **60**, *1266 (1988).*

[10] G. C. King, M. Zubek, P. M. Rutter, F. H. Read, A. A. MacDowell, J. B. West, and D. M. P. Holland, A study of threshold photoionisation and double photoionisation in helium, *J. Phys. B* **21**, *L403 (1988).*

[11] H. L. Rouzo and C. D. Cappello, Double photoionization of helium: Analysis of photoelectrons with respect to energies and angles, *Phys. Rev. A* **43**, *318 (1991).*

[12] A. Huetz, P. Selles, D. Waymel, and J. Mazeau, Wannier theory for double photoionization of noble gases, *J. Phys. B* **24**, *1917 (1991).*

[13] F. Maulbetsch and J. S. Briggs, Angular distribution of electrons following double photoionization, *J. Phys. B* **26**, *1679 (1993).*

[14] F. Maulbetsch and J. S. Briggs, Angular distribution of electrons following double photoionization, *J. Phys. B* **26**, *L647, (1993).*

[15] O. Schwarzkopf, B. Krässig, J. Elmiger, and V. Schmidt, Energy- and angle-resolved double photoionization in helium, *Phys. Rev. Lett.* **70**, *3008, (1993).*

[16] J. Z. Tang, and I. Shimamura, Double photoionization of helium at low photon energies, *Phys. Rev. A* **52**, *R3413 (1995).*

[17] K. W. Meyer and C. H. Greene, Double photoionization of helium using R-matrix methods, *Phys. Rev. A* **50**, *R3573 (1994).*

[18] M. Pont and R. Shakeshaft, Absolute cross sections for double photoionization of helium at energies from 0 to 80 eV above threshold, *J. Phys. B* **28**, *L571 (1995).*

[19] J. A. R. Samson, Z. X. He, L. Yin, and G. N. Haddad, Precision measurements of the absolute photoionization cross section of He, *J. Phys. B* **27**, *887 (1994).*

[20] J. C. Levin, G. B. Armen, and I. A. Sellin, Photoionization and Compton double ionization of helium from threshold to 20 keV, *Phys. Rev. Lett.* **76**, *1220 (1996).*

[21] R. Dörner, T. Vogt, V. Mergel, H. Khemliche, S. Kravis, C. L. Cocke, J. Ullrich, M. Unverzagt, L. Spielberger, M. Damrau, O. Jagutzki, I. Ali, B. Weaver, K. Ullmann, C. C. Hsu, M. Jung, E. P. Kanter, B. Sonntag, M. H. Prior, E. Rotenberg, J. Denlinger, T. Warwick, S. T. Manson, and H. Schmidt-Böcking, Ratio of cross sections for double to

single ionization of He by 85-400 eV photons, *Phys. Rev. Lett.* **76**, *2654 (1996).*

[22] C. Pan and H. P. Kelly, Calculation of the double-photoionization cross section of helium, *J. Phys. B* **28**, *5001 (1995).*

[23] T. Ishihara, K. Hino, and J. H. McGuire, Photoionization of two electrons in helium, *Phys. Rev. A* **44**, *R6980 (1991).*

[24] K. Hino, T. Ishihara, and J. H. McGuire, Double photoionization of helium using many-body perturbation theory, *Phys. Rev. A* **48**, *1271 (1993).*

[25] L. R. Andersson and J. Burgdörfer, Excitation ionization and double ionization of helium by high-energy photon impact, *Phys. Rev. Lett.* **5**, *50 (1993).*

[26] Z. Teng and R. Shakeshaft, Double ionization of helium by a single high-energy photon, *Phys. Rev. A* **47**, *R3487 (1993).*

[27] K. Hino, Double ionization of He by high-energy photon impact, *Phys. Rev. A* **47**, *4845 (1993).*

[28] M. A. Kornberg and J. E. Miraglia, Double photoionization of helium: Use of a correlated two-electron continuum wavefunction, *Phys. Rev. A* **48**, *3714 (1993).*

[29] R. C. Forrey, Z. Yan, H. R. Sadeghpour, and A. Dalgarno, Single and double photoionization from dipole response function, *Phys. Rev. Lett.* **78**, *3662 (1997).*

[30] F. W. Byron, Jr. and C. J. Joachain, Multiple ionization processes in helium, *Phys. Rev.* **1**, *146 (1966).*

[31] A. Dalgarno and H. Sadeghpour, Double photoionization of atomic helium and its isoelectronic partners at x-ray energies, *Phys. Rev. A* **46**, *3591 (1992).*

[32] L. I. Schiff, *Quantum mechanics, Third Edition,* McGraw-Hill, Inc. (1968)

[33] C. F. Fischer, *The Hartree-Fock method for atoms,* John Wiley, New York, (1977).

[34] J. F. Hart and G. Herzberg, Twenty-parameter eigenfunctions and energy values of the ground states of He and He-like ions, *Phys. Rev.* **1**, *57 (1957).*

[35] T. Kinoshita, Ground state of helium atom, *Phys. Rev.* **105**, *1490 (1957).*

[36] S. Chandrasekhar and G. Herzberg, Energies of the ground states of He, Li^+, and O^{6+}, *Phys. Rev.* **98**, *1050 (1958).*

[37] C. L. Pekeris, Ground state of two-electron atoms, *Phys. Rev.* **112**, *1649 (1958).*

[38] C. L. Pekeris, 1 ^1S and 2 ^3S states of helium, *Phys. Rev.* **115**, *1216 (1959).*

[39] C. Schwartz, Ground state of the helium atom, *Phys. Rev.* **3**, *1146 (1962).*

[40] R. A. Bonham and D. A. Kohl, Simple correlated wavefunctions for the ground state of heliumlike atoms, *Phys. Rev.* **45**, *2471 (1966).*

[41] Z. C. Yan and G. W. F. Drake, On the evaluation of two-electron integrals in Hylleraas coordinates, *Chem. Phys. Lett.* **259**, *96 (1996).*

[42] R. D. Cowan, *The theory of atomic structure and spectra,* University of California Press, Berkeley and Los Angeles, California, (1981).

[43] T. Kato, On the eigenfunctions of many-particle systems in quantum mechanics, *Commun. Pure. Appl. Math.* **10**, *151 (1957).*

[44] E. A. Hylleraas, *Z. Physik 54, 347, (1929).*

[45] J. Müller, Quantenmechanik klassisch chaotischer systeme, *Reihe Physik Bd.19 Verlag Harri Deutsch (1993).*

[46] V. A. Fock, *Izvest. Akad. Nauk SSSR Ser. Fiz.* **18**, *161 (1954).*

[47] R. A. Sack, Generalization of Laplace's expansion to arbitrary powers and functions of the distance between two points, *J. Math. Phys.* **5**, *245 (1964).*

[48] V. Jacobs, Low-energy photo-ionization of the 1^1S and 2^1S states of He, *Phys. Rev.* **3**, *289 (1971).*

[49] Y. Qiu, J. Müller, and J. Burgdörfer, Periodic orbit spectra of hydrogen and helium, *Phys. Rev.* **54**, *1922 (1996).*

[50] J. Burgdörfer, Y. Qiu, and J. Müller, Periodic Orbit Spectra of Simple Atoms, edited by H. Friedrich and B. Eckhardt, in *Classical, semiclassical and quantum dynamics in atoms,* (Springer-Verlag Berlin Heidelberg, 1997).

[51] L. Vainshtein, L. Presnyakov, and I. Sobelman, *Zh. Eksp. Teor. Fiz.* **45**, *2015 (1963) [Sov. Phys. JETP* **18**, *1383 (1964)].*

[52] M. R. H. Rudge and M. J. Seaton, The threshold law for ionizing collisions, *Proc. Phys. Soc.* **83**, *680 (1964).*

[53] R. K. Peterkop, *Theory of ionization of Atoms by the Electron Impact,* (Colorado Associated University Press, Bould, 1977).

[54] S. Jetzke and F. H. M. Faisal, coulomb correlations in electron and positron impact ionization of hydrogen at intermediate and higher energies, *J. Phys. B* **25**, *1543 (1992).*

[55] J. Berakdar, Approximate analytical solution of the quantum-mechanical three-body Coulomb continuum problem, *Phys. Rev. A* **53**, *2314, (1996).*

[56] J. Berakdar, Parabolic-hyperspherical approach to the fragmentation of three-particle Coulomb systems, *Phys. Rev. A* **54**, *1480, (1996).*

[57] G. Gasaneo, F. D. Colavecchia, C. R. Garibotti, J. E. Miraglia, and P. Macri, Correlated continuum wavefunctions for three particles with Coulomb interactions, *Phys. Rev. A* **55**, *2809, (1997).*

[58] G. Gasaneo, F. D. Colavecchia, C. R. Garibotti, J. E. Miraglia, P. A. Macri, Multivariable hypergeometric solutions for three charged particles, *J. Phys. B* **30**, *L265, (1997).*

[59] M. R. C. McDowell and J. P. Coleman, *Introduction to the theory of ion-atom Collisions*, North-Holland Publishing Company, Amsterdam-London, (1970).

[60] H. Friedrich, *Theoretical atomic physics*, Springer-Verlag Berlin Heidelberg, (1991).

[61] C. Pan and A. F. Starace, Target dependence of angular distributions for near-threshold (e,2e) processes, *Phys. Rev. Lett.* **8**, *185, (1991).*

[62] L. Rosenberg, Variational methods in charged-particle collision theory, *Phys. Rev. D* **8**, *1833, (1973).*

[63] C. R. Garibotti and J. E. Miraglia, Ionization and electron capture to the continuum in the H^+−hydrogen−atom collision, *Phys. Rev. A* **2**, *572, (1980).*

[64] M. Brauner, J. S. Briggs, and H. Klar, Triply-differential cross sections for ionization of hydrogen atoms by electrons and positrons, *J. Phys. B* **22**, *2265 (1989).*

[65] F. Maulbetsch and J. S. Briggs, Angular distribution of electrons following double photoionization, *J. Phys. B* **26**, *1679, (1993).*

[66] J. Berakdar and J. S. Briggs, Three-body Coulomb continuum problem, *Phys. Rev. A* **13**, *3799, (1994).*

[67] E. O. Alt and A. M. Mukhamedzhanov, Asymptotic solution of the Schrödinger equation for three charged particles, *Phys. Rev. A* **47**, *2004, (1993).*

[68] R. Wehlitz, I. A. Sellin, O. Hemmers, S. B. Whitfield, P. Glans, H. Wang, D. W. Lindle, B. Langer, N. Berrah, J. Viefhaus and U. Becker, Photon energy dependence of ionization-excitations in helium at medium energies, *J. Phys. B* **30**, *L51, (1997).*

[69] J. A. R. Samson, Private communication.

[70] L. Spielberger, O. Jagutzki, R. Dörner, J. Ullrich, U. Meyer, V. Mergel, M. Unverzagt, M. Damrau, T. Vogt, I. Ali, Kh. Khayyat, D. Bahr, H. G. Schmidt, R. Frahm, and H. Schmidt-Böcking, Separation of photoabsorption and Compton scattering contributions to He single and double ionization, *Phys. Rev. Lett.* **74**, *4615 (1995).*

[71] I. S. Gradshteyn and I. M. Ryzhik, *Table of integrals, series, and products, corrected and enlarged edition,* (Academic Press, Inc., New York, 1979)

[72] M. Rotenberg, R. Bivins, N. Metropolis, and J. K. Wooten, Jr. The 3-j and 6-j symbols (The technology press, Massachusetts institute of technology, Cambridge, Massachusetts, 1959).

[73] L. R. Andersson, *Notes for the evaluation of the double photoionization by partial wave analysis.*

[74] R. R. Lewis, Jr., Potential scattering of high-energy electrons in second Born approximation, *Phys. Rev. 102, 537 (1956).*

[75] T. A. Carlson, M. O. Krause, and W. E. Moddeman, *J. Phys. (Paris) 32, C4-76 (1971).*

[76] S. Svensson, B. Eriksson, N. Martensson, G. Wendin, and U. Gelius, *J. Elec. Spec. 47, 327, (1988).*

[77] J. C. Levin, D. W. Lindle, N. Keller, R. D. Miller, Y. Azuma, N. Berrah Mansour, H. G. Berry, and I. A. Sellin, Measurement of the ratio of double-to single photoionization of helium at 2.8 keV using synchrotron radiation, *Phys. Rev. Lett. 67, 968, (1991).*

[78] J. C. Levin, I. A. Sellin, B. M. Johnson, D. W. Lindle, R. D. Miller, N. Berrah, Y. Azuma, H. G. Berry, and D. H. Lee, High-energy behavior

of the double photoionization of helium from 2 to 12 keV, *Phys. Rev. A. 47, R16, (1993).*

[79] J. Z. Tang, (private communication) (1997).

[80] Y. Qiu, J. Z. Tang, J. Burgdörfer, J. Wang, Double photoionization of helium from threshold to high energies, to be published.

[81] T. Åberg, Asymptotic double-photoionization cross sections of the helium atom, *Phys. Rev. A 2, 1726 (1970).*

[82] R. L. Brown and R. J. Gould, *Phys. Rev. D* **1**, *2252 (1970).*

[83] M.Ya.Amusia, E.G.Drukarev, V.G.Gorshkov, and M.P.Kazachkov, Two-electron photoionization of helium, *J. Phys. B* **8**, *1248 (1975).*

[84] P. K. Kabir and E. E. Salpeter, Radiative corrections to the ground-state energy of the helium atom, *Phys. Rev.* **108**, *1256 (1957).*

[85] A. Dalgarno and A. L. Stewart, The Lamb shift of helium, *Proc. Phys. Soc. London* **76**, *49 (1960).*

[86] R. H. Pratt, A. Ron, and H. K. Tseng, *Rev. Mod. Phys.* **45**, *273 (1973).*

[87] M. A. Kornberg and J. E. Miraglia, Retardation effects and angular coefficients in double photoionization, *Phys. Rev. A* **52**, *2915 (1995).*

[88] J. Wang, J. H. McGuire, J. Burgdörfer, and Y. Qiu, Consistency test of double ionization of helium by photons and charged particles,, *Phys. Rev. A* **54**, *613 (1996).*

[89] J. Wang, J. H. McGuire, J. Burgdörfer, and Y. Qiu, Differential double ionization of He by Compton photons and charged particles at large energy transfers, *Phys. Rev. Lett.* **26**, *1723 (1996)*.

[90] J. B. Donahue, P. A. M. Gram, M. V. Hymes, R. W. Hamm, C. A. Frost, H. C. Bryant, K. B. Butterfield, David A. Clark and W. W. Smith, Observation of two-electron photoionization of the H^- ion near threshold, *Phys. Rev. Lett.* **48**, *1538 (1982)*.

[91] J. F. McCann and D. S. F. Crothers, Semiclassical (γ, 2e): absolute cross sections for H^- at threshold, *J. Phys. B* **19**, *L399 (1986)*.

[92] A. G. Abrashkevich and M. Shapiro, Photoionization of two-electron atoms via the hyperspherical artificial-channel method: Application to H^- and He, *Phys. Rev. A* **50**, *1205 (1994)*.

[93] J. T. Broad and W. P. Reinhardt, One- and two-electron photoejection from H^-1: A multichannel J-matrix calculation, *Phys. Rev. A* **14**, *2159 (1976)*.

[94] M. A. Kornberg and J. E. Miraglia, Scaling laws in double photoionization, *Phys. Rev. A* **49**, *5120 (1994)*.

[95] K. W. Meyer, C. H. Greene, and B. D. Esry, Two-electron photoejection of He and H^-, *Phys. Rev. Lett.* **78**, *4902 (1997)*.

[96] Y. Qiu, J. Z. Tang, J. Burgdörfer, and J. Wang, one- and two-electron emission from H^- by high-energy photons, *J. Phys. B* **30**, *L689 (1997)*.

[97] J. Z. Tang, J. Burgdörfer, excitation-ionization by photoabsorption at low and intermediate energies, *J. Phys. B* **30**, *L523, (1997).*

Vita

Yanghui Qiu was born on October 12, 1963 in Miluo county of Hunan province, P. R. China. He has two brothers and one sister. He was brought up by his grandfather and grandmother.

In 1979 he left his family for the first time. He entered the first high school of Miluo county that year. Two years later, he was admitted to Changsha Institute of Technology. He obtained the B. S. in 1985 and entered the Institute of Applied Physics and Computational Mathematics (IAPCM) in Beijing under the guidance of Professor Shichang Li, majoring in atomic physics. Yanghui Qiu graduated with his M. S. in 1988 and joined the atomic physics group in the IAPCM untill 1992. During the period he went to the atomic and molecular data unit, nuclear data section IAEA for half a year for atomic data management under the guidance of Professor Ratko Janev. In December 1992 he became a graduate student of Professor Joachim Burgdörfer at the department of physics and astronomy, the University of Tennessee. He is working on the double photoionization of helium and H^- in the high energy region and expects to receive his Ph. D. in December 1997.